Doctoral Dissertation

博士論文

Super-sample tidal effect on cosmological distortions

(超長波長スケールの潮汐力場が宇宙論的歪みに与える影響)

A Dissertation Submitted for
the Degree of Doctor of Philosophy December 2019

令和元年12月博士（理学）申請

Department of Physics, Graduate School of Science,
The University of Tokyo

東京大学大学院理学系研究科物理学専攻

Kazuyuki Akitsu

秋津 一之

Acknowledgments

The time has come to thank all the people and fortunes that made this work possible. First and foremost, I would like to express my deepest gratitude and appreciation to my supervisor, Masahiro Takada, for his generous guidance, patience, and support. Without his help, I would not be able to finish my Ph.D. course. He always encouraged me and his optimism saved me especially when I felt stuck and depressed.

During my Ph.D. course, I had a chance to work with excellent people from whom I learned a lot. I would like to thank Yin Li, Naonori S. Sugiyama, and Maresuke Shiraishi for fruitful collaborations. Yin taught me almost everything on simulations and Naonori and Maresuke introduced a new method to me. I really enjoyed discussing and working with them and I hope I continue to collaborate with them.

I am grateful to Takahiro Nishimichi, Chiaki Hikage, Atsushi Taruya, Misao Sasaki, and Fabian Schmidt for numerous invaluable discussions and advices. Conversations with them always inspired me. I am also happy to thank many (really many!) visitors who kindly discussed with me although I cannot name everyone here. It was my pleasure to study at Kavli IPMU.

I acknowledge the students at Kavli IPMU for everyday discussions and chats. They made my student life more enjoyable. Apart from the physics community, I thank to my friends from the undergrad, Saku, Mitsuki, Yosuke, Kento, and Yuuki for regular breaks. They enlightened me on various topics other than physics.

Finally I wish to thank my family for providing me with the best education possible, developing my interest in physics from my childhood, and supporting me.

Abstract

Although large-scale perturbations beyond a finite-volume survey region, called "super-sample modes", are not direct observables, these affect measurements of clustering statistics of small-scale (sub-survey) perturbations in the large-scale structure, compared with the ensemble average, via the mode-coupling effect. In this thesis we show that large-scale tides (super-sample tidal modes) induced by scalar perturbations cause apparent anisotropic distortions in the observed power spectrum of galaxies. Using the perturbation theory of structure formation, we derive a response function of the power spectrum to large-scale tides. In particular, we find that large-scale tides violates the statistical isotropy in the observed power spectrum and in the redshift-space power spectrum of galaxies this anisotropy depends on an alignment between the tide, wavevector of small-scale modes, and line-of-sight direction. We then quantify the impact of large-scale tides on estimation of cosmological distances (Alcock-Paczyński test) and the redshift-space distortion (RSD) parameter via the measured redshift-space power spectrum for a hypothetical large-volume survey, based on the Fisher information matrix formalism. We show that a degradation in the parameter estimation of cosmological distortions is restored if we employ the prior on the rms amplitude expected for the standard ΛCDM model. We also discuss whether the super-sample tidal modes can be constrained and find that the super-sample tides are detectable with an accuracy better than the ΛCDM prediction without degrading the accuracy of measurements of other cosmological distortions by using bipolar spherical harmonic (BipoSH) decomposition formalism to characterize statistically anisotropic power spectra. In addition, we develop the cosmological N-body simulation with the super-sample tidal modes to study effects of the large-scale tides on nonlinear structure formation in deeply nonlinear regime where the perturbation theory breaks down.

Contents

List of Figures

Chapter 1

Introduction

The large-scale structure (LSS) of the universe offers a powerful tool for measuring the cosmic expansion history of the universe. As the LSS keeps information on the initial state of the universe, its measurements can also be used to probe statistical properties of cosmic fluctuations that are generated in the early universe, as predicted by an inflationary scenario [1–4]. Actually, the LSS historically plays an important role as one of the key probes of cosmology. In 1990s, Refs. [5–8] already suggested a positive cosmological constant Λ from LSS observations. From the discovery of the evidence of Λ by Supernovae observations [9, 10] until the recent Planck satellite, most prominent results came from cleaner probes such as the cosmic microwave background (CMB) [11–13]. However, how to extract the cosmological information from he CMB fluctuations has been extensively discussed. Furthermore, the CMB is limited on the two-dimensional sphere and its available Fourier modes are $N_{\rm modes}^{\rm CMB} \sim \ell_{\rm max}^2 \sim 10^7$, while the LSS, distributed in three-dimensional volume V, has lots of modes $N_{\rm modes}^{\rm LSS} \sim V k_{\rm max}^3 \sim 10^{11}$ for $V \sim (10^4 {\rm Mpc}/h)^3$ and $k_{\rm max} \sim 0.3h/{\rm Mpc}$. Given the great success of the SDSS III BOSS project [14], various next-generation galaxy surveys such as Prime Focus Spectrograph (PFS) [15], Large Synoptic Survey Telescope (LSST) [16], Dark Energy Spectroscopic Instrument (DESI) [17], Wide-Field Infrared Survey Telescope (WFIRST) [18], Euclid [19], and Spectro-Photometer for the History of the universe, Epoch of Reionization, and Ices Explorer (SPHEREx) [20] are being planned. Thus now, again, a new golden age of the LSS will come.

For interpreting upcoming unprecedentedly high-quality data correctly, it is of crucial importance to accurately model various nonlinear corrections imprinted in the observed galaxy clustering: nonlinear gravitational instabilities [21], nonlinear galaxy biases [22] and nonlinear redshift-space distortions [23]. The linear perturbation theory can accurately describe the time evolution of large-scale perturbations in

structure formation, based on the standard Λ and cold dark matter dominated cosmology with Gaussian adiabatic initial conditions (hereafter ΛCDM) [24], which successfully reproduces the high-precision measurements of CMB anisotropies, yielding stringent constraints on the cosmological parameters [13]. The linear theory, however, breaks down in the late-time universe, where galaxy surveys explore, because the nonlinear structure formation induces a mode coupling between different Fourier modes of the perturbations owing to the nature of nonlinear and long-range gravity. As a result, the power spectrum of LSS probes, measured from a galaxy survey, no longer carries the full information unlike CMB anisotropies and the statistical properties display a substantial non-Gaussianity that is described by higher-order correlation functions [25]. A better understanding of the nonlinear structure formation is thus required in order to attain the full potential of wide-area galaxy surveys.

Even though a wide-area galaxy survey is to cover a huge cosmological volume, there is an unavoidable uncertainty in the statistical analysis of LSS probes arising due to the finite survey volume as well as the nonlinear mode coupling, as studied in Refs. [26–39]. A finite-volume survey realization is generally embedded into longer-wavelength perturbations than survey scales – which are called "super-sample modes" [30, 33] (see Fig. 1.1). Although the super-sample modes are not directly observable, have small amplitudes, and are well in the linear regime for a wide-area galaxy survey, it causes a non-negligible effect on small-scale perturbations due to the nonlinear mode coupling, compared with the statistical accuracies in measurements of the small-scale perturbations. Hence, it is necessary to include the effects in the cosmological analysis (e.g. [40]) in order not to have any biased estimation in cosmological parameters as well as not to have too optimistic cosmological constraints.

Various works have studied the super-sample effects for cosmological observables such as the weak lensing correlation functions [30–34, 41]. They focused on the effects of the large-scale coherent overdensity, denoted by $\delta_{\rm b}$ (see [30], for a unified formulation of the effect). However, the effects of the large-scale coherent gravitational tidal force on short-wavelength modes have yet to be fully studied. Since the coherent overdensity and the coherent tidal force are both related to the Hessian of the gravitational potential, it is expected that they have comparable amplitudes in each realization. Therefore, the purpose of this thesis lies in investigating how the super-sample coherent tidal force affects cosmological observables in galaxy redshift surveys. We show that the super-sample coherent tidal force causes an apparent anisotropic clustering in the galaxy distribution. Based on this result, firstly we study the impact of the super-sample tidal field on the measurement of other cos-

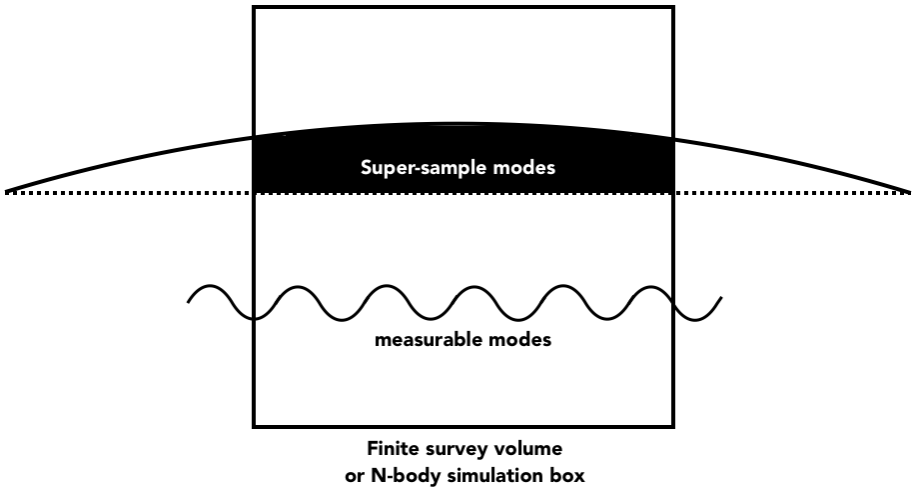

Figure 1.1: A schematic picture describing the super-sample modes. What we can directly measure in surveys are shorter-wavelength modes than the survey scale. The super-sample modes are longer-wavelength modes than the survey scale and thus we cannot measure those perturbations directly. However, due to the nonlinear mode-coupling, the super-sample modes have an effect on all short-wavelength modes.

mological distortions, assuming the ΛCDM cosmology. In particular, we investigate the effect on the measurement of the redshift-space distortion [42, 43] arising from the peculiar velocities of LSS tracers as well as the Alcock-Paczyński (AP) distortion [44–46] arising from the use of an incorrect cosmological model in the clustering analysis. Then, we pursue another possibility to measure or reconstruct the large-scale tidal field beyond the survey region from the short-wavelength observables by making use of the anisotropic imprint of the super-sample modes on small-scale modes without assuming the ΛCDM model, i.e., providing a tool to test the isotropy of our universe in the regime where we cannot directly access.

Besides observational aspects, the super-sample modes are tricky to consider, because their effects vanish in N-body simulations with periodic boundary conditions which have no contribution of long-wavelength modes outside the simulation box. The effect of the super-sample density filed on sub-survey modes for ΛCDM cosmology can be absorbed into an apparent curvature parameter of the local volume — a separate universe picture [27, 31, 35, 47–49]. This approach allows us to include the fully nonlinear mode-coupling of long-wavelength modes with all short-wavelength modes, by performing N-body simulations on a perturbed background correctly capturing the local expansion. However, a technique to implement the large-scale tidal filed beyond the simulation box has yet to be studied. In this thesis, we develop a method to include the super-sample tidal field in N-body simulation by introducing

perturbed scale factors along each coordinate axis.

This thesis is laid out as follows. In Chapter 2, we give a brief summary of the cosmological perturbation theory, including both the linear perturbation theory and nonlinear perturbation theory for structure formation. Then we review observational effects which we have to consider in galaxy redshift surveys in Chapter 3. In Chapter 4, following Refs. [37, 50, 51], we study the effect of the super-sample tidal modes on the observed power spectrum and discuss its possible impact and application. Chapter 5 is devoted to the discussion on the cosmological N-body simulation with the large-scale tides. In Chapter 6 we summarize results with an outlook.

Chapter 2

Cosmological perturbation theory

Contents

In this chapter, we review the cosmological perturbation theory, especially the dark matter perturbation, which is necessary to understand the following chapter. On the first half, we describe the linear perturbation theory in general relativity. On the latter half, we introduce the standard perturbation theory for structure formation, which solves the nonlinear fluid equations in cosmological background in Newtonian limit. Finally we discuss the momentum transfer from short-modes to long-modes and vice versa.

2.1 Linear perturbation theory

We consider the perturbed flat FLRW metric in the conformal Newtonian gauge,

$$\begin{aligned} ds^2 &= a^2(\tau)\left[\eta_{\mu\nu} + h_{\mu\nu}\right] dx^\mu dx^\nu \\ &= a^2(\tau)\left[(-1 - 2\Phi(\tau, \mathbf{x}))d\tau^2 + (1 + 2\Psi(\tau, \mathbf{x}))d\mathbf{x}^2\right], \end{aligned} \tag{2.1}$$

where τ is the conformal time, $a(\tau)$ is the scale factor, Φ is the gravitatioanl potential perturbation, and Ψ is the spatial curvature perturbation. In this thesis, we consider only scalar perturbations. The goal of this section is to explain the shape of the linear matter power spectrum.

2.1.1 Equations

The dynamics of our universe is governed by Einstein equation,

$$R^\mu{}_\nu - \frac{1}{2}R\delta^\mu{}_\nu + \Lambda\delta^\mu{}_\nu = 8\pi G T^\mu{}_\nu, \tag{2.2}$$

where $T^\mu{}_\nu$ is the energy momentum tensor. The background equations are given by

$$\mathcal{H}^2 = \frac{8\pi G}{3}a^2\bar{\rho} + \frac{\Lambda}{3}a^2, \tag{2.3}$$

$$\mathcal{H}' = -\frac{4\pi G}{3}a^2\left(\bar{\rho} + 3\bar{\mathcal{P}}\right) + \frac{\Lambda}{3}a^2, \tag{2.4}$$

where $' \equiv d/d\tau$, $\mathcal{H} \equiv a'/a$, $\bar{\rho}$ is the mean energy density and $\bar{\mathcal{P}}$ is the mean pressure of cosmic fluid. The conformal Hubble parameter $\mathcal{H}$ is related to the Hubble parameter $H \equiv \frac{da}{dt}/a$ through $\mathcal{H} = aH$ with t being the physical time. Defining the energy density parameters via

$$\Omega_i \equiv \frac{8\pi G a^2 \bar{\rho}_i}{3\mathcal{H}^2}, \tag{2.5}$$

and denoting its value at present as Ω_{i0}, the Friedmann equation can be rewritten as

$$H^2 = H_0\left[\frac{\Omega_{r0}}{a^4} + \frac{\Omega_{m0}}{a^3} + \Omega_{\Lambda 0}\right], \tag{2.6}$$

with $i = r, m, \Lambda$ refers to the radiation, the matter, and the cosmological constant, respectively.

Given the metric Eq. (2.1), the 00-component and ij-component of linearly perturbed Einstein equations are calculated as

$$3\mathcal{H}(\mathcal{H}\Phi - \Psi') + \nabla^2\Psi = -4\pi G a^2\bar{\rho}\delta, \tag{2.7}$$

$$\nabla^2(\Phi + \Psi) + 3(\mathcal{H}^2 + 2\mathcal{H}')\phi + 3\mathcal{H}\Phi' - 6\mathcal{H}\Psi' - 3\Psi'' = 12\pi G a^2\delta\mathcal{P}, \tag{2.8}$$

$$\Phi + \Psi = -8\pi G a^2\Pi, \tag{2.9}$$

where we have introduced the perturbed energy momentum tensor

$$\bar{T}^0_{\ 0} + \delta T^0_{\ 0} = -\bar{\rho}(1+\delta), \tag{2.10}$$

$$\delta T^0_{\ i} = (\bar{\rho} + \bar{\mathcal{P}})v_i, \tag{2.11}$$

$$\delta T^i_{\ 0} = -(\bar{\rho} + \bar{\mathcal{P}})v^i, \tag{2.12}$$

$$\bar{T}^i_{\ j} + \delta T^i_{\ j} = \left(\bar{P} + \delta\mathcal{P}\right)\delta^i_{\ j} + \Pi^i_{\ j}, \tag{2.13}$$

with $\Pi^i_{\ j}$ being the anisotropic stress and Π being its scalar component.

To solve these equations, we need to know the time evolution of the energy momentum tensor. In order to follow the full dynamics, we have to consider the Boltzmann equations. However, it is possible to extract the dynamics of each component from the conservation of the energy-momentum tensor, $\nabla_\mu T^\mu_{\ \nu} = 0$, in the limit where effects of the higher order moments (higher than two) can be neglected. Although the higher order moments are important for photons and neutrinos, we focus on dark matter, so we derive the evolution of each component from the the conservation of the energy-momentum tensor: $\nabla_\mu T^\mu_{\ \nu} = 0$ yields

$$\delta' + (1+w)(\theta + 3\Psi') = 0, \tag{2.14}$$

$$\theta' + \mathcal{H}(1-3w)\theta + \frac{w}{1+w}\nabla^2\delta + \nabla^2\Phi = 0, \tag{2.15}$$

where $\theta = \nabla^i v_i$ is the velocity potential and $w = \mathcal{P}/\rho$ is the parameter for the equation of state. For the photon $w = 1/3$ and dark matter $w = 0$, we obtain

$$\delta_r' + \frac{4}{3}\theta_r + 4\Psi' = 0, \tag{2.16}$$

$$\theta_r' + \frac{1}{4}\nabla^2\delta_r + \nabla^2\Phi = 0, \tag{2.17}$$

$$\delta_m' + \theta_m + 3\Psi' = 0, \tag{2.18}$$

$$\theta_m' + \mathcal{H}\theta + \nabla^2\Phi = 0. \tag{2.19}$$

Since photons have interaction with baryons via Thomson scattering with electrons and protons before the recombination, the energy momentum tensor of photons did not actually conserve. In this thesis, however, we treat photons and baryons as a single fluid component in a radiation-dominated era and δ_r and θ_r are interpreted as the fluctuations of the photon-baryon fluid.

2.1.2 Time evolution of density perturbations

In this subsection, we derive the solutions of the gravitational potential Φ and the fluctuations of dark matter δ and θ in radiation–dominated, matter-dominated, and

matter-and-Λ-dominated eras. In the following, we move to Fourier space. We define the Fourier transformation as

$$\Phi(\mathbf{x}) = \int \frac{d^3\mathbf{k}}{(2\pi)^3}\, \tilde{\Phi}(\mathbf{k}) e^{i\mathbf{k}\cdot\mathbf{x}}, \tag{2.20}$$

$$\tilde{\Phi}(\mathbf{k}) = \int d^3\mathbf{x}\, \Phi(\mathbf{x}) e^{-i\mathbf{k}\cdot\mathbf{x}}, \tag{2.21}$$

and similar to other quantities. Hereafter we omit the tilde on the quantities in Fourier space for notational simplicity. Ignoring the effect of neutrinos, the anisotropic stress Π can be neglected, so in the following we have $\Psi = -\Phi$ from Eq. (2.9). Then, the Einstein equations reduce to

$$\Phi'' + 3(1+w)\mathcal{H}\Phi + wk^2\Phi + \Lambda a^2(1+w)\Phi = 0, \tag{2.22}$$

$$3\mathcal{H}^2\Phi + 3\mathcal{H}\Phi' + k^2\Phi = -\frac{3}{2}\mathcal{H}^2(\delta_r + \delta_m). \tag{2.23}$$

In the radiation-dominated era where $w = 1/3$ and $\Lambda = 0$, the Friedmann equation (2.3) gives

$$a \propto \tau, \qquad \mathcal{H} = \frac{1}{\tau}, \tag{2.24}$$

so we have

$$\Phi'' + \frac{4}{\tau}\Phi' + \frac{k^2}{3}\Phi = 0. \tag{2.25}$$

The solution for this equation is given by

$$\Phi(\tau, k) = A_k j_1(x) + B_k n_1(x), \tag{2.26}$$

with $x \equiv k\tau/\sqrt{3}$, $j_n(x)$ being the n-th order spherical Bessel function, and $n_n(x)$ being the n-th order spherical Neumann function. Neglecting the decaying solution, we find

$$\Phi = \frac{9\Phi_\mathrm{p}}{k^2\tau^2}\left[\frac{\sqrt{3}}{k\tau}\sin\frac{k\tau}{\sqrt{3}} - \cos\frac{k\tau}{\sqrt{3}}\right], \tag{2.27}$$

where Φ_p denotes the primordial value of the potential, which means $\Phi \to \Phi_\mathrm{p}$ in the superhorizon limit $k\tau \to 0$. In the subhohizon limit $k\tau \gg 1$, we have $\Phi \to -9\Phi_\mathrm{p}\cos(k\tau/\sqrt{3})/(k\tau)^2$, which means the gravitational potential follows the damped oscillation. Given this solution, we can find a solution for δ_r via Eq. (2.23)

$$\delta_r = -\frac{2}{3}(k\tau)^2\Phi - 2\tau\Phi' - 2\Phi. \tag{2.28}$$

Thus, while $\delta_r \to -2\Phi_{\rm p}$ outside the horizon, in the subhorizon we have $\delta_r \to 6\Phi_{\rm p}\cos(k\tau/\sqrt{3})$. This oscillatory feature inside the horizon reflects the pressure of the photon and leads to the so-called Baryon-Acoustic Oscillations (BAO). In order to determine how to evolve the dark matter perturbation in the radiation-dominated era, we use Eqs. (2.18) and (2.19). In the subhorizon limit, these equations reduce to

$$\delta_m'' + \mathcal{H}\delta_m' + k^2\Phi = 0. \tag{2.29}$$

As seen above, the gravitational potential Φ in the radiation-dominated era oscillates rapidly inside the horizon so the *time-averaged* gravitational potential does not contribute to the evolution of the density perturbations of the dark matter [52]. Therefore what we have to solve is $\delta_m'' + \delta_m'/\tau = 0$ and the solution is found to be $\delta_m \propto \ln\tau \propto \ln a$.

Next we consider the matter-dominated era. In the matter-dominated era, the Friedmann equation (2.3) gives

$$a \propto \tau^2, \qquad \mathcal{H} = \frac{2}{\tau}, \tag{2.30}$$

so the evolution of the gravitational potential is governed by

$$\Phi'' + \frac{6}{\tau}\Phi' = 0. \tag{2.31}$$

Neglecting the decaying mode $\propto \tau^{-5}$, the solution for Φ is

$$\Phi = \Phi_m \propto \tau^0, \tag{2.32}$$

where Φ_m is a constant. Thus the gravitational potential remains constant in the matter-dominated era for all scales. With this solution, δ_m is determined by Eq. (2.23),

$$\delta_m = -\frac{1}{6}(k\tau)^2\Phi - 2\Phi. \tag{2.33}$$

Thus δ_m does not evolve outside the horizon while $\delta_m \to -(k\tau)^2\Phi/6 \propto a$ inside the horizon.

Finally, let us focus on the matter-and-Λ-dominated universe. In this epoch, the gravitational potential obeys

$$\Phi'' + 3\mathcal{H}\Phi' + \Lambda a^2\Phi = 0. \tag{2.34}$$

By making use of the decaying mode solution $\Phi \propto \mathcal{H}^3/a$, we can construct the growing mode solution as follows,

$$\Phi = C\frac{\mathcal{H}^3}{a}\int_0^a \frac{da}{\mathcal{H}^3}, \tag{2.35}$$

with C being a constant. Normalizing $\Phi \to \Phi_m$ as $a \to 0$, we get $C = 5\Phi_m\Omega_m(a)a\mathcal{H}^2/2$, which leads to

$$\Phi = \Phi_m \times \frac{5}{2}\Omega_m(a)\mathcal{H}^5 \int_0^a \frac{da}{\mathcal{H}^3}. \tag{2.36}$$

Since in the subhorizon limit the Poisson equation Eq. (2.23) becomes $k^2\Phi = -3\mathcal{H}^2\delta_m/2$, we have

$$\delta_m = -\frac{2}{3}\frac{k^2}{\mathcal{H}^2}\Phi = -\frac{5}{3}\Phi_m k^2\Omega_m(a)\mathcal{H}^3 \int_0^a \frac{da}{\mathcal{H}^3}. \tag{2.37}$$

We identify the time dependent part of this solution as the linear growth factor $D(a)$ with normalizing $D(a) \to a$ as $a \to 0$:

$$D(a) \equiv \frac{5}{2}\Omega_m(a)\mathcal{H}^3 \int_0^a \frac{da}{\mathcal{H}^3} = \frac{5}{2}\Omega_{m,0}H_0\frac{\mathcal{H}}{a}\int_0^a \frac{da}{\mathcal{H}^3}, \tag{2.38}$$

where we have used $\Omega_m(a) = \Omega_{m,0}H_0^2/(a\mathcal{H}^2)$. Using the linear growth factor, $\delta_m = -2k^2\Phi_m D(a)/3$. Given this expression, the velocity potential θ_m inside the hosizon reads via Eq. (2.19)

$$\theta_m = -\delta_m' = \frac{2}{3}k^2\Phi_m\mathcal{H}f(a)D(a) = -\delta_m\mathcal{H}f(a)D(a), \tag{2.39}$$

where we have introduced the linear growth rate $f(a)$ defined as

$$f(a) \equiv \frac{d\ln D}{d\ln a}, \tag{2.40}$$

which takes unity in the matter domination.

2.1.3 Initial conditions

According to the discussion in the previous subsection, the gravitational potential is frozen on the superhorizon scales. So the initial condition is naturally given when the wavelength of perturbations is longer than the horizon scale. It is useful to introduce the comoving curvature perturbation $\mathcal{R}$, which is related to the gravitational potential as

$$\mathcal{R} = -\Phi - \frac{2}{3+3w}\left(\frac{\Phi'}{\mathcal{H}} + \Phi\right) \overset{k\ll\mathcal{H}}{\to} \frac{5+3w}{3+3w}\Phi, \tag{2.41}$$

since the comoving curvature perturbation is gauge-invariant and conserved on the superhorizon [53].

The initial condition for the structure formation is given only statistically, rather than the specific value at a specific position. The standard (single-field slow-roll)

inflation predicts that the initial fluctuation follows the Gaussian distribution and its spectrum is scale-invariant, i.e., the initial condition is characterized by the power spectrum of the comoving curvature perturbation,

$$\Delta^2_{\mathcal{R}}(k) = \frac{k^3 P_{\mathcal{R}}(k)}{2\pi^2} = A_s \left(\frac{k}{k_*}\right)^{n_s - 1}, \tag{2.42}$$

where $\langle \mathcal{R}(\mathbf{k})\mathcal{R}(\mathbf{k}')\rangle = (2\pi)^3 \delta^3_{\rm D}(\mathbf{k}+\mathbf{k}')P_{\mathcal{R}}(k)$, A_s is the amplitude of the primordial curvature perturbation, n_s is the spectral index, and k_* is the pivot scale. The observational constrains from the Planck satelite are consistent with $A_s = 2.105 \times 10^{-9}$ and $n_s = 0.9665$ for $k_* = 0.05$ Mpc^{-1} [13].

2.1.4 Linear matter power spectrum

Here we summarize the results derived in the previous subsection. We show the linear matter power spectrum at late time. The linear matter power spectrum fully characterizes statistical properties of density perturbations in the linear regime for the Gaussian initial conditions. The linear matter power spectrum is defined through

$$\langle \delta_m(\mathbf{k}; a)\delta_m(\mathbf{k}'; a)\rangle = (2\pi)^3 \delta^3_{\rm D}(\mathbf{k}+\mathbf{k}')P_{\rm lin}(k; a). \tag{2.43}$$

In the linear perturbation theory, each Fourier mode evolves independently, so we can simply relate the density perturbation at late time to the primordial one as

$$\delta_m(\mathbf{k}; a) = \mathcal{M}(k, a)\mathcal{R}(\mathbf{k}), \tag{2.44}$$

where $\mathcal{M}(k, a)$ is called the transfer function. Notice that the transfer function depends on only amplitudes of wavenumber because of the isotropy of the FRLW background. Using the transfer function, the linear matter power spectrum can be written as

$$P_{\rm lin}(k; a) = \mathcal{M}^2(k, a)P_{\mathcal{R}}(k). \tag{2.45}$$

Thus the shape of the linear matter power spectrum is determined by the spectrum of the initial condition and the the transfer function.

The perturbation whose wavenumber k is smaller than $k_{\rm eq} \equiv \mathcal{H}(\tau_{\rm eq})$ with $\tau_{\rm eq}$ being the epoch of the matter-radiation equality enters the horizon when the universe is matter dominated. Since in the matter-dominated era the gravitational potential Φ does not change, its power spectrum remains scale-invariant $P_\Phi(k) \propto P_{\mathcal{R}}(k) \propto k^{n_s-4}$. Thus for $k < k_{\rm eq}$, via the Poisson equation, we have

$$P_{\rm lin}(k) \propto k^4 \times k^{n_s-4} = k^{n_s}. \tag{2.46}$$

On the other hand, the Fourier modes with $k > k_{\rm eq}$ enters the horizon during the radiation-dominated era. In that stage, neglecting the oscillation term, Φ follows $\propto 1/(k\tau)^2$, which leads to

$$P_{\rm lin}(k) \propto k^4 \times k^{n_s-4} \times k^{-4} = k^{n_s-4}. \tag{2.47}$$

Fig. 2.1 shows the linear matter power spectrum computed from the Boltzmann code `CLASS` [54]. As clearly seen, the asymptotic scaling of the linear matter power spectrum changes around $k_{\rm eq}$. The wiggly feature around $k \sim 0.1\ h/{\rm Mpc}$ is an imprint of the BAOs.

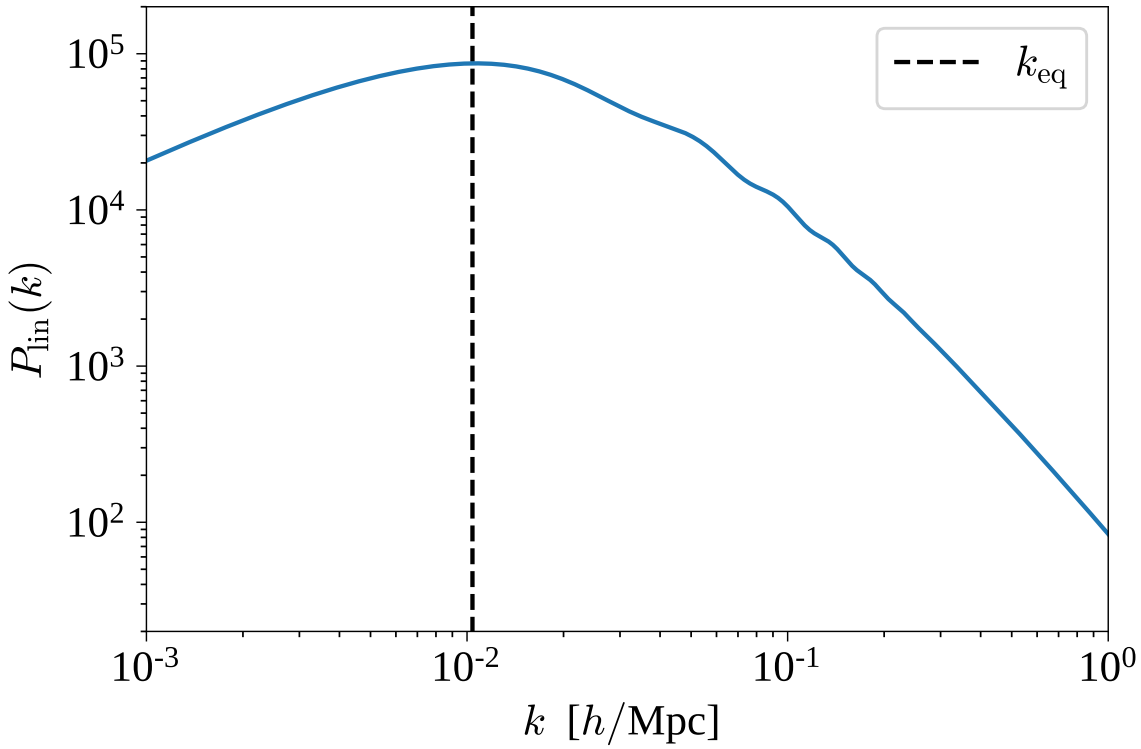

Figure 2.1: The linear matter power spectrum at $z = 0$, computed by the `CLASS` [54]. The black-dashed line corresponds to $k_{\rm eq} = 0.0104\ h/{\rm Mpc}$, around which the matter power spectrum turns over. Here we employ cosmological parameters that are consistent with the Planck 2018 results [13].

2.2 Nonlinear perturbation theory

Unlike the CMB fluctuations, the nonlinear effect is of great importance in the matter distribution at late times, so we have to take into account the nonlinear evolution of density perturbations to compare theoretical prediction with observations. Fortunately, however, since the large-scale structure forms hierarchically from small to large scales, density perturbation we are interested in lies in nonlinear but subhorizon scales, so we can use Newtonian description to follow the nonlinear evolution. Here we summarize the method to handle nonlinearities due to gravity in an analytical way.

2.2.1 Standard perturbation theory

In this subsection, we review the standard perturbation theory for the structure formation beyond the linear approximation [21]. We start from the collisionless Boltzmann equation (or Vlasov equation) in non-relativistic limit,

$$\frac{df}{d\tau} = \frac{\partial f}{\partial \tau} + \frac{\partial f}{\partial \mathbf{x}} \cdot \frac{d\mathbf{x}}{d\tau} + \frac{\partial f}{\partial \mathbf{p}} \cdot \frac{d\mathbf{p}}{d\tau} = 0, \tag{2.48}$$

where $\mathbf{x}$ is comoving coordinate and

$$\mathbf{p} \equiv am\frac{d\mathbf{x}}{d\tau}, \tag{2.49}$$

$$\frac{d\mathbf{p}}{d\tau} = -am\frac{\partial \Phi}{\partial \mathbf{x}}, \tag{2.50}$$

with Φ being the gravitational potential. By "non-relativistic limit" we mean ignoring the higher order terms in the metric perturbations (see e.g. [55]). We thus have

$$\frac{\partial f}{\partial \tau} + \frac{\mathbf{p}}{am} \cdot \frac{\partial f}{\partial \mathbf{x}} - am\nabla\Phi \cdot \frac{\partial f}{\partial \mathbf{p}} = 0. \tag{2.51}$$

This is a six dimensional differential equation in phase space. Therefore it is very challenging to solve this equation directly. One way to proceed is to take moments of the Vlasov equation. The moments of the distribution function $f(\tau, \mathbf{x}, \mathbf{p})$ is defined as

$$\rho(\tau, \mathbf{x}) \equiv \frac{m}{a^3} \int \frac{d^3\mathbf{p}}{(2\pi)^3} f(\tau, \mathbf{x}, \mathbf{p}), \tag{2.52}$$

$$v^i(\tau, \mathbf{x}) \equiv \int \frac{d^3\mathbf{p}}{(2\pi)^3} \frac{p^i}{am} f(\tau, \mathbf{x}, \mathbf{p}) \Big/ \int \frac{d^3\mathbf{p}}{(2\pi)^3} f(\tau, \mathbf{x}, \mathbf{p}), \tag{2.53}$$

$$\sigma^{ij}(\tau, \mathbf{x}) \equiv \int \frac{d^3\mathbf{p}}{(2\pi)^3} \frac{p^i p^j}{a^2 m^2} f(\tau, \mathbf{x}, \mathbf{p}) \Big/ \int \frac{d^3\mathbf{p}}{(2\pi)^3} f(\tau, \mathbf{x}, \mathbf{p}) - v^i(\tau, \mathbf{x}) v^j(\tau, \mathbf{x}) \tag{2.54}$$

Then, taking the moments of Eq. (2.51) gives nonlinear fluid equations,

$$\frac{\partial \delta}{\partial \tau} + \frac{\partial}{\partial x^i}\left[(1+\delta)v^i\right] = 0, \tag{2.55}$$

$$\frac{\partial v^i}{\partial \tau} + \mathcal{H}v^i + v^j\frac{\partial v^i}{\partial x^j} = -\frac{\partial \Phi}{\partial x^i} - \frac{1}{\rho}\frac{\partial \sigma^{ij}}{\partial x^j}. \tag{2.56}$$

The gravitational potential Φ is determined by the Poisson equation,

$$\nabla^2\Phi = \frac{3}{2}\mathcal{H}^2\Omega_m\delta. \tag{2.57}$$

As *cold* dark matter has a negligible velocity dispersion, we work with the single stream approximation, which means the velocity shear σ^{ij} and other higher order multipoles are simply neglected to truncate the Boltzmann hierarchy. Therefore our perturbative description is no longer valid inside halos where multi stream motion becomes important. Furthermore, we consider the matter-dominated era ($\Omega_m = 1$), the main stage of the structure formation.

First, under these setups, we show that the vorticity is not generated even at the nonlinear level unless there initially exists vorticity. The vorticity is the curl component of the velocity, which is defined as

$$\omega^i \equiv \epsilon^{ijk}\partial^j v^k, \tag{2.58}$$

with ϵ^{ijk} being the Levi-Chivita tensor. Taking the curl of the Euler equation Eq. (2.56), we obtain

$$\frac{\partial \omega^i}{\partial \tau} + \mathcal{H}\omega^i = \frac{\partial}{\partial x^j}\left(v^i\omega^j - v^j\omega^i\right). \tag{2.59}$$

Thus the voticity remains zero when it is initially zero. Note however that the vorticity is generated in highly nonlinear regime where the single stream approximation is no longer valid.

We derive the second order solution in real space for clarity. Vanishing the vorticity, the velocity potential $\theta \equiv \partial_i v^i$ contains full information on the velocity field,

$$v^i = \frac{\partial^i}{\nabla^2}\theta, \tag{2.60}$$

so we focus on the second order solution for δ and θ. Rewriting the time variable from the conformal time τ to the scale factor a, the nonlinear equations for δ and θ become

$$\mathcal{H}\left[a^2\frac{\partial^2\delta}{\partial a^2} + \frac{3}{2}a\frac{\partial\delta}{\partial a} - \frac{3}{2}\delta\right] = \mathcal{H}(a\frac{\partial}{\partial a} + 1)\alpha - \beta, \tag{2.61}$$

$$\theta = -a\mathcal{H}\frac{\partial\delta}{\partial a} + \alpha, \tag{2.62}$$

where we introduced the nonlinear interaction terms

$$\alpha \equiv -\partial_i(\delta v^i) = -\partial_i\left(\delta\frac{\partial^i}{\nabla^2}\theta\right), \tag{2.63}$$

$$\beta \equiv -\partial_i(v^j\partial_j v^i) = -\partial_i\left(\frac{\partial^j}{\nabla^2}\theta\frac{\partial_j\partial^i}{\nabla^2}\theta\right). \tag{2.64}$$

Because there are only quadratic nonlinear terms, in general the n-th order solutions $\delta^{(n)}$ and $\theta^{(n)}$ can be found by following steps; (1) Substitute the lower order solutions $\delta^{(m)}$ and $\theta^{(m)}$ $(m < n)$ into the right-hand side of Eq. (2.61), (2) Constitute $\delta^{(n)}$ by using the Green's function for Eq. (2.61) and (3) Compute $\theta^{(n)}$ from Eq. (2.62).

To proceed, we need to calculate the retarded Green's function for Eq. (2.61). This Green's function $G(a, a')$ solves Eq. (2.61) with replacing the right-hand side with the Dirac delta function,

$$\mathcal{H}\left[a^2\frac{\partial^2 G(a,a')}{\partial a^2} + \frac{3}{2}a\frac{\partial G(a,a')}{\partial a} - \frac{3}{2}G(a,a')\right] = \delta_{\rm D}(a-a'), \tag{2.65}$$

with the boundary condition $G(a < a', a') = 0$. The solution to this equation is found to be

$$G(a,a') = \begin{cases} 0 & (a < a') \\ \frac{2}{5H_0}\left[\frac{a}{a'} - \left(\frac{a'}{a}\right)^{3/2}\right] & (a > a'), \end{cases} \tag{2.66}$$

where we have used $\mathcal{H} = H_0/\sqrt{a}$ in matter dominated era.

Now we can get the second order solutions by following general procedure mentioned above. Recalling that in a matter-dominated era we have $\delta^{(1)} \propto D(a) = a$ and $\theta^{(1)} = -\mathcal{H}f\delta^{(1)} \propto -H_0\sqrt{a}$ at linear order, the second-order source term for Eq. (2.61) is given by

$$S_2(a) = H_0 a\left[\frac{5}{2}\partial_i\left(\delta^{(1)}\frac{\partial_i}{\nabla^2}\delta^{(1)}\right) + \partial_i\left(\frac{\partial_i}{\nabla^2}\delta^{(1)}\frac{\partial_i\partial_j}{\nabla^2}\delta^{(1)}\right)\right]. \tag{2.67}$$

Then, the second order solution for δ can be computed by

$$\begin{aligned}\delta^{(2)}(a) =& \int_0^a da' G(a,a')S_2(a') = \frac{2}{7}a^2\left[\frac{5}{2}\partial_i\left(\delta^{(1)}\frac{\partial_i}{\nabla^2}\delta^{(1)}\right) + \partial_i\left(\frac{\partial_i}{\nabla^2}\delta^{(1)}\frac{\partial_i\partial_j}{\nabla^2}\delta^{(1)}\right)\right] \\ =& a^2\left[\frac{5}{7}\left(\delta^{(1)}\right)^2 + \left(\frac{\partial_i}{\nabla}\delta^{(1)}\right)\partial_i\delta^{(1)} + \frac{2}{7}\left(\frac{\partial_i\partial_j}{\nabla^2}\delta^{(1)}\right)^2\right].\end{aligned} \tag{2.68}$$

The second order solution for θ is

$$\begin{aligned}\theta^{(2)}(a) =& -\mathcal{H}a\frac{\partial\delta^{(2)}}{\partial a} - \partial_i\left(\delta^{(1)}\frac{\partial_i}{\nabla^2}\theta^{(1)}\right) \\ =& -\mathcal{H}fa^2\left[\frac{3}{7}\left(\delta^{(1)}\right)^2 + \left(\frac{\partial_i}{\nabla}\delta^{(1)}\right)\partial_i\delta^{(1)} + \frac{4}{7}\left(\frac{\partial_i\partial_j}{\nabla^2}\delta^{(1)}\right)^2\right].\end{aligned} \tag{2.69}$$

To interpret each term arisen in $\delta^{(2)}$ physically, we define the displacement field $\Psi_i(\mathbf{x})$ and the gravitational tidal field $s_{ij}(\mathbf{x})$ as

$$\Psi_i(\mathbf{x}) \equiv -\frac{\partial_i}{\nabla^2}\delta^{(1)}(\mathbf{x}) = \int \frac{d^3\mathbf{q}}{(2\pi)^3}\frac{iq_i}{q^2}\delta^{(1)}(\mathbf{q})e^{i\mathbf{q}\cdot\mathbf{x}}, \tag{2.70}$$

$$s_{ij}(\mathbf{x}) \equiv \left(\frac{\partial_i\partial_j}{\nabla^2} - \frac{1}{3}\delta_{ij}\right)\delta^{(1)}(\mathbf{x}) = \int \frac{d^3\mathbf{q}}{(2\pi)^3}\left(\frac{q_iq_j}{q^2} - \frac{1}{3}\delta_{ij}\right)\delta^{(1)}(\mathbf{q})e^{i\mathbf{q}\cdot\mathbf{x}}. \tag{2.71}$$

We call $\Psi_i(\mathbf{x})$ as the displacement field because $\Psi_i(\mathbf{x})$ corresponds to the gradient of the gravitatioanl potential $\partial_i\Phi(\mathbf{x})$ or equivalently velocity field $v_i(\mathbf{x})$. The reason why we call $s_{ij}(\mathbf{x})$ as the tidal field is that $s_{ij}(\mathbf{x})$ is equivalent to $(\partial_i\partial_j - \delta_{ij}\nabla^2/3)\Phi(\mathbf{x})$. In terms of $\Psi_i(\mathbf{x})$ and $s_{ij}(\mathbf{x})$, we can rewrite $\delta(\mathbf{x})$ with the second-order correction as

$$\delta^{(1)}(\mathbf{x}) + \delta^{(2)}(\mathbf{x}) = \delta^{(1)}(\mathbf{x}) - \Psi_i(\mathbf{x})\partial^i\delta^{(1)}(\mathbf{x}) + \frac{17}{21}\left(\delta^{(1)}(\mathbf{x})\right)^2 + \frac{2}{7}s_{ij}(\mathbf{x})s_{ij}(\mathbf{x}) \tag{2.72}$$

$$\simeq \delta^{(1)}(\mathbf{x} - \mathbf{\Psi}) + \frac{17}{21}\left(\delta^{(1)}(\mathbf{x})\right)^2 + \frac{2}{7}s_{ij}(\mathbf{x})s_{ij}(\mathbf{x}), \tag{2.73}$$

where we suppressed the time argument a for notational simplicity. From this expression, one can see the first term in the second-order correction describes the displacement of the density field caused by the gravitatioanl potential sourced by other perturbations, so this term is called as the shift term. The second term corresponds to the nonlinear growth by the density fields and the third term represents the nonlinear growth by interaction with the tidal fields.

In practice, we want to get the Fourier space expression for the nonlinear correction. Fourier transforms of Eqs. (2.68) and (2.69) are given by

$$\delta^{(2)}(\mathbf{k}) = a^2\int\frac{d^3\mathbf{q_1}}{(2\pi)^3}\int\frac{d^3\mathbf{q_2}}{(2\pi)^3}\left[\frac{5}{7} + \frac{(\mathbf{q_1}\cdot\mathbf{q_2})}{q_1^2} + \frac{2}{7}\frac{(\mathbf{q_1}\cdot\mathbf{q_2})^2}{q_1^2q_2^2}\right] \times \delta^{(1)}(\mathbf{q_1})\delta^{(1)}(\mathbf{q_2})(2\pi)^3\delta_{\rm D}^3(\mathbf{q_1}+\mathbf{q_2}), \tag{2.74}$$

$$\theta^{(2)}(\mathbf{k}) = -\mathcal{H}fa^2\int\frac{d^3\mathbf{q_1}}{(2\pi)^3}\int\frac{d^3\mathbf{q_2}}{(2\pi)^3}\left[\frac{3}{7} + \frac{(\mathbf{q_1}\cdot\mathbf{q_2})}{q_1^2} + \frac{4}{7}\frac{(\mathbf{q_1}\cdot\mathbf{q_2})^2}{q_1^2q_2^2}\right] \times \delta^{(1)}(\mathbf{q_1})\delta^{(1)}(\mathbf{q_2})(2\pi)^3\delta_{\rm D}^3(\mathbf{q_1}+\mathbf{q_2}). \tag{2.75}$$

These expression are not so convenient since these kernels are not symmetric in momentum variables, $\mathbf{q}_1$ and $\mathbf{q}_2$. So it is common to use the symmetrized kernels,

$$F_2(\mathbf{q}_1,\mathbf{q}_2) = \frac{5}{7} + \frac{1}{2}\left(\frac{1}{q_1^2}+\frac{1}{q_2^2}\right)(\mathbf{q_1}\cdot\mathbf{q_2}) + \frac{2}{7}\frac{(\mathbf{q_1}\cdot\mathbf{q_2})^2}{q_1^2q_2^2}, \tag{2.76}$$

$$G_2(\mathbf{q}_1,\mathbf{q}_2) = \frac{3}{7} + \frac{1}{2}\left(\frac{1}{q_1^2}+\frac{1}{q_2^2}\right)(\mathbf{q_1}\cdot\mathbf{q_2}) + \frac{4}{7}\frac{(\mathbf{q_1}\cdot\mathbf{q_2})^2}{q_1^2q_2^2}. \tag{2.77}$$

The higher order kernels can be obtained by iterating the steps described here. Actually, there are recursion relation for F_n and G_n,

$$nF_n(\mathbf{q}_1,\cdots,\mathbf{q}_n) - G_n(\mathbf{q}_1,\cdots,\mathbf{q}_n) = \sum_{i=1}^{n-1}\alpha(\mathbf{q}_{1\cdots i},\ \mathbf{q}_{i+1\cdots n})G_i(\mathbf{q}_1,\cdots,\mathbf{q}_i)F_{n-i}(\mathbf{q}_{i+1},\cdots,\mathbf{q}_n), \tag{2.78}$$

$$\frac{3}{2}F_n(\mathbf{q}_1,\cdots,\mathbf{q}_n) - \left(\frac{1}{2}+n\right)G_n(\mathbf{q}_1,\cdots,\mathbf{q}_n) = -\sum_{i=1}^{n-1}\beta(\mathbf{q}_{1\cdots i},\ \mathbf{q}_{i+1\cdots n})G_i(\mathbf{q}_1,\cdots,\mathbf{q}_i)G_{n-i}(\mathbf{q}_{i+1},\cdots,\mathbf{q}_n), \tag{2.79}$$

where $\mathbf{q}_{1\cdots i}\equiv\mathbf{q}_1+\cdots+\mathbf{q}_i$ and α and β are the wavevectoer dependent parts of the Fourier transform of Eq. (2.63) and Eq. (2.64),

$$\alpha(\mathbf{q_1},\mathbf{q_2}) = \frac{\mathbf{q_1}\cdot(\mathbf{q}_1+\mathbf{q}_2)}{q_1^2}, \tag{2.80}$$

$$\beta(\mathbf{q_1},\mathbf{q_2}) = \frac{1}{2}(\mathbf{q}_1+\mathbf{q}_2)^2\,\frac{\mathbf{q}_1\cdot\mathbf{q}_2}{q_1^2q_2^2}. \tag{2.81}$$

From these relations, for instance, we find the symmetrized third order kernels are expressed as

$$\begin{aligned}F_3(\mathbf{q}_1,\mathbf{q}_2,\mathbf{q}_3) =& \frac{2q_{123}^2}{54}\left[\frac{\mathbf{q}_1\cdot\mathbf{q}_{23}}{q_1^2q_{23}^2}G_2(\mathbf{q}_2,\mathbf{q}_3)+2\text{ permutations}\right]\\ &+\frac{7}{54}\mathbf{q}_{123}\cdot\left[\frac{\mathbf{q}_{12}}{q_{12}^2}G_2(\mathbf{q}_1,\mathbf{q}_2)+2\text{ perms.}\right]\\ &+\frac{7}{54}\mathbf{q}_{123}\cdot\left[\frac{\mathbf{q}_1}{q_1^2}F_2(\mathbf{q}_2,\mathbf{q}_3)+2\text{ perms.}\right],\end{aligned} \tag{2.82}$$

$$\begin{aligned}G_3(\mathbf{q}_1,\mathbf{q}_2,\mathbf{q}_3) =& \frac{q_{123}}{9}\left[\frac{\mathbf{q}_1\cdot\mathbf{q}_{23}}{q_1^2q_{23}^2}G_2(\mathbf{q}_2,\mathbf{q}_3)+2\text{ permutations}\right]\\ &+\frac{1}{18}\mathbf{q}_{123}\cdot\left[\frac{\mathbf{q}_{12}}{q_{12}^2}G_2(\mathbf{q}_1,\mathbf{q}_2)+2\text{ perms.}\right]\\ &+\frac{1}{18}\mathbf{q}_{123}\cdot\left[\frac{\mathbf{q}_1}{q_1^2}F_2(\mathbf{q}_2,\mathbf{q}_3)+2\text{ perms.}\right].\end{aligned} \tag{2.83}$$

By making use of the n-th order kernels, the n-th order solutions in Fourier space can be written as

$$\delta^{(n)}(\mathbf{k}) = a^n\prod_{i=1}^{n}\left\{\int\frac{d^3\mathbf{q}_i}{(2\pi)^3}\delta^{(1)}(\mathbf{q}_i)\right\}F_n(\mathbf{q}_1,\ldots,\mathbf{q}_n)(2\pi)^3\delta_{\rm D}^3(\mathbf{k}-\mathbf{q}_{1\cdots n}), \tag{2.84}$$

$$\theta^{(n)}(\mathbf{k}) = a^n\prod_{i=1}^{n}\left\{\int\frac{d^3\mathbf{q}_i}{(2\pi)^3}\delta^{(1)}(\mathbf{q}_i)\right\}G_n(\mathbf{q}_1,\ldots,\mathbf{q}_n)(2\pi)^3\delta_{\rm D}^3(\mathbf{k}-\mathbf{q}_{1\cdots n}), \tag{2.85}$$

where we have used $\delta^{(n)} \propto a^n$ and $\theta^{(n)} \propto \mathcal{H} f a^n$, which can be straightforwardly shown by using the Green's function Eq. (2.66).

As an application of the nonlinear perturbation theory, let us compute the tree-level bispectrum and the nonlinear matter power spectrum with the one-loop correction. In the linear theory, the three point correlation function or bispectrum vanishes since the initial condition predicted by the single field inflation is given by the Gaussian random field. But nonlinear growth by gravity induces the non-Gaussianity and generates a non-vanishing bispectrum. The leading order three point function is given by

$$\begin{aligned}\langle\delta(\mathbf{k}_1)\delta(\mathbf{k}_2)\delta(\mathbf{k}_3)\rangle =&\langle\delta^{(2)}(\mathbf{k}_1)\delta^{(1)}(\mathbf{k}_1)\delta^{(1)}(\mathbf{k}_1)\rangle + 2 \text{ permutations}\\ =&(2\pi)^3\delta_{\rm D}^3(\mathbf{k}_1+\mathbf{k}_2+\mathbf{k}_3)\left[F_2(\mathbf{k}_2,\mathbf{k}_3)P_{\rm lin}(k_2,a)P_{\rm lin}(k_3,a) + \text{perms.}\right],\end{aligned} \tag{2.86}$$

where we have used Wick's theorem and $P_{\rm lin} \propto a^2$. The tree-level bispectrum $B_{211}(\mathbf{k}_1,\mathbf{k}_2,\mathbf{k}_3)$ corresponds to the inside of the bracket.

The nonlinear two point function up to the one-loop correction is

$$\begin{aligned}\langle\delta(\mathbf{k})\delta(\mathbf{k}')\rangle =&\langle\delta^{(1)}(\mathbf{k})\delta^{(1)}(\mathbf{k}')\rangle + \langle\delta^{(2)}(\mathbf{k})\delta^{(2)}(\mathbf{k}')\rangle + 2\langle\delta^{(1)}(\mathbf{k})\delta^{(3)}(\mathbf{k}')\rangle\\ =&(2\pi)^3\delta_{\rm D}^3(\mathbf{k}+\mathbf{k}')\left[P_{\rm lin}(k,a) + P_{22}(k,a) + 2P_{13}(k,a)\right],\end{aligned} \tag{2.87}$$

where $P_{\rm lin}(k,a) \propto a^2$ and $P_{22}(k,a) \propto P_{13}(k,a) \propto a^4$ and we call the inside of the bracket as $P_{1-\rm loop}(k)$. The explicit expressions of $P_{22}(k)$ and $P_{13}(k)$ are given by

$$P_{22}(k) = \int \frac{d^3\mathbf{q}}{(2\pi)^3} P_{\rm lin}(q)P_{\rm lin}(|\mathbf{k}-\mathbf{q}|)|F_2(\mathbf{q},\mathbf{k}-\mathbf{q})|^2, \tag{2.88}$$

$$P_{13}(k) = 3P_{\rm lin}(k)\int \frac{d^3\mathbf{q}}{(2\pi)^3} P_{\rm lin}(q)F_3(\mathbf{k},\mathbf{q},-\mathbf{q}). \tag{2.89}$$

Note that $F_2(\mathbf{k}_1,\mathbf{k}_2)$ kernel has a divergence in the squeezed limit, $k_1 \ll k_2$,

$$F_2(\mathbf{k}_1,\mathbf{k}_2) \simeq \frac{\mathbf{k}_1\cdot\mathbf{k}_2}{2k_1} \gg 1, \tag{2.90}$$

while the bispectrum and one-loop power spectrum have no such divergence. In the next subsection, we explicitly show the cancellation of the infrared divergence for one-loop matter power spectrum. In general, when one wavevector in the arguments of the kernels $\mathbf{q}_i \to 0$, F_n and G_n have an infrared divergence $\propto \mathbf{q}_i/q_i^2$, while the correlators have no infrared divergence. This is a consequence of the so-called consistency relations of the large-scale structure, which states that the equivalence principle enforces the cancellation of the effect from long modes for equal-time correlatiors [56–62]. This is because the long-wavelength gravitational potential Φ and

its derivative $\partial_i \Phi \sim q_i/q^2 \times \delta(\mathbf{q})$, which corresponds to the divergent terms in F_n and G_n kernels, can be eliminated by performing a local coordinate transformation to choose a free-falling observer frame.

So far, we consider the matter-dominated era where the time evolution is simply given by $\delta^{(n)} \propto a^n$ and $\theta^{(n)} \propto \mathcal{H} f a^n$. It is natural to ask whether perturbative solutions derived in this section can be useful for other cosmology, especially for ΛCDM cosmology. The difference between the Einstein-de Sitter universe ($\Omega_m = 1$) and other cosmology lies in only the time dependence; i.e., the form of equations Eqs. (2.55)-(2.57) remains the same except for the time dependence of coefficients. However, the time dependence for arbitrary cosmology can be almost captured by replacing $a^n \to D^n(a)$. This simple prescription gives a very good approximation [63].

2.2.2 Mode-coupling between long- and short- wavelength perturbations

As shown in the previous subsection, the nonlinear interaction induces mode-couplings among different Fourier modes. In contrast to the linear theory, taking into account nonlinear effects, a perturbation of a given Fourier mode $\mathbf{k}$ is affected by other Fourier mode $\mathbf{q} \neq \mathbf{k}$. In this subsection, using the one-loop matter power spectrum, we discuss impact of nonlinear mode-coupling effects on a featured perturbation with a wavevector $\mathbf{k}$ from (1) a shorter-wavelength perturbation, i.e., $k \ll q$ and (2) a longer-wavelength perturbation, i.e., $k \gg q$.

First let us focus on the effect from short-wavelength perturbation. In the low-k limit $k \ll q$, we have

$$P_{22}(k) \overset{k\ll q}{\to} \frac{9}{98} k^4 \int \frac{d^3\mathbf{q}}{(2\pi)^3} \frac{P_{\rm lin}^2(q)}{q^4} + \mathcal{O}\left(k^6/q^6\right), \tag{2.91}$$

$$P_{13}(k) \overset{k\ll q}{\to} -\frac{1}{3} k^2 P_{\rm lin}(k) \int \frac{d^3\mathbf{q}}{(2\pi)^3} \frac{P_{\rm lin}(q)}{q^2} \left(\frac{61}{210} - \frac{2}{35}\frac{k^2}{q^2}\right) + \mathcal{O}\left(k^6/q^6\right). \tag{2.92}$$

Thus in the standard cosmology, the leading order nonlinear correction induced by short modes is suppressed by $\mathcal{O}(k^2/q^2)$. Furthermore, if one considers long modes sourced by pure short modes, there appears an additional suppression. Suppose that there are initially only short-wavelength perturbations but no long-wavelength perturbations, then $P_{13}(k)$ vanishes in $k \to 0$ limit while $P_{22}(k)$ results in $\mathcal{O}(k^4/q^4)$ contribution [64]. Therefore long-wavelength perturbations induced by short-wavelength perturbations shows $\propto k^4$ scaling at leading order. This is a universal feature of self-gravitating system and a consequence of the momentum conservation in large scales as described below, following the discussion in Ref. [65].

Imagine that matter is almost uniformly distributed at the initial time with small short-wavelength fluctuations of scale $\sim 1/q$ but without long modes, i.e., $\delta_{\rm init}(\mathbf{k}) = 0$. Dividing space into cells of size $\sim R_n$, in which the matter collapses into a point particle with mass m_n at the cell center of mass, we can write a final density contrast as

$$\delta_{\rm fin}(\mathbf{k}) = \frac{1}{\bar{\rho}} \sum_n m_n e^{i\mathbf{k}\cdot\mathbf{x}_n}, \tag{2.93}$$

where $\bar{\rho}$ is the mean density. Denoting the initial density of n-th cell as $\rho_n(\mathbf{x})$, the mass in n-th cell is given by

$$m_n = \int_{R_n} d^3\mathbf{y}\ \rho_n(\mathbf{x}_n + \mathbf{y}), \tag{2.94}$$

where $-\mathbf{y}$ corresponds to the displacement from the initial position $\mathbf{x}$ to final position $\mathbf{x}_n$. No initial long mode means that there are initially no spatial correlations beyond R_n; in other words, we choose R_n so that the spatial correlations beyond R_n vanish initially. Therefore we can consider the Fourier transform of the initial density field as the sum of each cells. This leads to

$$\begin{aligned} 0 =& \frac{1}{\bar{\rho}} \int d^3\mathbf{x}\, \bar{\rho}\, e^{i\mathbf{k}\cdot\mathbf{x}} = \frac{1}{\bar{\rho}} \sum_n \int_{R_n} d^3\mathbf{y}\, \rho_n(\mathbf{x}_n + \mathbf{y})\, e^{i\mathbf{k}\cdot(\mathbf{x}_n+\mathbf{y})} \\ =& \frac{1}{\bar{\rho}} \sum_n e^{i\mathbf{k}\cdot\mathbf{x}_n} \left[m_n + ik^i d_n^i - k^i k^j Q_n^{ij} + \mathcal{O}(k^3/q^3) \right], \end{aligned} \tag{2.95}$$

where we have used $y \sim \mathcal{O}(1/q)$ and defined the moments of the matter distribution in the n-th cell as follows,

$$d_n^i = \int_{R_n} d^3\mathbf{y}\, y^i \rho(\mathbf{x}_n + \mathbf{y}), \tag{2.96}$$

$$Q_n^{ij} = \int_{R_n} d^3\mathbf{y}\, y^i y^j \rho(\mathbf{x}_n + \mathbf{y}). \tag{2.97}$$

Using Eq. (2.93), we obtain

$$\delta_{\rm fin}(\mathbf{k}) = -\frac{ik^i}{\bar{\rho}} \sum_n d_n^i e^{i\mathbf{k}\cdot\mathbf{x}_n} + \frac{k^i k^j}{\bar{\rho}} \sum_n Q_n^{ij} e^{i\mathbf{k}\cdot\mathbf{x}_n} + \mathcal{O}(k^3/q^3). \tag{2.98}$$

Since $\mathbf{y} = \mathbf{x} - \mathbf{x}_n$, the first term on the right-hand side can be rewritten as

$$\sum_n \mathbf{d}_n e^{i\mathbf{k}\cdot\mathbf{x}_n} = \sum_n m_n \left(\mathbf{x}_n^{\rm CM} - \mathbf{x}_n\right) e^{i\mathbf{k}\cdot\mathbf{x}_n}, \tag{2.99}$$

where $\mathbf{x}_n^{\rm CM}$ denotes the center of mass position of each cell. In the absence of the long-wavelength modes, which can generate the difference $(\mathbf{x}_n^{\rm CM} - \mathbf{x}_n)$ by the coherent

momentum transfer over longer separations than the cell size $R_n \sim 1/q$, $(\mathbf{x}_n^{\rm CM} - \mathbf{x}_n)$ should be zero. In other words, the momentum in each cell should be conserved if there is no the long-wavelength perturbation beyond cells. Therefore the remaining contribution starts the second term on the right-hand side in Eq. (2.98), and hence

$$P_{\rm fin}(k \to 0) \propto k^4. \tag{2.100}$$

Now we turn to consider the effect from long-wavelength perturbation on short-wavelength one. The high-k limit $k \gg q$ of Eqs. (2.88) and (2.89) with Eqs. (2.76) and (2.82) yields

$$\begin{aligned} P_{22}(k) \overset{k\gg q}{\to}& \frac{1}{3}k^2 P_{\rm lin}(k) \int \frac{d^3\mathbf{q}}{(2\pi)^3}\frac{P_{\rm lin}(q)}{q^2} \\ &+ \left[\frac{569}{735}P_{\rm lin}(k) - \frac{47}{105}k\frac{dP_{\rm lin}(k)}{dk} + \frac{1}{10}k^2\frac{d^2P_{\rm lin}(k)}{dk^2}\right]\int \frac{d^3\mathbf{q}}{(2\pi)^3}P_{\rm lin}(q) \\ &+ \mathcal{O}\left(\frac{q^2}{k^2}\right), \end{aligned} \tag{2.101}$$

$$\begin{aligned} P_{13}(k) \overset{k\gg q}{\to}& -\frac{1}{6}k^2 P_{\rm lin}(k) \int \frac{d^3\mathbf{q}}{(2\pi)^3}\frac{P_{\rm lin}(q)}{q^2} \\ &+ \frac{58}{415}P_{\rm lin}(k)\int \frac{d^3\mathbf{q}}{(2\pi)^3}P_{\rm lin}(q) + \mathcal{O}\left(\frac{q^2}{k^2}\right). \end{aligned} \tag{2.102}$$

We can see that the $\mathcal{O}(k^2/q^2)$ contribution in the first term in $P_{22}(k)$ exactly cancels out with the first term in $2P_{13}(k)$. Again, this is an example of the consistency relation of large-scale structure, which is a consequence of the equivalence principle. Thus, the leading order correction starts from $\mathcal{O}(k^0/q^0)$, so the nonlinear correction is not suppressed by the small parameter q/k. Comparing this with the result in the low-k limit, where the nonlinear correction is suppressed by k/q, this implies the effect of the long modes is more important than the short modes. While here we use the perturbation theory, the importance of the momentum transfer from the long modes to the short modes is confirmed by the N-body simulations [66].

Chapter 3

Observational effects

Contents

In this chapter, we describe several observational effects relevant to galaxy spectroscopic surveys such as the galaxy bias, redshift-space distortion, and Alcock-Paczyński effect. These effects make it difficult to interpret observed data. At the same time, however, these also provide probes of cosmological information. For instance, the primordial non-Gaussianity introduces the scale-dependent bias [67] at least on large scales, so we can extract the dynamics during the inflation by measuring this bias. As discussed below, the redshift-space distortion contains the information on the velocity field, or equivalently the growth rate. Anisotropies induced by Alcock-Paczyński effect can be used to calibrate the distance measurements.

3.1 Galaxy bias

In this section, we discuss the so-called galaxy bias issues, following a comprehensive review [22]. Basically, the bias is a statistical relation between the observed distribution of tracers (e.g. galaxies) and the underlying matter fluctuations. Because we cannot yet understand or simulate the formation of galaxies from the first principles, we need to introduce nuisance parameters that model the relation — the so-called galaxy bias parameters. Then we need to derive cosmological constraints from clustering observables after marginalizing over the galaxy bias parameters. Here we are limited to the case where the initial fluctuations obeys the Gaussian and our discussion focuses on the halo bias since on large scales the description of the halo biases can be applied to galaxies. Indeed, the derived relations is valid for actual galaxy surveys such as Ref [14]. Thus, in the following we identify halos as galaxies.

3.1.1 Simple model: the peak theory in Lagrangian space

First, let us consider the bias expansion in Lagrangian space in which we specifies the initial positions of dark matter particles and halos. We denote the Lagrangian position by $\mathbf{q}$. In the simple peak theory, we assume that dark matter halos are formed in overdense regions in Lagrangian space, that is, peaks above a threshold of dark matter fluctuations collapse to form halos, in which galaxies are formed. Because the dark matter density field in Lagrangian space $\delta(\mathbf{q})$ corresponds to the initial density field, $\delta^{(1)}(\mathbf{q})$ is to be close to uniform. Hence, the volume of a halo with mass M in Lagrangian space can be identified as $M/\bar{\rho}_m$ and we can define the *Lagrangian radius* R of halos through $R(M) \equiv (3M/4\pi\bar{\rho}_m)^{1/3}$. Then, in order to characterize the thresholed regions, it is natural to introduce the smoothed density field with R,

$$\delta_R^{(1)} \equiv \int d^3\mathbf{q}\; W_R(\mathbf{q})\delta^{(1)}(\mathbf{q}), \tag{3.1}$$

with $W_R(\mathbf{q})$ being the filter function that smooths out small-scale fluctuations less than R. Here we denote the Lagrangian density field with subscript $^{(1)}$ to stress that this field is the linear density field. Although the top-hat or the Gaussian function is commonly used for $W_R(\mathbf{q})$, the choice of the filter function is not important for the bias. Using this filtered density field δ_R, we define the comoving Lagrangian number density of halos as

$$n_g(\mathbf{q}) \equiv N\Theta_H(\delta^{(1)}(\mathbf{q}) - \delta_{\rm cr}), \tag{3.2}$$

where we introduce a density threshold $\delta_{\rm cr}$, Θ_H is the Heaviside step function and N is a normalization factor, which does not affect the calculation of the bias. This num-

ber density $n_g(\mathbf{q})$ corresponds to cumulative number density of halos with masses larger than M.

Since the initial condition is supposed to obey the Gaussian distribution, the statistics of the random field $\delta_R^{(1)}$ are completely specified by the two-point correlation function:

$$\xi_{R,\mathrm{lin}}(r) = \langle \delta_R^{(1)}(\mathbf{q}) \delta_R^{(1)}(\mathbf{q}+\mathbf{r}) \rangle. \tag{3.3}$$

The expectation values of Eq. (3.2) gives the mean number density of halos:

$$\bar{n}_g = \langle n_g(\mathbf{q}) \rangle = N \int d\delta \, \mathcal{N}[\delta] \Theta_{\mathrm{H}}(\delta - \delta_{\mathrm{cr}}) = \frac{N}{2} \mathrm{erfc}\left[\frac{\nu_c}{\sqrt{2}} \right], \tag{3.4}$$

where $\mathcal{N}[\delta]$ is the Gaussian distribution function and we define the normalized threshold $\nu_c \equiv \delta_{\mathrm{cr}}/\sigma_R$ with the variance $\sigma_R^2 \equiv \langle \delta_R^2 \rangle = \xi_{R,\mathrm{lin}}(0)$ of the smoothed density field. This shows that the high-peak (massive) limit $\nu_c \gg 1$ corresponds to rare objects. The two-point correlation function of halos in Lagrangian space is defined by [21, 65]

$$1 + \xi_g(r) \equiv \frac{\langle n_g(\mathbf{q}) n_g(\mathbf{q}+\mathbf{r}) \rangle}{\langle n_g \rangle^2} = \frac{N^2}{\bar{n}_g^2} \int d\delta_1 d\delta_2 \, \mathcal{N}[\delta_1, \delta_2] \Theta_H(\delta_1 - \delta_{\mathrm{cr}}) \Theta_H(\delta_2 - \delta_{\mathrm{cr}}), \tag{3.5}$$

where $\mathcal{N}[\delta_1, \delta_2]$ denotes the joint Gaussian distribution function with the covariance

$$\mathrm{Cov} = \begin{pmatrix} \sigma_R^2 & \xi_{R,\mathrm{lin}}(r) \\ \xi_{R,\mathrm{lin}}(r) & \sigma_R^2 \end{pmatrix}. \tag{3.6}$$

Using these expressions, we get

$$\xi_g(r) = \sqrt{\frac{2}{\pi}} \left[\mathrm{erfc}\left(\frac{\nu_c}{\sqrt{2}} \right) \right]^{-2} \int_{\nu_c}^{\infty} d\nu \, e^{-\nu^2/2} \exp\left[\frac{\nu_c \sigma_R^2 - \nu \xi_{R,\mathrm{lin}}(r)}{\sqrt{2(\sigma_R^4 - \xi_{R,\mathrm{lin}}^2(r))}} \right] - 1. \tag{3.7}$$

Notice that r-dependence of $\xi_g(r)$ is characterized only by $\xi_{R,\mathrm{lin}}(r)$. Then, if the smoothed two-point function $\xi_{R,\mathrm{lin}}(r)$ is small, we can expand Eq. (3.7) in terms of $\xi_{R,\mathrm{lin}}(r)$,

$$\xi_g(r) = \sum_{N=1}^{\infty} \frac{1}{N!} (b_N^{\mathrm{L}})^2 \left[\xi_{R,\mathrm{lin}}(r) \right]^N, \tag{3.8}$$

where b_N^{L} are called as the *Lagrangian bias parameters*, which are r-independent constants and the subscript $^{\mathrm{L}}$ means these bias parameters are defined with respect

to the *Lagrangian* density field. $b_N^{\rm L}$ can be calculated by comparing Eq. (3.7) to Eq. (3.8):

$$b_N^{\rm L} = \sqrt{\frac{2}{\pi}}\left[\mathrm{erfc}\left(\frac{\nu_c}{\sqrt{2}}\right)\right]^{-1}\frac{e^{-\nu_c/2}}{\sigma_R^N}H_{N-1}(\nu_c) \overset{\nu_c\gg 1}{=} \frac{\nu_c^N}{\sigma_R^N} + \mathcal{O}(\nu_c^{N-1}), \tag{3.9}$$

where $H_N(\nu_c)$ is the N-th order Hermite polynomial. In the high-park limit, we obtain the simple relation $b_N^{\rm L} = \nu_c^N/\sigma_R^N$, which implies that the rare (or equivalently massive) object has a high bias [68, 69]. Conversely, in the low-mass limit which corresponds $R \to 0$ we have $\sigma_R \to \infty$ leading to $b_N^{\rm L} \to 0$. This incorrect result implies the simple description for halos Eq. (3.2) is not valid for low-mass objects due to the miscounting the number of low-mass clumps, which is called as the "cloud-in-cloud" problem [70].

In reality, fluctuations of matter density field become small on large scales in the standard cosmology, so we can use the first few terms in Eq. (3.8) to describe the halo two-point correlation function or the power spectrum on large scales.

The same result can be obtained from more general ansatz [71]. In fact, suppose that $\delta_g(\mathbf{q}) \equiv n_g(\mathbf{q})/\bar{n}_g - 1$ is a functional of the smoothed matter density fluctuations $\delta_R(\mathbf{q})$, then we can formally expand in a series of $\delta_R^{(1)}(\mathbf{q})$,

$$\begin{aligned}\delta_g(\mathbf{q}) = \mathcal{F}[\delta_R^{(1)}(\mathbf{q})] &= \left(\frac{\partial\mathcal{F}}{\partial\delta_R}\right)_{\delta_R=0}\delta_R^{(1)}(\mathbf{q}) + \frac{1}{2}\left(\frac{\partial^2\mathcal{F}}{\partial\delta_R^2}\right)_{\delta_R=0}\left(\left[\delta_R^{(1)}(\mathbf{q})\right]^2 - \sigma_R^2\right) + \cdots \\ &= \sum_{N=1}^{\infty}\frac{1}{N!}b_N^{\rm L}\left(\left[\delta_R^{(1)}(\mathbf{q})\right]^N - \langle\left[\delta_R^{(1)}(\mathbf{q})\right]^N\rangle\right).\end{aligned} \tag{3.10}$$

Here we introduce σ_R^2 and $\langle\left[\delta_R^{(1)}(\mathbf{q})\right]^N\rangle$ terms to guarantee $\langle\delta_g(\mathbf{q})\rangle$ to be zero for all orders. Then, Eq. (3.8) holds for this ansatz. Furthermore, using this ansatz, we can easily predict not only two-point function but also N-point function of halos. This expansion is called as the *local Lagrangian bias* since the halo density field is determined only by the *local* overdensity field $\delta_R(\mathbf{q})$ and does not depends on the non-local quantities such as the tidal field $s_{ij}(\mathbf{q})$.

3.1.2 Bias expansion in Eulerian space

In the previous subsection, we consider the *Lagrangian bias*, i.e., the relation between density field of halos and matter fluctuations in *Lagrangian* space. In practice, however, we observe galaxies in *Eulerian* coordinates, not in Lagrangian coordinates where the Lagrangian coordinates are the initial positions of particles while the Eularian coordinates roughly correspond to the final positions of halos. Therefore we want to determine the bias expansion in Eulerian space, which requires the discussion of the gravitational evolution.

In order to find out the relation between the Lagrangian and Eulerian bias, let us start with the relation between the Eulerian and Lagrangian coordinates,

$$\mathbf{x} = \mathbf{q} + \mathbf{\Psi}(\mathbf{q}), \tag{3.11}$$

where $\mathbf{\Psi}(\mathbf{q})$ is the displacement field. The number conservation of dark matter and halos gives

$$[1+\delta(\mathbf{x})]\, d^3\mathbf{x} = d^3\mathbf{q}, \qquad \left[1+\delta_g^{\rm E}(\mathbf{x})\right] d^3\mathbf{x} = \left[1+\delta_g^{\rm L}(\mathbf{q})\right] d^3\mathbf{q}, \tag{3.12}$$

where the subscript $^{\rm E}$ and $^{\rm L}$ depict the "Eulerian" and "Lagrangian" respectively. These two equations lead to the following relation,

$$\delta_g^{\rm E}(\mathbf{x}) = \delta_g^{\rm L}(\mathbf{q}) + \delta_g^{\rm L}(\mathbf{q})\delta(\mathbf{x}) + \delta(\mathbf{x}). \tag{3.13}$$

With the local Lagrangian bias expansion Eq. (3.10), at the first order in the perturbation theory, we find

$$\delta_g^{\rm E,(1)}(\mathbf{x}) = \delta_g^{\rm L,(1)}(\mathbf{x}) + \delta^{(1)}(\mathbf{x}) = \left[b_1^{\rm L}+1\right]\delta^{(1)}(\mathbf{x}) = b_1^{\rm E}\delta^{(1)}(\mathbf{x}), \tag{3.14}$$

where we set $\mathbf{x} = \mathbf{q}$ from Eq. (3.11). Hence,

$$b_1^{\rm E} = 1 + b_1^{\rm L}. \tag{3.15}$$

At second order, Eqs. (3.11) and (3.13) yield

$$\delta_g^{\rm E,(2)}(\mathbf{x}) = \delta_g^{\rm L,(2)}(\mathbf{x}) - \mathbf{\Psi}^{(1)}\cdot\nabla\delta_g^{\rm L,(1)}(\mathbf{x}) + \delta_g^{\rm L,(1)}(\mathbf{x})\delta^{(1)}(\mathbf{x}) + \delta^{(2)}(\mathbf{x}), \tag{3.16}$$

where we have used $\delta_g^{\rm L,(2)}(\mathbf{q}) = \delta_g^{\rm L,(2)}(\mathbf{x}-\mathbf{q}) = \delta_g^{\rm L,(2)}(\mathbf{x}) - \mathbf{\Psi}^{(1)}\cdot\nabla\delta_g^{\rm L,(1)}(\mathbf{x})$. Recall that the second-order density is given by Eq. (2.72):

$$\delta^{(2)}(\mathbf{x}) = \frac{17}{21}\left(\delta^{(1)}(\mathbf{x})\right)^2 - \mathbf{\Psi}^{(1)}\cdot\nabla\delta^{(1)}(\mathbf{x}) + \frac{2}{7}s_{ij}(\mathbf{x})s_{ij}(\mathbf{x}). \tag{3.17}$$

Then, we obtain

$$\begin{aligned}
\delta_g^{\rm E,(2)}(\mathbf{x}) =& \frac{1}{2}b_2^{\rm L}\left(\delta^{(1)}\right)^2 - b_1^{\rm L}\mathbf{\Psi}^{(1)}\cdot\nabla\delta^{(1)} + b_1^{\rm L}\left(\delta^{(1)}\right)^2 + \delta^{(2)} \\
=& \left[\frac{1}{2}b_2^{\rm L} + \frac{4}{21}b_1^{\rm L}\right]\left(\delta^{(1)}\right)^2 + \left[b_1^{\rm L}+1\right]\delta^{(2)} - \frac{2}{7}b_1^{\rm L}\left(s_{ij}^{(1)}\right)^2 \\
=& \frac{1}{2}b_2^{\rm E}\left(\delta^{(1)}(\mathbf{x})\right)^2 + b_1^{\rm E}\delta^{(2)}(\mathbf{x}) + \frac{1}{2}b_{s^2}^{\rm E}\left(s_{ij}^{(1)}(\mathbf{x})\right)^2,
\end{aligned} \tag{3.18}$$

where we define the second-order Eulerian bias parameters

$$b_2^{\rm E} = b_2^{\rm L} + \frac{8}{21}b_1^{\rm L}, \qquad b_{s^2}^{\rm E} = -\frac{4}{7}b_1^{\rm L}, \tag{3.19}$$

where $b^{\rm E}_{s^2}$ is called the tidal bias. Up to the second order, we thus have

$$\delta^{\rm E}_g(\mathbf{x}) = b^{\rm E}_1\left(\delta^{(1)}(\mathbf{x}) + \delta^{(2)}(\mathbf{x})\right) + \frac{1}{2}b^{\rm E}_2\left(\delta^{(1)}(\mathbf{x})\right)^2 + \frac{1}{2}b^{\rm E}_{s^2}\left(s^{(1)}_{ij}(\mathbf{x})\right)^2. \tag{3.20}$$

Notice that even when assuming *local* Lagrangian bias Eq. (3.10), due to the non-linear gravitational evolution, there appears the *non-local* bias $b^{\rm E}_{s^2}$ which describes the dependence of halo overdensity field on the tidal field [72]. Indeed, there is evidence for the tidal bias from N-body simulations [73, 74]. As long as the *local* Lagrangian bias ansatz is valid, Eqs. (3.15) and (3.19) give rise to the consistency between higher Eulerian bias parameters, $b^{\rm E}_{s^2} = -\frac{4}{7}(b^{\rm E}_1 - 1)$, which can be used as the prior for higher-order bias.

Similarly to the discussion in the local Lagrangian bias, these results can be derived from the effective field theory approach [75, 76]. Assuming that the galaxy formation is solely determined by gravity, which is a reasonable ansatz in large scale limit, the galaxy density field can be considered as a functional of the large-scale gravitational potential. Here a relevant symmetry is the equivalent principle, which states the local physics does not depends on the gradient of the long-wavelength gravitational potential. Thus, the galaxy density field consists of the second (and higher) derivatives of the gravitational potential, which can be decomposed into its trace part $\delta^K_{ij}\partial^i\partial^j\Phi \propto \delta$ and its traceless part $(\partial^i\partial^j - \delta^K_{ij}/3)\Phi \propto s_{ij}$. At linear order, galaxy density field δ_g does not depend on the tidal field s_{ij} because δ_g is a scalar while s_{ij} is a tensor. At second order, however, δ_g can depend on the trace of the product of s_{ij}, i.e., $s_{ij}s_{ij}$. These consideration leads to

$$\begin{aligned}\delta_g(\mathbf{x}) =& \mathcal{F}[\partial_i\partial_j\Phi_L(\mathbf{x}), \dots] \\ =& \left(\frac{\partial\mathcal{F}}{\partial\delta}\right)_{\delta=0}\delta(\mathbf{x}) + \frac{1}{2}\left(\frac{\partial^2\mathcal{F}}{\partial\delta^2}\right)_{\delta=0}\delta^2(\mathbf{x}) + \frac{1}{2}\left(\frac{\partial^2\mathcal{F}}{\partial(s_{ij})^2}\right)_{s_{ij}=0}s^2_{ij}(\mathbf{x}) + \cdots.\end{aligned} \tag{3.21}$$

This gives the same results as Eq. (3.20).

3.1.3 Galaxy power spectrum and bispectrum

To sum up, at leading order, the galaxy power spectrum is simply given by

$$P_g(k) = b_1^2 P_{\rm lin}(k). \tag{3.22}$$

In order to consider the next-to-leading order power spectrum of galaxies, we have to include not only the second order biases but also the third-order biases. In addition, at one-loop order we have to renormalize the biases [77–80] and its explicit form is

found in Refs. [78, 80]. The tree-level galaxy bispectrum in real space is given by

$$B_{ggg}(\mathbf{k}_1,\mathbf{k}_2,\mathbf{k}_3) = 2b_1^2\left[\left(b_1F_2(\mathbf{k}_1,\mathbf{k}_2)+\frac{b_2}{2}+\frac{b_{s^2}}{2}\left[\frac{\mathbf{k}_1\cdot\mathbf{k}_2}{k_1k_2}-\frac{1}{3}\right]\right)P_{\rm lin}(k_1)P_{\rm lin}(k_2) + \text{ perms.}\right], \quad (3.23)$$

and the galaxy-galaxy-matter bispectrum, which is defined via $\langle\delta_g(\mathbf{k}_1)\delta_g(\mathbf{k}_2)\delta_m(\mathbf{k}_3)\rangle = (2\pi)^3\delta_{\rm D}^3(\mathbf{k}_1+\mathbf{k}_2+\mathbf{k}_3)B_{ggm}(\mathbf{k}_1,\mathbf{k}_2,\mathbf{k}_3)$, is explicitly given by

$$\begin{aligned} B_{ggm}(\mathbf{k}_1,\mathbf{k}_2,\mathbf{k}_3) = 2\Bigg[&b_1^2\left(b_1F_2(\mathbf{k}_1,\mathbf{k}_2)+\frac{b_2}{2}+\frac{b_{s^2}}{2}\left[\frac{\mathbf{k}_1\cdot\mathbf{k}_2}{k_1k_2}-\frac{1}{3}\right]\right)P_{\rm lin}(k_1)P_{\rm lin}(k_2)\\ &+b_1\left(b_1F_2(\mathbf{k}_2,\mathbf{k}_3)+\frac{b_2}{2}+\frac{b_{s^2}}{2}\left[\frac{\mathbf{k}_2\cdot\mathbf{k}_3}{k_2k_3}-\frac{1}{3}\right]\right)P_{\rm lin}(k_2)P_{\rm lin}(k_3)\\ &+b_1\left(b_1F_2(\mathbf{k}_1,\mathbf{k}_3)+\frac{b_2}{2}+\frac{b_{s^2}}{2}\left[\frac{\mathbf{k}_1\cdot\mathbf{k}_3}{k_1k_3}-\frac{1}{3}\right]\right)P_{\rm lin}(k_1)P_{\rm lin}(k_3)\Bigg]. \end{aligned} \quad (3.24)$$

3.2 Redshift-space distortion

In this section, we give a brief summary on the redshift-space distortion effect.

3.2.1 The linear Kaiser formula

In a redshift galaxy survey, the radial position of each galaxy needs to be inferred from its observed redshift, by using the fact that it is dominated by the Hubble flow. However, it can be modified by a peculiar velocity of galaxy through the Doppler effect, causing an apparent displacement of the inferred galaxy position from the true position:

$$\mathbf{s} = \mathbf{x} + \frac{v_\parallel(\mathbf{x})}{\mathcal{H}(z)}\hat{n}, \tag{3.25}$$

where $\mathbf{s}$ is the inferred position of galaxy in redshift space, $\mathbf{x}$ is the comoving true position in real space, $v_\parallel = \mathbf{v}\cdot\hat{n}$ is the radial component of peculiar velocity, $\mathcal{H}(z)$ is the comoving Hubble rate, and $\hat{n}$ is the unit vector of the line-of-sight direction. With this coordinate transformation, the density field in redshift space can be expressed as

$$\rho_s(\mathbf{s}) = \int d^3\mathbf{x}\ \rho(\mathbf{x})\ \delta_{\rm D}^3\left(\mathbf{s} - \mathbf{x} - \frac{v_\parallel(\mathbf{x})}{\mathcal{H}(z)}\hat{n}\right), \tag{3.26}$$

where $\rho_s(\mathbf{s})$ or $\rho(\mathbf{x})$ denotes the redshift- or real-space density field of galaxies, respectively. In the following quantities with subscript "s" denote their redshift-space quantities. Fourier-transforming Eq. (3.26), $\int d^3\mathbf{s}\ e^{i\mathbf{k}\cdot\mathbf{s}}$, yields

$$\delta_{\rm D}^3(\mathbf{k}) + \delta_s(\mathbf{k}) = \int d^3\mathbf{x}\ [1+\delta_g(\mathbf{x})]e^{-i\mathbf{k}\cdot\mathbf{x} - i(\mathbf{k}\cdot\hat{n})\frac{v_\parallel}{\mathcal{H}}}. \tag{3.27}$$

This transformation is exact even if multiple galaxies are mapped to the same position in redshift space, which can happen, e.g. in a nonlinear high-density region. Such multi-streaming regions are beyond the scope of this thesis, and we ignore the effects in this thesis for simplicity. Then we can rewrite Eq. (3.27) as

$$\begin{aligned}\delta_s(\mathbf{k}) &= \int d^3\mathbf{x}\left[1 + \delta_g(\mathbf{x}) - \left|\frac{\partial s_i}{\partial x_j}\right|\right] e^{-i\mathbf{k}\cdot\mathbf{x} - i(\mathbf{k}\cdot\hat{n})\frac{v_\parallel}{\mathcal{H}}} \\ &\simeq \int d^3\mathbf{x}\left[\delta_g(\mathbf{x}) - \frac{1}{\mathcal{H}(z)}\frac{\partial v_\parallel}{\partial\hat{n}}\cdot\hat{n}\right] e^{-i\mathbf{k}\cdot\mathbf{x} - i(\mathbf{k}\cdot\hat{n})\frac{v_\parallel}{\mathcal{H}}},\end{aligned} \tag{3.28}$$

where we kept the peculiar velocity up to the linear order in an expansion of the Jacobian, $|\partial s_i/\partial x_j|$, assuming $|v_\parallel/\mathcal{H}| \ll 1$. In the absence of vorticity, from Eq. (2.39) the linear velocity is expressed as,

$$v_i(\mathbf{k}, z) = \frac{ik_i}{-k^2}\theta(\mathbf{k}, z) = \frac{ik_i}{k^2}\delta_m(\mathbf{k}, z)\mathcal{H}(z)f(z). \tag{3.29}$$

Substituting this into Eq. (3.28) , at leading order we find [42]

$$\delta_s(\mathbf{k}) \simeq \left(b_1 + f\mu^2\right) \delta_m(\mathbf{k}), \tag{3.30}$$

where we have used $\delta_g = b_1\delta_m$ and $\mu = \mathbf{k}\cdot\hat{n}/k$ is the directional cosine of the wavevector and the line-of-sight. Note that here we assume that there is no velocity bias, i.e., $\mathbf{v}_g = \mathbf{v}_m$, which is valid at large scales. Given Eq. (3.30), the galaxy power spectrum in redshift space yields

$$P_s(k,\mu) = \left(b_1 + f\mu^2\right)^2 P_{\rm lin}(k). \tag{3.31}$$

This is the Kaiser formula that describes the observed power spectrum of galaxies on large scales. Notice that there appears the anisotropy called as the redshift-space distortion (RSD). This Kaiser anisotropy represents the infall motion. At linear order, this anisotroy is proportional to the linear growth rate f. This implies that by measuring anisotropic signals on large scales we can infer f, or the velocity field. Compared to the general relativity, alternative gravity theories predict different values for f , so we can use the RSD to test theories of gravity.

In practice, to measure the anisotropic power spectrum we use its Legendre coefficients;

$$P_s(k,\mu) = \sum_\ell P_\ell(k)\mathcal{L}_\ell(\mu), \tag{3.32}$$

where $\mathcal{L}_\ell(\mu)$ is the ℓ-th order Legendre polynomial. The Kaiser formula Eq. (3.31) contains the monopole, quadrupole and hexadecapole power spectra as follows:

$$P_0(k) = \left(b_1^2 + \frac{2}{3}b_1 f + \frac{1}{5}f^2\right) P_{\rm lin}(k), \tag{3.33}$$

$$P_2(k) = \left(\frac{4}{3}b_1 f + \frac{4}{7}f^2\right) P_{\rm lin}(k), \tag{3.34}$$

$$P_4(k) = \frac{8}{35}f^2 P_{\rm lin}(k). \tag{3.35}$$

Because $f < 1$ in the nearby universe, the amplitudes of the multipole power spectra follows $P_0(k) > P_2(k) > P_4(k)$ and thus most of information comes from the monopole and quarupole power spectra.

3.2.2 Nonlinear RSD in the standard perturbation theory

In order to obtain the higher order perturbative results beyond linear theory, we expand the exponent in Eq. (3.28),

$$\delta_s(\mathbf{k}) = \sum_{n=1}^{\infty}\prod_{m=1}^{n}\left\{\int\frac{d^3\mathbf{q}_m}{(2\pi)^3}\right\}\delta_{\rm D}^3(\mathbf{k}-\mathbf{q}_{1\cdots n})\left[\delta_g(\mathbf{k}_1)-f\mu^2\theta(\mathbf{k}_1)\right] \times\frac{(f\mu k)^{n-1}}{(n-1)!}\prod_{m=2}^{n}\left\{\frac{\mu_m}{q_m}\theta(\mathbf{q}_m)\right\}, \tag{3.36}$$

where $\mu_m \equiv \mathbf{q}_m\cdot\hat{n}/q_m$. Using the perturbative results for $\delta_g(\mathbf{k})$ and $\theta(\mathbf{k})$, we can write the redshift-space density field as the power series of the linear matter density field as follows

$$\delta_s(\mathbf{k}) = \sum_{n=1}^{\infty}\prod_{i=1}^{n}\left\{\int\frac{d^3\mathbf{q}_i}{(2\pi)^3}\delta^{(1)}(\mathbf{q}_i)\right\}\delta_{\rm D}^3(\mathbf{k}-\mathbf{q}_{1\cdots n})Z_n(\mathbf{q}_1,\cdots,\mathbf{q}_n), \tag{3.37}$$

where $Z_n(\mathbf{q}_1,\cdots,\mathbf{q}_n)$ is the n-th redshift-space kernel function, which reads from Eqs. (3.36) and (2.76)-(2.77),

$$Z_1(\mathbf{k}) = b_1 + f\mu^2, \tag{3.38}$$

$$Z_2(\mathbf{q}_1,\mathbf{q}_2) = b_1F_2(\mathbf{q_1},\mathbf{q_2}) + \frac{b_2}{2} + \frac{b_{s^2}}{2}\left(\frac{\mathbf{q}_1\cdot\mathbf{q}_2}{q_1q_2}-\frac{1}{3}\right) + f\mu^2G_2(\mathbf{q_1},\mathbf{q_2}) - \frac{f\mu k}{2}\left[\frac{\mu_1}{q_1}(b_1+f\mu_1^2)+\frac{\mu_2}{q_2}(b_1+f\mu_2^2)\right]. \tag{3.39}$$

Here we have consistently included both the nonlinear biases and nonlinear gravitational evolution up to the second order.

Using these kernels, the tree-level bispectrum in redshift space can be written as

$$B_{sss}(\mathbf{k}_1,\mathbf{k}_2,\mathbf{k}_3) = 2\left[Z_1(\mathbf{k}_1)Z_1(\mathbf{k}_2)Z_2(\mathbf{k}_1,\mathbf{k}_2)P_{\rm lin}(k_1)P_{\rm lin}(k_2)+{\rm perms.}\right], \tag{3.40}$$

and the galaxy-galaxy-matter bispectrum in redshift space, which is define through $\langle\delta_s(\mathbf{k}_1)\delta_s(\mathbf{k}_2)\delta_m(\mathbf{k}_3)\rangle = (2\pi)^3\delta_{\rm D}^3(\mathbf{k}_1+\mathbf{k}_2+\mathbf{k}_3)B_{ssm}(\mathbf{k}_1,\mathbf{k}_2,\mathbf{k}_3)$, as

$$B_{ssm}(\mathbf{k}_1,\mathbf{k}_2,\mathbf{k}_3) = 2\left[Z_1(\mathbf{k}_1)Z_1(\mathbf{k}_2)Z_2(\mathbf{k}_1,\mathbf{k}_2)P_{\rm lin}(k_1)P_{\rm lin}(k_2) + Z_1(\mathbf{k}_2)Z_2(\mathbf{k}_2,\mathbf{k}_3)P_{\rm lin}(k_2)P_{\rm lin}(k_3) + Z_1(\mathbf{k}_1)Z_2(\mathbf{k}_1,\mathbf{k}_3)P_{\rm lin}(k_1)P_{\rm lin}(k_3)\right]. \tag{3.41}$$

3.3 Alcock-Paczyński test

The two-point correlation function of galaxies is measured as a function of the separation lengths between paired galaxies. To measure this separation, the position of each galaxy needs to be inferred from the measured redshift and angular position by means of the angular diameter distance and the Hubble law. Then the separation lengths perpendicular and parallel to the line-of-sight direction from the measured quantities are given as

$$x_\perp = (1+z) D_A(z) \Delta\theta, \tag{3.42}$$

$$x_\parallel = \frac{1+z}{H(z)} \Delta z, \tag{3.43}$$

with $\Delta\theta$ and Δz being the differences between the angular positions and the redshifts of the paired galaxies and

$$D_A(z) = \frac{1}{1+z} \int_0^z \frac{dz'}{H(z')}. \tag{3.44}$$

To convert the observables ($\Delta\theta$, Δz) to the comoving quantities ($x_\perp, x_\parallel$), one has to assume a fiducial cosmological model. If the fiducial cosmological model we use differs from the underlying true cosmological model, the relation between the comoving true distance and observed distance is given by

$$x_{\perp,\mathrm{true}} = \frac{D_A(z)}{D_{A,\mathrm{fid}}(z)} x_{\perp,\mathrm{obs}}, \tag{3.45}$$

$$x_{\parallel,\mathrm{true}} = \frac{H_{\mathrm{fid}}(z)}{H(z)} x_{\parallel,\mathrm{obs}}, \tag{3.46}$$

where the quantities with subscript "true" refer to the underlying true values and the quantities with "obs" are obtained from the assumed fiducial cosmological model. In terms of the wavevector, this transformation results in

$$k_{\perp,\mathrm{true}} = \frac{D_{A,\mathrm{fid}}(z)}{D_A(z)} k_{\perp,\mathrm{obs}}, \tag{3.47}$$

$$k_{\parallel,\mathrm{true}} = \frac{H(z)}{H_{\mathrm{fid}}(z)} k_{\parallel,\mathrm{obs}}. \tag{3.48}$$

Then the magnitude and line-of-sight component of the comoving wavevector become

$$\begin{aligned} k^{\rm true} =& \sqrt{|\vec{k}_\perp^{\rm true}|^2 + |\vec{k}_\parallel^{\rm true}|^2} = \sqrt{\left(\frac{D_A^{\rm fid}}{D_A}\right)^2 |\vec{k}_\perp^{\rm obs}|^2 + \left(\frac{H}{H^{\rm fid}}\right)^2 |\vec{k}_\parallel^{\rm obs}|^2} \\ =& k^{\rm obs}\sqrt{\left(\frac{D_A^{\rm fid}}{D_A}\right)^2 (1-\mu_{\rm obs}^2) + \left(\frac{H}{H^{\rm fid}}\right)^2 \mu_{\rm obs}^2} \\ \equiv& \frac{k^{\rm obs}}{\alpha(D_A^{\rm fid}, H^{\rm fid}, \mu_{\rm obs})}, \end{aligned} \tag{3.49}$$

$$\begin{aligned} \mu^{\rm true} =& \frac{k_\parallel^{\rm true}}{k^{\rm true}} = \alpha(D_A^{\rm fid}, H^{\rm fid}, \mu_{\rm obs}) \frac{H}{H^{\rm fid}} \frac{k_\parallel^{\rm obs}}{k^{\rm obs}} \\ =& \frac{\alpha H}{H^{\rm fid}} \mu^{\rm obs}. \end{aligned} \tag{3.50}$$

This leads to the observed power spectrum in redshift space,

$$P_{\rm obs}(k^{\rm obs}, \mu^{\rm obs}) = \frac{H}{H^{\rm fid}} \left(\frac{D_A^{\rm fid}}{D_A}\right)^2 P(k^{\rm true}, \mu^{\rm true}), \tag{3.51}$$

where we have used $P_{\rm obs}(\mathbf{k}^{\rm obs}) d^3\mathbf{k}_{\rm obs} = P(\mathbf{k}^{\rm true}) d^3\mathbf{k}_{\rm true}$.

Since the fiducial cosmological model we assume generally differs from the underlying true cosmology and $D_A(z)$ and $H(z)$ depend on the cosmological parameters differently, an apparent geometrical distortion is caused in the two-dimensional pattern of galaxy clustering. In principle, this distortion could be measured using only the isotropy of clustering statistics, the so-called Alcock-Paczyński (AP) test [44, 81, 82], but a more robust measurement of both $D_A(z)$ and $H(z)$ can be obtained by searching for the "common" BAO scales in the pattern of galaxy clustering, as the standard ruler, in combination with the CMB constraints [45, 46]. This is because the AP effect anisotropically alters the characteristic scales imprinted on the power spectrum, as shown in Eq. (3.49), $k \to k/\alpha$ [14, 83, 84].

Eq. (3.51) implies that there appear the higher-order multipoles than $\ell = 4$ if the fiducial cosmology deviates from the underlying true cosmology. In general, the AP effect makes the galaxy clustering anisotropic even in the absence of the RSD. Notice that, however, the generated anisotropic signals are confined into the line-of-sight direction and there is no anisotropic distortion in the plane perpendicular to the line-of-sight due to the AP effect. In other words, the AP effect leaves the redshift-space power spectrum two-dimensional one, which still respects the three-dimensionally rotational symmetry around the observer.

Chapter 4

Super-sample tidal effect

Contents

According to the discussion in Section 2.2, the nonlinear growth of the LSS produces the mode-coupling of different scales. The mode-coupling naturally predicts that long-wavelength fluctuations beyond a given survey region may affect the observed galaxy clustering within a finite survey region, which is known as the super-sample or super-survey effect [30, 33]. We cannot directly measure these long-wavelength fluctuations (called as the super-sample or super-survey modes) in a finite volume survey. However, through the non-linear mode coupling between different Fourier modes, the super-sample modes change both the amplitude and the comoving scale of the short-wavelength fluctuations, which is known as the growth and dilation effect, respectively [26, 28, 31].

The effects of the super-sample modes on the real-space power spectrum have been extensively studied in Refs. [26, 29–32, 37, 41]. The uncertainty of the amplitude of the super-sample modes forces us to add a new term to the power spectrum covariance, dubbed as the super-sample covariance [30, 31, 41]. Physical effects of the super-sample modes originate from the second derivatives of large-scale gravitational potential, which can be decomposed into the trace (mean overdensity) and the traceless (large-scale tidal field) parts [37]. Thus, there are super-sample tidal components that are expected to be of the same order of magnitude as those of isotropic ones, whereas previous studies have focused on the isotropic super-sample mode because the impact of super-sample tidal components on the real-space power spectrum vanishes after the spherical average.

As discussed in Section 3.2 and 3.3, however, in spectroscopic surveys what we observe is not the real-space power spectrum but redshift-space power spectrum. The super-sample tidal mode is likely to produce similar anisotropic effects. Hence, the purpose of this chapter is to study the effects of the large-scale tides on the redshift-space power spectrum, based on the perturbation theory. To do this, in Sections 4.2-4.4 we derive *response* functions of the power spectrum to super-sample modes, which describe how the super-sample modes in a given survey realization affect the power spectrum, after giving the definition of the super-sample modes in Section 4.1. We then discuss the impact of the large-scale tide on estimation of cosmological distances and the redshift-space distortion parameter via a measurement of the redshift-space power spectrum for a hypothetical large-volume galaxy survey, using the Fisher matrix formalism in Section 4.5. We further explore the possibility to treat the super-sample tidal modes as a new signal in Section 4.6.

4.1 Observed density field and the super-sample modes

The number density field of galaxies observed in a finite-volume survey region can be expressed, using the survey window function $W(x)$, following the formulation in Ref.[30]

$$\delta_W(\mathbf{x}) = W(\mathbf{x})\delta(\mathbf{x}), \tag{4.1}$$

where $\delta_W(\mathbf{x})$ is the observed density field, $\delta(\mathbf{x})$ is the underlying true density field, and the survey window is defined such that $W(x) = 1$ if $\mathbf{x}$ is inside the survey geometry, and otherwise $W(x) = 0$. Throughout this thesis we assume that a survey window is given in the background comoving coordinate. The survey volume V is defined in terms of the survey window as

$$V = \int d^3\mathbf{x}\, W(\mathbf{x}). \tag{4.2}$$

In the following we do not consider effects of masks that might cause additional mode-coupling between high-k modes in the observed power spectrum. The Fourier transform of the density field is

$$\delta_W(\mathbf{k}) = \int \frac{d^3\mathbf{q}}{(2\pi)^3} W(\mathbf{q})\delta(\mathbf{k}-\mathbf{q}), \tag{4.3}$$

where we distinguish real-space quantities from their Fourier transforms by their arguments. The Fourier transform of the survey window $W(\mathbf{k})$ is nonvanishing for $k \ll 1/L$ while $W(\mathbf{k}) \simeq 0$ for $k \gg L$, where $L \sim V^{1/3}$ is a typical scale of the survey volume. The equation above explicitly shows that the Fourier transform of the observed field has a contribution from long-wavelength modes beyond a survey window, i.e. super-sample or super-survey modes, via a convolution with the survey window.

An estimator of the *three-dimensional* power spectrum for a given survey window is defined as

$$\hat{P}_{\rm obs}(\mathbf{k}) \equiv \frac{1}{V}\int_{\mathbf{k}'\in\mathbf{k}} \frac{d^3\mathbf{k}'}{V_{\mathbf{k}}} \delta_W(\mathbf{k}')\delta_W(-\mathbf{k}'), \tag{4.4}$$

where the integration is done over a volume element around the mode $\mathbf{k}$ (a target wavevector for the power spectrum measurement), and $V_{\mathbf{k}}$ is the volume: $V_{\mathbf{k}} \equiv \int_{\mathbf{k}'\in\mathbf{k}} d^3\mathbf{k}'$. If a bin width around the bin $\mathbf{k}$ is given by Δk, $V_{\mathbf{k}} \simeq (\Delta k)^3$. This definition does *not* include an angle average of $d^2\hat{k}$, unlike a definition of the monopole power spectrum. Hence, at this point, the power spectrum $\hat{P}(\mathbf{k})$ is given as a

function of the three-dimensional vector, $\mathbf{k}$. This is because the large-scale tides generally cause anisotropic distortions in the clustering pattern of galaxies in all three-dimensional directions. Note that the power spectrum estimator satisfies a parity invariance:

$$\hat{P}_{\rm obs}(\mathbf{k}) = \hat{P}_{\rm obs}(-\mathbf{k}). \tag{4.5}$$

Given the definition of the power spectrum $\langle\delta(\mathbf{k})\delta(\mathbf{k}')\rangle \equiv (2\pi)^3\delta_{\rm D}^3(\mathbf{k}+\mathbf{k}')P(\mathbf{k})$, the ensemble average of the estimator (Eq. (4.4)) is found to be an unbiased estimator of the underlying power spectrum for modes with $k \gg 1/L$:

$$\begin{aligned}\left\langle \hat{P}_{\rm obs}(\mathbf{k})\right\rangle =& \frac{1}{V}\int_{\mathbf{k}\in\mathbf{k}'}\frac{d^3\mathbf{k}'}{V_{\mathbf{k}}}\int\frac{d^3\mathbf{q}}{(2\pi)^3}\left|W(\mathbf{q})\right|^2 P(\mathbf{k}'-\mathbf{q})\\ \simeq& \frac{1}{V}\int_{\mathbf{k}\in\mathbf{k}'}\frac{d^3\mathbf{k}'}{V_{\mathbf{k}}}P(\mathbf{k}')\int\frac{d^3\mathbf{q}}{(2\pi)^3}\left|W(\mathbf{q})\right|^2\\ \simeq& \frac{P(\mathbf{k})}{V}\int\frac{d^3\mathbf{q}}{(2\pi)^3}\left|W(\mathbf{q})\right|^2 = P(\mathbf{k}).\end{aligned} \tag{4.6}$$

Here we have used $P(\mathbf{k}'-\mathbf{q}) \simeq P(\mathbf{k}')$ over the integration rage of $d^3\mathbf{q}$ which the window function supports and assumed that $P(\mathbf{k})$ is not a rapidly varying function within the $\mathbf{k}$-bin. In addition, we have used the general identity for the window function [30]:

$$V = \int d^3\mathbf{x}\; W^n(\mathbf{x}) = \left[\prod_{i=1}^{n}\int\frac{d^3\mathbf{q}_i}{(2\pi)^3}W(\mathbf{q}_i)\right](2\pi)^3\delta_{\rm D}^3(\mathbf{q}_{1\cdots n}), \tag{4.7}$$

where $\mathbf{q}_{1\cdots n} \equiv \mathbf{q}_1+\mathbf{q}_2+\cdots+\mathbf{q}_n$.

The super-sample modes we focus on are the large-scale density contrast (corresponding to the *background* density fluctuation) and the large-scale tides, defined in terms of the *linear* matter density fluctuation field as

$$\begin{aligned}\delta_{\rm b} \equiv& \frac{1}{V}\int d^3\mathbf{x}\; W(\mathbf{x})\delta_m^{\rm lin}(\mathbf{x}) = \frac{1}{V}\int\frac{d^3\mathbf{q}}{(2\pi)^3}\delta_m^{\rm lin}(\mathbf{q})W(-\mathbf{q}),\\ \tau_{ij} \equiv& \frac{1}{4\pi G\bar{\rho}_{\rm m}a^2V}\int d^3\mathbf{x}\; W(\mathbf{x})\left[\partial_i\partial_j\Phi(\mathbf{x}) - \frac{\delta_{ij}^K}{3}\nabla^2\Phi(\mathbf{x})\right]\\ =& \frac{1}{V}\int\frac{d^3\mathbf{q}}{(2\pi)^3}\left(\hat{q}_i\hat{q}_j - \frac{\delta_{ij}^K}{3}\right)\delta_m^{\rm lin}(\mathbf{q})W(-\mathbf{q}),\end{aligned} \tag{4.8}$$

where $\hat{q}_i \equiv q_i/q$, $\hat{q}_i\hat{q}^i = 1$, δ_{ij}^K is the Kronecker delta and $\Phi(\mathbf{x})$ is the gravitational potential field. The window function picks up the longer-wavelength fluctuations than a typical scale of survey volume. Throughout this thesis, we assume that a given survey volume is so large that the matter density fields contributing the

super-sample modes are in the linear regime, denoted as $\delta_m^{\rm lin}(\mathbf{x})$. Under this setting, $|\delta_{\rm b}|, |\tau_{ij}| \ll 1$. These super-sample modes are not direct observables and vary with survey realizations, because the super-sample modes depend on the position and shape of specific surveys. For a given survey realization, $\delta_{\rm b}$ and τ_{ij} are constant. Although $\delta_{\rm b}$ and τ_{ij} are related through $\tau_{ij} = \partial_i\partial_j\partial^{-2}\delta_{\rm b}$ in real space, the values of τ_{ij} cannot be inferred from $\delta_{\rm b}$ due to the non-local nature of a tidal field (suggested by the appearance of inverse Laplacian ∂^{-2}, see Refs. [35, 36] for details). The *expectation* values of the super-sample modes, i.e. the averages over different, possible survey realizations for a fixed volume, are $\langle\delta_{\rm b}\rangle = \langle\tau_{ij}\rangle = 0$ and the variances are computed if the linear matter power spectrum at long wavelengths for super-sample modes, $P_{\rm lin}(k)$, is given for a given cosmological model:

$$\sigma_{\rm b}^2 \equiv \langle\delta_{\rm b}^2\rangle = \frac{1}{V^2}\int\frac{d^3\mathbf{q}}{(2\pi)^3}P_{\rm lin}(q)\,|W(\mathbf{q})|^2\,, \tag{4.9}$$

$$\langle\delta_{\rm b}\tau_{ij}\rangle = \frac{1}{V^2}\int\frac{d^3\mathbf{q}}{(2\pi)^3}\left(\hat{q}_i\hat{q}_j - \frac{1}{3}\delta^K_{ij}\right)P_{\rm lin}(q)\,|W(\mathbf{q})|^2\,, \tag{4.10}$$

$$\langle\tau_{ij}\tau_{lm}\rangle = \frac{1}{V^2}\int\frac{d^3\mathbf{q}}{(2\pi)^3}\left(\hat{q}_i\hat{q}_j - \frac{1}{3}\delta^K_{ij}\right)\left(\hat{q}_l\hat{q}_m - \frac{1}{3}\delta^K_{lm}\right)P_{\rm lin}(q)\,|W(\mathbf{q})|^2\,. \tag{4.11}$$

In this thesis we consider an isotropic window for simplicity; $W(\mathbf{q}) = W(q)$. In this case the variances of large-scale tides are simplified as

$$\langle\delta_{\rm b}\tau_{ij}\rangle = 0, \tag{4.12}$$

$$\begin{aligned}\langle\tau_{ij}\tau_{\ell m}\rangle =& \frac{1}{V^2}\int\frac{d^3\mathbf{q}}{(2\pi)^3}\left(\hat{q}_i\hat{q}_j - \frac{1}{3}\delta^K_{ij}\right)\left(\hat{q}_\ell\hat{q}_m - \frac{1}{3}\delta^K_{\ell m}\right)P_{\rm lin}(q)|W(\mathbf{q})|^2 \\ =& \left(-\frac{2}{45}\delta^K_{ij}\delta^K_{\ell m} + \frac{3}{45}\delta^K_{i\ell}\delta^K_{jm} + \frac{3}{45}\delta^K_{im}\delta^K_{j\ell}\right)\sigma_{\rm b}^2,\end{aligned} \tag{4.13}$$

$$\sigma_\tau^2 \equiv \langle(\tau_{11})^2\rangle = \langle(\tau_{22})^2\rangle = \langle(\tau_{33})^2\rangle = \frac{3}{4}\langle(\tau_{ij})^2\rangle_{i\neq j} = \frac{4}{45}\sigma_{\rm b}^2. \tag{4.14}$$

4.2 Response and the squeezed bispectrum

We now consider how super-sample modes affect the power spectrum observed in a finite-volume survey. These long-wavelength perturbations affect the small-scale clustering due to the nonlinear mode-coupling by gravity. Following the discussion in Refs. [30, 37], in the presence of super-sample modes $(\delta_{\rm b}, \tau_{ij})$ for a given survey realization, the "observed" power spectrum is formally expressed, up to the first order of super-sample modes, as

$$P_{\rm obs}(\mathbf{k};\delta_{\rm b},\tau_{ij}) = P(\mathbf{k})|_{\delta_{\rm b}=0,\tau_{ij}=0} + \frac{\partial P(\mathbf{k})}{\partial\delta_{\rm b}}\delta_{\rm b} + \frac{\partial P(\mathbf{k})}{\partial\tau_{ij}}\tau_{ij}. \tag{4.15}$$

Here we explicitly denote that the observed spectrum $P_{\rm obs}(\mathbf{k};\delta_{\rm b},\tau_{ij})$ depends on the super-sample modes of a given survey realization, and the first term in the right-hand side is the power spectrum without the super-sample modes. The functions $\partial P(\mathbf{k})/\partial\delta_{\rm b}$ and $\partial P(\mathbf{k})/\partial\tau_{ij}$ are so-called "response" functions describing a response of the power spectrum to the super-sample modes via mode couplings in the nonlinear structure formation. We again stress that the super-sample modes, $\delta_{\rm b}$ and τ_{ij}, are "constant" numbers for a particular survey realization. Hence, the above equation assumes that a shift in the power spectrum due to all modes with wavelengths longer than a size of survey volume is described by the product of the response function and $\delta_{\rm b}$ or τ_{ij}. Furthermore, the response function is given as a function of sub-survey modes, even down to an arbitrary large k in the deeply nonlinear regime, if it is not non-vanishing. That is, we assume that, as long as the super-sample modes are in the linear regime (a survey volume is sufficiently large) and if the response function is obtained, the effects on all the small-scale modes are described by the above equation. Thus Eq. (4.15) rests on a non-trivial assumption, but is quite useful if Eq. (4.15) holds a good approximation, which is indeed the case for $\delta_{\rm b}$ as shown by many works e.g.[31].

Now we derive the response function using the perturbation theory. The simplest way to do this is considering a squeezed-limit bispectrum that arises from correlations between two short modes and one long mode (corresponding to super-sample modes) [85]. More specifically, let us consider a correlation of $\hat{P}_{\rm obs}(\mathbf{k})$ (Eq. (4.4)) with the large-scale matter density field, $\delta_m^{\rm lin}(\mathbf{q}) = \delta^{(1)}(\mathbf{q})$ ($\mathbf{q}$ is the long mode):

$$\begin{aligned}\left\langle \hat{P}_{\rm obs}(\mathbf{k})\delta_m^{(1)}(\mathbf{q})\right\rangle =& \frac{1}{V}\int_{\mathbf{k}'\in\mathbf{k}}\frac{d^3\mathbf{k}'}{V_{\mathbf{k}}}\int\frac{d^3\mathbf{q}_1}{(2\pi)^3}\frac{d^3\mathbf{q}_2}{(2\pi)^3}\left\langle\delta(\mathbf{k}'-\mathbf{q}_1)\delta(-\mathbf{k}'-\mathbf{q}_2)\delta(\mathbf{q})\right\rangle W(\mathbf{q}_1)W(\mathbf{q}_2)\\ =& \frac{1}{V}\int_{\mathbf{k}'\in\mathbf{k}}\frac{d^3\mathbf{k}'}{V_{\mathbf{k}}}\int\frac{d^3\mathbf{q}_1}{(2\pi)^3}\frac{d^3\mathbf{q}_2}{(2\pi)^3}B(\mathbf{k}'-\mathbf{q}_1,-\mathbf{k}'-\mathbf{q}_2,\mathbf{q})(2\pi)^3\delta_{\rm D}^3(\mathbf{q}_{12}-\mathbf{q})\\ &\times W(\mathbf{q}_1)W(\mathbf{q}_2),\end{aligned} \tag{4.16}$$

where we have used the definition of the bispectrum:

$$\langle\delta(\mathbf{k}_1)\delta(\mathbf{k}_2)\delta(\mathbf{q})\rangle \equiv B(\mathbf{k}_1,\mathbf{k}_2,\mathbf{q})(2\pi)^3\delta_{\rm D}^3(\mathbf{k}_1+\mathbf{k}_2+\mathbf{q}). \tag{4.17}$$

Due to the window function, the contribution of the above integrand comes when $q_1, q_2 \ll k$ if we are interested in $k \gg 1/L$. For the case that $k \gg q_1, q_2, q$, the bispectrum in the above equation arises from so-called squeezed triangles where two sides are nearly equal and in opposite direction. To see this, we can make the variable changes $\mathbf{k}' - \mathbf{q}_1 \leftrightarrow \mathbf{k}'$ and $\mathbf{q}_1 + \mathbf{q}_2 \leftrightarrow \mathbf{q}$ under the delta function condition $\mathbf{q}_{12} + \mathbf{q} = \mathbf{0}$ and the approximation that $k \ll q$. The bispectrum we are interested in reads

$$\lim_{q\to 0} B(\mathbf{k}', -\mathbf{k}' - \mathbf{q}, \mathbf{q}). \tag{4.18}$$

In this limit,

$$\begin{aligned}\left\langle \hat{P}_{\rm obs}(\mathbf{k})\delta_m^{(1)}(\mathbf{q})\right\rangle =& \frac{1}{V}\int_{\mathbf{k}'\in\mathbf{k}}\frac{d^3\mathbf{k}'}{V_{\mathbf{k}}}B(\mathbf{k}', -\mathbf{k}'-\mathbf{q}, \mathbf{q})\int\frac{d^3\mathbf{q}_1}{(2\pi)^3}W(\mathbf{q}_1)W(\mathbf{q}-\mathbf{q}_1)\\ =& \frac{B(\mathbf{k}, -\mathbf{k}-\mathbf{q}, \mathbf{q})W(\mathbf{q})}{V},\end{aligned} \tag{4.19}$$

where we have used

$$\int\frac{d^3\mathbf{q}_1}{(2\pi)^3}W(\mathbf{q}_1)W(\mathbf{q}-\mathbf{q}_1) = W(\mathbf{q}), \tag{4.20}$$

which is followed from $W^2(\mathbf{x}) = W(\mathbf{x})$ in real space. On the other hand, correlating Eq. (4.15) with $\delta^{(1)}(\mathbf{q})$ results in

$$\begin{aligned}\left\langle \hat{P}_{\rm obs}(\mathbf{k};\delta_{\rm b},\tau_{ij})\delta_m^{(1)}(\mathbf{q})\right\rangle =& P(\mathbf{k})\left\langle\delta^{(1)}(\mathbf{q})\right\rangle + \frac{\partial P(\mathbf{k})}{\partial\delta_{\rm b}}\left\langle\delta_{\rm b}\delta^{(1)}(\mathbf{q})\right\rangle + \frac{\partial P(\mathbf{k})}{\partial\tau_{ij}}\left\langle\tau_{ij}\delta^{(1)}(\mathbf{q})\right\rangle.\\ =& \frac{1}{V}\int\frac{d^3\mathbf{q}'}{(2\pi)^3}\left[\frac{\partial P(\mathbf{k})}{\partial\delta_{\rm b}} + \frac{\partial P(\mathbf{k})}{\partial\tau_{ij}}\left(\hat{q}_i'\hat{q}_j' - \frac{\delta_{ij}^K}{3}\right)\right]\\ &\times\left\langle\delta^{(1)}(\mathbf{q}')\delta^{(1)}(\mathbf{q})\right\rangle W(-\mathbf{q}')\\ =& \frac{1}{V}\left[\frac{\partial P(\mathbf{k})}{\partial\delta_{\rm b}} + \frac{\partial P(\mathbf{k})}{\partial\tau_{ij}}\left(\hat{q}_i\hat{q}_j - \frac{\delta_{ij}^K}{3}\right)\right]P_{\rm lin}(q)W(\mathbf{q}).\end{aligned} \tag{4.21}$$

Thus, the triangle configuration describes how the power spectrum $P(\mathbf{k})$ is modulated by the super-sample mode $\delta^{(1)}(\mathbf{q})$. Comparing Eq. (4.19) with Eq. (4.21), the squeezed bispectrum can be described by the response of $P(\mathbf{k})$ to the super-sample modes as

$$\lim_{q\to 0} B(\mathbf{k}, -\mathbf{k}-\mathbf{q}, \mathbf{q}) = \left[\frac{\partial P(\mathbf{k})}{\partial\delta_{\rm b}} + \left(\hat{q}_i\hat{q}_j - \frac{1}{3}\delta_{ij}^K\right)\frac{\partial P(\mathbf{k})}{\partial\tau_{ij}}\right]P_{\rm lin}(q). \tag{4.22}$$

From Eq. (4.22), we can derive the response function $\partial P(\mathbf{k})/\partial\delta_{\rm b}$ from the angle average of the squeezed bispectrum over $d^3\mathbf{q}$ as

$$\frac{\partial P(\mathbf{k})}{\partial\delta_{\rm b}}P_{\rm lim}(q) \simeq \lim_{q\to 0}\int\frac{d^2\hat{q}}{4\pi}\,B(\mathbf{k},-\mathbf{k}-\mathbf{q},\mathbf{q}). \tag{4.23}$$

With this derivation, the response to the large-scale tide, $\partial P(\mathbf{k})/\partial\tau_{ij}$, can be found from

$$\frac{\partial P(\mathbf{k})}{\partial\tau_{ij}} \longleftarrow \text{coefficients in } \left(\hat{q}_i\hat{q}_j - \frac{\delta^K_{ij}}{3}\right)P_{\rm lin}(q) \text{ in } \lim_{q\to 0}B(\mathbf{k},-\mathbf{k}-\mathbf{q},\mathbf{q}). \tag{4.24}$$

Therefore, we can predict the response function by computing the squeezed bispectrum using the perturbation theory.

Eq. (4.15) implies that we can also extract the response function from the collapsed trispectrum (4-point function) $\left\langle \hat{P}_{\rm obs}(\mathbf{k})\hat{P}_{\rm obs}(\mathbf{k}')\right\rangle$, which is related to the covariance. The derivation of the response function through the collapsed trispectrum is presented in Appendix B. In the following, we calculate the response function from the squeezed bispectrum.

4.3 Real space results

In this section, using the standard perturbation theory we give an expression of the response function in matter and galaxy power spectrum in real space.

4.3.1 Growth and dilation effects

The response of the matter power spectrum in real space is the simplest case. What we need to consider is the squeezed matter bispectrum Eq. (2.86), which at leading order is given by

$$\begin{aligned} B_{mmm}(\mathbf{k},-\mathbf{k}-\mathbf{q},\mathbf{q}) \simeq & 2F_2(\mathbf{k},\mathbf{q})P_{\rm lin}(k)P_{\rm lin}(q)+2F_2(-\mathbf{k}-\mathbf{q},\mathbf{q})P_{\rm lin}(|\mathbf{k}+\mathbf{q}|)P_{\rm lin}(q) \\ \simeq & \left[\frac{13}{7}+\frac{8}{7}\left(\hat{k}\cdot\hat{q}\right)^2-\left(\hat{k}\cdot\hat{q}\right)^2\frac{d\ln P_{\rm lin}(k)}{d\ln k}\right]P_{\rm lin}(k)P_{\rm lin}(q). \end{aligned} \tag{4.25}$$

Thus we have

$$\frac{\partial P_m(k)}{\partial\delta_{\rm b}}=\left[\frac{47}{21}-\frac{1}{3}\frac{d\ln P_{\rm lin}(k)}{d\ln k}\right]P_{\rm lin}(k), \tag{4.26}$$

$$\frac{\partial P_m(\mathbf{k})}{\partial\tau_{ij}}=\left[\frac{8}{7}-\frac{d\ln P_{\rm lin}(k)}{d\ln k}\right]\hat{k}_i\hat{k}_jP_{\rm lin}(k). \tag{4.27}$$

Notice that while the response to the isotropic super-sample mode $\delta_{\rm b}$ can depend only on the magnitude of the wavevector due to the symmmetry, the response to the large-scale tides τ_{ij} has the angular dependence.

Next we consider the response function of the galaxy power spectrum in real space. To derive that, we should consider the galaxy-galaxy-matter bispectrum Eq. (3.24). This bispectrum in sqeezed limit yeilds

$$\begin{aligned} B_{ggm}(\mathbf{k},-\mathbf{k}-\mathbf{q},\mathbf{q}) \simeq & \left[\frac{13}{7}b_1^2+2b_1b_2-\frac{2}{3}b_1b_{s^2}+\left(\frac{8}{7}b_1^2+2b_1b_{s^2}\right)\left(\hat{k}\cdot\hat{q}\right)^2\right. \\ & \left.-b_1^2\left(\hat{k}\cdot\hat{q}\right)^2\frac{d\ln P_{\rm lin}(k)}{d\ln k}\right]P_{\rm lin}(k)P_{\rm lin}(q), \end{aligned} \tag{4.28}$$

which leads to

$$\frac{\partial P_g(k)}{\partial\delta_{\rm b}}=\left[\frac{47}{21}b_1^2+2b_1b_2-\frac{1}{3}b_1^2\frac{d\ln P_{\rm lin}(k)}{d\ln k}\right]P_{\rm lin}(k), \tag{4.29}$$

$$\frac{\partial P_g(\mathbf{k})}{\partial\tau_{ij}}=\left[\frac{8}{7}b_1^2+2b_1b_{s^2}-b_1^2\frac{d\ln P_{\rm lin}(k)}{d\ln k}\right]\hat{k}_i\hat{k}_jP_{\rm lin}(k). \tag{4.30}$$

The expressions above exhibit the physical effects of the super-sample modes on small-scale fluctuations. There are two types of the super-sample effects. First, the

super-sample modes enhance or suppress the growth of the short-modes depending on the sign of the super-sample modes and directions of small-scale fluctuations: speeding up the growth in the denser region and slowing down in the less dense region. As for τ_{ij}, if the large-scale tide along a particular direction is positive, say $\tau_{ii} > 0$, the expansion of a local volume along the direction is slower than that of the global universe, so the growth of short modes with $\mathbf{k}$ along the direction can be enhanced. This growth effect corresponds to the terms with no derivatives. Second, the super-sample modes cause a dilation of the comoving scale since the local expansion history is altered by the super-sample modes. The comoving wavelengths which an observer infers are modulated by the super-sample modes, which imprints a modulation in the power spectrum. This dilation effect is described by the derivative terms. While the mean density mode $\delta_{\rm b}$ generates an isotropic shift for all scales, the tidal modes τ_{ij} cause an ellipsoidal expansion in a local region and this leads to an anisotropic shift. Thus the large-scale tides cause modifications in the clustering pattern along all the three directions.

In particular, this dilation leaves a characteristic imprint on the BAOs feature in the power spectrum. Specifically, the isotropic super-sample mode shifts the observed BAO scale in an isotropic way, whereas the anisotropic super-sample modes shift in an anisotropic way. Neglecting the growth terms, we can rewrite the real-space galaxy power spectrum with responses as

$$\begin{aligned} P_g(\mathbf{k};\delta_{\rm b},\tau_{ij}) =& b_1^2 P_{\rm lin}(k) + b_1^2\left(-\frac{1}{3}\delta_{\rm b} - \hat{k}_i\hat{k}_j\tau_{ij}\right)\frac{\partial P_{\rm lin}(k)}{\partial \ln k} \\ \simeq& b_1^2 P_{\rm lin}\left(k/\alpha(\hat{k})\right), \end{aligned} \tag{4.31}$$

where

$$\begin{aligned} \alpha(\hat{k}) =& \left[1 - \frac{1}{3}\delta_{\rm b} - \hat{k}_i\hat{k}_j\tau_{ij} + \mathcal{O}(\delta_{\rm b}^2,\tau_{ij}^2)\right]^{-1} \\ \simeq& 1 + \frac{1}{3}\delta_{\rm b} + \hat{k}_i\hat{k}_j\tau_{ij} \end{aligned} \tag{4.32}$$

parameterizes the direction-dependent shift in the BAO peak. When there is no BAO peak shift, $\alpha = 1$ holds. From this expression, one can easily see that the large-scale tides generate three-dimensionally anisotropic distortions in the BAO peak position, while the large-scale mean density causes only isotropic distortion.

4.3.2 Modulation of the mean galaxy overdensity

In the previous subsection, we implicitly assume that the overdensity field of galaxies is defined to the global (background) mean number density of galaxies. In a spectroscopic survey of galaxies, however, we measure the overdensity field defined to the

"local" mean number density in the survey region. Because the super-sample modes behave like the background in the local survey area, these also make a difference between the "local" mean number density $\bar{n}_g^{\rm global}$ and the "global" mean number density $\bar{n}_g^{\rm global}$ such that $\bar{n}_g^{\rm local} = \bar{n}_g^{\rm global}(1+\delta_{\rm b}^g)$ with $\delta_{\rm b}^g$ being the mean galaxy over-density in the specific survey due to the super-sample modes. In a galaxy redshift survey, therefore, the observed number density fluctuation of galaxies $\delta_g^{\rm local}(\mathbf{k})$ which is defined through $n_g(\mathbf{k}) = \bar{n}_g^{\rm local}[1+\delta_g^{\rm local}(\mathbf{k})]$ is related to that defined to the "global" mean density through $n_g(\mathbf{k}) = \bar{n}_g^{\rm global}[1+\delta_g^{\rm global}(\mathbf{k})]$ as follows [29],

$$\delta_g^{\rm local}(\mathbf{k}) = \frac{\delta_g^{\rm global}(\mathbf{k})}{1+\delta_{\rm b}^g} + \frac{1}{1+\delta_{\rm b}^g} \simeq (1-\delta_{\rm b}^g)\delta_g^{\rm global}(\mathbf{k}), \tag{4.33}$$

where we omit the constant contribution because the Fourier transform of the constant is not relevant for $\mathbf{k} \neq 0$ modes. Eq. (4.33) results in

$$P_g^{\rm local}(\mathbf{k}) \simeq (1-2\delta_{\rm b}^g)P_g^{\rm global}(\mathbf{k}). \tag{4.34}$$

Since $\delta_{\rm b}^g = b_1\delta_{\rm b}$ in real space, we finally obtain

$$\begin{aligned} P_g^{\rm local}(\mathbf{k}) \simeq & (1-2\delta_{\rm b}^g)\left[P_g(k) + \frac{\partial P_m(k)}{\partial\delta_{\rm b}}\delta_{\rm b} + \frac{\partial P_m(\mathbf{k})}{\partial\tau_{ij}}\tau_{ij}\right] \\ \simeq & b_1^2 P_{\rm lin}(k) + P_{\rm lin}(k)\left[\frac{5}{21}b_1^2 + 2b_1b_2 - \frac{1}{3}b_1^2\frac{d\ln P_{\rm lin}(k)}{d\ln k}\right]\delta_{\rm b} \\ & + P_{\rm lin}(k)\left[\frac{8}{7}b_1^2 + 2b_1b_{s^2} - b_1^2\frac{d\ln P_{\rm lin}(k)}{d\ln k}\right]\hat{k}_i\hat{k}_j\tau_{ij}, \end{aligned} \tag{4.35}$$

where we have replaced $P_g(k)$ with $b_1^2 P_{\rm lin}(k)$, which is valid at leading order. Note that the response to $\delta_{\rm b}$ suffers from the modulation of the mean galaxy density and the growth term almost cancels out, but the response to τ_{ij} does not suffer in real space. Note also that the effect from τ_{ij} vanishes if one considers the monopole power spectrum.

4.4 Redshift space results

As discussed in the previous section, the large-scale tidal field does not have an effect on the monopole power spectrum in real space. In redshift space, however, anisotropic signals indueced by the large-scale tidal field mimics cosmological distortions such as the RSD and AP effect.

4.4.1 The responses in full three-dimensional redshift-space power spectrum

In order to derive the response functions in redshift space, we compute the galaxy-galaxy-matter bispectrum Eq. (3.41) in the squeezed limit,

$$
\begin{aligned}
B_{ssm}(\mathbf{k},-\mathbf{k}-\mathbf{q},\mathbf{q}) \simeq & 2Z_1(\mathbf{k}+\mathbf{q})Z_2(\mathbf{k}+\mathbf{q},-\mathbf{q})P_{\rm lin}(|\mathbf{k}+\mathbf{q}|)P_{\rm lin}(q) \\
& + 2Z_1(\mathbf{k})Z_2(\mathbf{k},\mathbf{q})P_{\rm lin}(k)P_{\rm lin}(q) \\
= & \left[\frac{13}{7}b_1^2 + 2b_1b_2 - \frac{2}{3}b_1b_{s^2} + \frac{18}{7}b_1f\mu_k^2 + 2b_1^2f\mu_k^2 \right. \\
& \left. +2b_2f\mu_k^2 - \frac{2}{3}b_{s^2}f\mu_k^2 + \frac{5}{7}f^2\mu_k^4 + 2b_1f^2\mu_k^4\right] P_{\rm lin}(k)P_{\rm lin}(q) \\
& + \left[\frac{8}{7}b_1^2 + 2b_1b_{s^2} + \frac{24}{7}b_1f\mu_k^2 + 2b_{s^2}f\mu_k^2 - \frac{16}{7}f^2\mu_k^2 - f^2\mu_k^4 \right. \\
& \left. - \left(b_1^2 + 2b_1f\mu_k^2 + f^2\mu_k^4\right)\frac{d\ln P_{\rm lin}(k)}{d\ln k}\right](\hat{k}\cdot\hat{q})^2P_{\rm lin}(k)P_{\rm lin}(q) \\
& + \left[4b_1f^2\mu_k^3 + 4f^3\mu_k^5 \right. \\
& \left. - \left(b_1^2 + 2b_1f\mu_k^2 + f^2\mu_k^4\right)f\mu_k\frac{d\ln P_{\rm lin}(k)}{d\ln k}\right]\mu_q(\hat{k}\cdot\hat{q})P_{\rm lin}(k)P_{\rm lin}(q) \\
& + \left(b_1^2 - f^2\mu_k^4\right)f\mu_q^2P_{\rm lin}(k)P_{\rm lin}(q), \qquad (4.36)
\end{aligned}
$$

where $\mu_k = \hat{k}\cdot\hat{n}$ and $\mu_q = \hat{q}\cdot\hat{n}$. Substituting this result into Eqs. (4.23) and (4.24), the response of the redshift-space galaxy power spectrum to the large-scale overdensity $\delta_{\rm b}$ is read off as [50]

$$
\begin{aligned}
\frac{\partial P_s(k,\mu)}{\partial\delta_{\rm b}} = & \left[\frac{47}{21}b_1 + 2b_2 - \frac{1}{3}b_1\frac{d\ln P_{\rm lin}(k)}{d\ln k}\right]b_1P_{\rm lin}(k) \\
& + \left[\frac{1}{3}b_1^2 + \mu^2\left(\frac{26}{7}b_1 + 2b_1^2 + 2b_2\right) - \frac{\mu^2}{3}b_1(2+b_1)\frac{d\ln P_{\rm lin}(k)}{d\ln k}\right]fP_{\rm lin}(k) \\
& + \left[\frac{1}{21}(31+70b_1) - \frac{1}{3}(1+2b_1)\frac{d\ln P_{\rm lin}(k)}{d\ln k}\right]f^2\mu^4P_{\rm lin}(k) \\
& + \left[\frac{1}{3}(4\mu^2-1) - \frac{1}{3}\mu^2\frac{d\ln P_{\rm lin}(k)}{d\ln k}\right]f^3\mu^4P_{\rm lin}(k), \qquad (4.37)
\end{aligned}
$$

and to the large-scale tides τ_{ij} as [50]

$$\begin{aligned}\frac{\partial P_s(\mathbf{k},\hat{n})}{\partial \tau_{ij}} &= \left[\frac{8}{7}b_1 + 2b_{s^2} - b_1\frac{d\ln P_{\rm lin}(k)}{d\ln k}\right]\hat{k}_i\hat{k}_j b_1 P_{\rm lin}(k) \\ &+ \left[b_1^2\hat{n}_i\hat{n}_j + \left(\frac{24}{7}b_1 + 2b_{s^2}\right)\mu^2\hat{k}_i\hat{k}_j - b_1\mu\left(2\mu\hat{k}_i\hat{k}_j + b_1 h_{ij}\right)\frac{d\ln P_{\rm lin}(k)}{d\ln k}\right] f P_{\rm lin}(k) \\ &+ \left[\frac{16}{7}\mu\hat{k}_i\hat{k}_j + 4b_1 h_{ij} - \left(\mu\hat{k}_i\hat{k}_j + 2b_1 h_{ij}\right)\frac{d\ln P_{\rm lin}(k)}{d\ln k}\right]\mu^3 f^2 P_{\rm lin}(k) \\ &+ \left[(4\mu h_{ij} - \hat{n}_i\hat{n}_j) - \mu h_{ij}\frac{d\ln P_{\rm lin}(k)}{d\ln k}\right]\mu^4 f^3 P_{\rm lin}(k), \end{aligned} \tag{4.38}$$

where $h_{ij} \equiv k_{(i}n_{j)} = \frac{1}{2}(k_i n_j + n_i k_j)$. These are the full expressions of the responses of redshift-space power spectrum to the large-scale perturbations. Compared with the results in real space Eq. (4.30), there are additional effects of the super-sample modes on the redshift-space power spectrum, that is, there are terms including the couplings between the large-scale tide τ_{ij} and the line-of-sight direction $\hat{n}$ as expected. In the limit $f \to 0$, the above equations reduce to the real-space results Eqs. (4.29) and (4.30) and the response function for $\delta_{\rm b}$, $\partial P_s(k,\mu)/\partial\delta_{\rm b}$, agrees with Eq. (65) in Ref. [86] if we set $b_1 = 1$ and $b_2 = b_{s^2} = 0$ in the above equation. Notice that the response to the isotropic super-sample mode $\delta_{\rm b}$ can depend on only k and μ because it preserves the rotational symmetry around the observer.

From Eq. (4.38) we can find several types of anisotropies in the redshift-space power spectrum: the standard RSD effect $\mu^2 = \hat{k}_i\hat{k}_j\hat{n}_i\hat{n}_j$ (Kaiser factor), and the effects due to τ_{ij} that have dependences of $\tau_{ij}\hat{k}_i\hat{k}_j$, $\tau_{ij}\hat{k}_i\hat{n}_j$, and $\tau_{ij}\hat{n}_i\hat{n}_j$, respectively. First, let us remind of the physical origin of the Kaiser factor. It comes from $\partial_i v_j \hat{n}_i\hat{n}_j$ (see Eq. (3.28)). This means that the Kaiser anisotropy reflects the projection of the velocity shear ($\partial_{(i}v_{j)}$, in Fourier space $\propto \hat{k}_i\hat{k}_j$) onto the line-of-sight direction. In other words, since the velocity shear corresponds to the tidal field, the Kaiser factor can be interpreted as the projection of the short-mode tidal field onto the line-of-sight direction. The terms proportional to $\tau_{ij}\hat{k}_i\hat{k}_j$ represent a coupling between the large-scale tide τ_{ij} and the small-scale tide, where the latter has directional dependences given by $\propto \left(\hat{k}_i\hat{k}_j - \frac{1}{3}\delta^K_{ij}\right)$. The terms of $\tau_{ij}\hat{n}_i\hat{n}_j$ are like the Kaiser factor, that is, the projection of the large-scale tide τ_{ij} onto the line-of-sight direction. Note that the terms proportional to h_{ij} always appear with $\mu = \hat{k}\cdot\hat{n}$, because of the parity invariance of the power spectrum, i.e. $P_s(\mathbf{k}) = P_s(-\mathbf{k})$. Then, $\tau_{ij}\hat{k}_i\hat{n}_j\mu = \tau_{ij}\hat{k}_i\hat{k}_\ell\hat{n}_j\hat{n}_\ell$ is a consequence of the projection of the coupling between the large-scale tide τ_{ij} and the small-scale velocity $\propto \hat{k}_i$ onto the line-of-sight direction.

Finally, let us consider the mean density modulation effect in redshift space. In redshift space, the Kaiser formula Eq. (3.30) tells that $\delta^g_{\rm b}$ is related to the super-

sample modes,

$$\delta_{\rm b}^g = \left[b_1 + f(\hat{q}\cdot\hat{n})^2\right]\delta_{\rm b} = \left(b_1 + \frac{1}{3}f\right)\delta_{\rm b} + f\tau_{ij}\hat{n}^i\hat{n}^j, \tag{4.39}$$

at lowest order. After all, at leading order of the super-sample modes, the observed power spectrum of galaxies with the effects of the super-sample modes is expressed as

$$\begin{aligned} P_s^{\rm local}(\mathbf{k},\hat{n}) \simeq & (1-2\delta_{\rm b}^g)P_s^{\rm global}(\mathbf{k},\hat{n}) \\ = & (b_1+f\mu^2)^2 P_{\rm lin}(k) \\ & + \left[-2\left(b_1+\frac{1}{3}f\right)(b_1+f\mu^2)P_{\rm lin}(k) + \frac{\partial P_s(k,\mu)}{\partial\delta_{\rm b}}\right]\delta_{\rm b} \\ & + \left[-2f(b_1+f\mu^2)^2 P_{\rm lin}(k)\hat{n}^i\hat{n}^j + \frac{\partial P_s(\mathbf{k},\hat{n})}{\partial\tau_{ij}}\right]\tau_{ij}. \end{aligned} \tag{4.40}$$

We use this power spectrum in the Fisher analysis.

4.4.2 The large-scale mode effects on the two-dimensional redshift-space power spectrum: $P_s^{\rm 2D}(k_\parallel, k_\perp)$

One of the main purposes of this thesis is to estimate the impact of super-sample modes on the RSD measurements as well as the Alcock-Paczyński (AP) test through a measurement of the redshift-space power spectrum. To do this, we employ the standard approach used in an analysis of the redshift-space power spectrum. Since the RSD and AP effect are only along the line-of-sight direction and does not affect the clustering pattern in the two-dimensional plane perpendicular to the line-of-sight direction, a usual way to measure the redshift-space power spectrum is making the angle average given as

$$P_s^{\rm 2D}(k_\parallel, k_\perp; \delta_{\rm b}, \tau_{ij}) \equiv \int_0^{2\pi}\frac{d\varphi_{\mathbf{k}_\perp}}{2\pi}\, P_s(\mathbf{k}; \delta_{\rm b}, \tau_{ij}), \tag{4.41}$$

where we have set the line-of-sight direction as z-axis, $\hat{n}_i = \delta_{i3}^K$ and used the decomposition of wavevector, $\mathbf{k} = (k_\perp\cos\varphi_{\mathbf{k}_\perp}, k_\perp\sin\varphi_{\mathbf{k}_\perp}, k_\parallel)$ with the conditions $(k_\perp, k_\parallel) = k\left(\sqrt{1-\mu^2}, \mu\right)$.

By inserting Eqs.(4.40) and (4.37)-(4.38) into Eq. (4.41) we can find

$$\begin{aligned}
P_s^{\rm 2D}(k_\perp, k_\parallel; \delta_{\rm b}, \tau_{ij}) =& (b_1 + f\mu^2)^2 P_{\rm lin}(k) \\
&+ \left[-2\left(b_1 + \frac{1}{3}f\right)(b_1 + f\mu^2)P_{\rm lin}(k) + \frac{\partial P_s(k,\mu)}{\partial \delta_{\rm b}}\right]\delta_{\rm b} \\
&+ b_1\left[\left(\frac{8}{7}b_1 + 2b_{s^2}\right)P_{\rm lin}(k) - b_1\frac{dP_{\rm lin}(k)}{d\ln k}\right]\frac{3\mu^2-1}{2}\tau_{33} \\
&+ f\left[\left\{b_1^2 + \left(\frac{12}{7}b_1 + b_{s^2}\right)\mu^2(3\mu^2-1)\right\}P_{\rm lin}(k)\right. \\
&\qquad \left. - b_1\mu^2\left\{b_1 + (3\mu^2-1)\right\}\frac{dP_{\rm lin}(k)}{d\ln k}\right]\tau_{33} \\
&+ f^2\mu^4\left[\left\{4b_1 + \frac{8}{7}(3\mu^2-1)\right\}P_{\rm lin}(k)\right. \\
&\qquad \left. - \left(2b_1 + \frac{3\mu^2-1}{2}\right)\frac{dP_{\rm lin}(k)}{d\ln k}\right]\tau_{33} \\
&+ f^3\mu^4\left[\left(4\mu^2-1\right)P_{\rm lin}(k) - \mu^2\frac{dP_{\rm lin}(k)}{d\ln k}\right]\tau_{33}, \qquad (4.42)
\end{aligned}$$

where we have used the following identities under the presence of the line-of-sight direction

$$\begin{aligned}
\int_0^{2\pi}\frac{d\varphi_{\mathbf{k}_\perp}}{2\pi}\hat{k}_i\hat{k}_j &= \frac{1-\mu^2}{2}\delta^K_{ij} + \frac{3\mu^2-1}{2}\hat{n}_i\hat{n}_j, \\
\int_0^{2\pi}\frac{d\varphi_{\mathbf{k}_\perp}}{2\pi}\hat{k}_i &= \mu\hat{n}_i, \qquad (4.43)
\end{aligned}$$

with the trace-less condition of τ_{ij}, i.e. $\tau_{ij}\delta^K_{ij} = 0$. Notice that while τ_{ij} has the five degrees of freedom there remains only one component, τ_{33}, in the two-dimensional power spectrum after the angle average. Eq. (4.42) shows that the large-scale density field and large-scale tide cause an additional anisotropic clustering in the two-dimensional redshift-space power spectrum in addition to the Kaiser distortion. The super-smaple modes cause anisotropic distortions up to the order of μ^6, while the standard Kaiser RSD effect causes distortions up to μ^4 (Multipole power spectra are presented in Appendix C). The amount of the distortion depends on $\delta_{\rm b}$ and the line-of-sight component of the tide, τ_{33}, in a given survey realization. Thus the super-sample modes in a given survey realization cause a bias in the redshift-space power spectrum. There are two ways to take into account the effect. One way is to include the effect as an additional noise in the error covariance matrix of the power spectrum as studied in Ref. [31, 37]. An alternative approach, which we adopt in this thesis, is to treat the effect as an additional parameter rather than noise [32]. We can model this effect by treating the bias as a purely systematic additive shift

in the redshift-space power spectrum, where an amount of the bias is given by the power spectrum response multiplied by a free parameter $\delta_{\rm b}$ and τ_{33}. In the next subsection, we study how the large-scale tide could cause a degradation in cosmological parameters.

4.5 Impact on the estimation of cosmological parameters

In this section, following Refs. [45] and [46], we study how the large-scale tide affects the BAO and RSD measurements in the redshift-space power spectrum, based on the Fisher information matrix formalism. In the following we focus on τ_{33}, and we do not consider the response for $\delta_{\rm b}$ because the effect of $\delta_{\rm b}$ can be estimated by lensing surveys [31, 32].

4.5.1 Fisher information matrix for the two-dimensional power spectrum

As a theoretical template of the power spectrum, taking into account the RSD and AP effect, we use the following redshift-space galaxy power spectrum measured in a hypothetical survey realization in linear regime,

$$P^{\rm 2D}_{s,{\rm obs}}(k_{\parallel,{\rm obs}}, k_{\perp,{\rm obs}}; \tau_{33}) = \frac{D^2_{A,{\rm fid}} H}{D^2_A H_{\rm fid}} P^{\rm 2D}_s\left(k_\parallel, k_\perp; \tau_{33}\right) + P_{\rm sn}, \tag{4.44}$$

where $P^{\rm 2D}_{s,{\rm obs}}$ is the "observed" or "estimated" power spectrum from a given survey realization, $P^{\rm 2D}_s$ on the right-hand side is the underlying true power spectrum (Eq. (4.42)), measured if an observer employs the true cosmological model, and $P_{\rm sn}$ is a parameter (constant number) to model a possible contamination of a residual shot noise to the power spectrum measurement.

The Fisher information matrix for the two-dimensional power spectrum is given by

$$\begin{aligned} F_{\alpha\beta} &= -\left\langle \frac{\partial^2 \log L}{\partial\theta_\alpha \partial\theta_\beta} \right\rangle \\ &= \sum_{kk'} \sum_{\mu\mu'} \frac{\partial P^{\rm 2D}_{s,{\rm obs}}(k,\mu)}{\partial\theta_\alpha} {\rm Cov}^{-1}\left[P^{\rm 2D}_{s,{\rm obs}}(k,\mu), P^{\rm 2D}_{s,{\rm obs}}(k',\mu')\right] \frac{\partial P^{\rm 2D}_{s,{\rm obs}}(k',\mu')}{\partial\theta_\beta}, \end{aligned} \tag{4.45}$$

where L is the likelihood, θ_α is the α-th parameter of interest and $\partial P^{\rm 2D}_{s,{\rm obs}}/\partial\theta_\alpha$ is the partial derivative of the galaxy power spectrum (Eq. (4.44)) with respect to the α-th parameter around the fiducial cosmological model. The Cramér-Rao bound states that the minimum possible errors on parameter α, marginalized over all other parameters, are given by the square root of the diagonal components of the inverse of the Fisher matrix as

$$\Delta\theta_\alpha \geq \sqrt{(F^{-1})_{\alpha\alpha}}, \tag{4.46}$$

while the unmarginalized ones are given by $\Delta\theta_\alpha = 1/\sqrt{F_{\alpha\alpha}}$. The cross-correlation coefficients $c_{\alpha\beta}$ are defined through

$$c_{\alpha\beta} = \frac{(F^{-1})_{\alpha\beta}}{\sqrt{(F^{-1})_{\alpha\alpha}(F^{-1})_{\beta\beta}}}. \tag{4.47}$$

The covariance matrix for the two-dimensional redshift-space power spectrum of galaxies is given in the Gaussian limit as [87]

$$\mathrm{Cov}\left[P^{\mathrm{2D}}_{s,\mathrm{obs}}(k,\mu), P^{\mathrm{2D}}_{s,\mathrm{obs}}(k',\mu')\right] = \frac{2}{N_k}\left[P^{\mathrm{2D}}_{s,\mathrm{obs}}(k,\mu) + \frac{1}{\bar{n}_g}\right]^2 \delta^3_{\mathrm{D}}(\mathbf{k}-\mathbf{k}'), \tag{4.48}$$

where $N_k = 4\pi k^2 \Delta k V/(2\pi)^3$ is the number of modes with survey volume V and the interval between each Fourier mode Δk, $\bar{n}_g$ is the mean number density of galaxies and $1/\bar{n}_g$ term represents the Poisson shot noise. Then, taking the continuum limit, the Fisher information matrix can be rewritten as

$$\begin{aligned} F^{\mathrm{galaxy}}_{\alpha\beta} &= \int_{-1}^{1}\frac{d\mu}{2}\int_{k_{\mathrm{min}}}^{k_{\mathrm{max}}}\frac{k^2\mathrm{d}k}{4\pi^2}\frac{\partial \ln P^{\mathrm{2D}}_{s,\mathrm{obs}}(k,\mu;z_i)}{\partial\theta_\alpha}\frac{\partial \ln P^{\mathrm{2D}}_{s,\mathrm{obs}}(k,\mu;z_i)}{\partial\theta_\beta} \\ &\quad \times V_{\mathrm{eff}}(k;z_i)\exp\left[-k^2\Sigma_\perp^2 - k^2\mu^2(\Sigma_\parallel^2-\Sigma_\perp^2)\right], \end{aligned} \tag{4.49}$$

where the effective survey volume V_{eff} is defined as

$$V_{\mathrm{eff}}(k,\mu;z_i) \equiv \left[\frac{\bar{n}_g(z_i)P^{\mathrm{2D}}_{s,\mathrm{obs}}(k,\mu;z_i)}{\bar{n}_g(z_i)P^{\mathrm{2D}}_{s,\mathrm{obs}}(k,\mu;z_i)+1}\right]^2 V(z_i), \tag{4.50}$$

with $V(z_i)$ being the comoving volume of a galaxy survey centered at redshift z_i and the exponential damping factor we have introduced outside of the derivatives of $P^{\mathrm{2D}}_{s,\mathrm{obs}}$ in Eq. (4.49) explains the smearing effect, which arises from the highly nonlinear gravitational evolution. Here the Lagrangian displacement fields $\Sigma_\parallel$ and Σ are given as

$$\Sigma_\perp(z) \equiv c_{\mathrm{rec}}D(z)\Sigma_0, \tag{4.51}$$

$$\Sigma_\parallel(z) \equiv c_{\mathrm{rec}}D(z)(1+f)\Sigma_0, \tag{4.52}$$

where Σ_0 is the Lagrangian linear displacement field at the present, computed as $\Sigma_0 = 11h^{-1}\mathrm{Mpc}$ for $\sigma_8 = 0.8$, and c_{rec} is a parameter to control the BAO reconstruction method, which is briefly explained below [88].

The nonlinear gravitational evolution pushes galaxies from their initial position, which erases the higher harmonics of the BAO feature in the power spectrum [89]. However, since the large-scale velocity field of galaxies resided in the large-scale structure can be inferred from the measured galaxy density field via the continuity equation, by using this inferred velocity field, we can pull back each galaxy to its

position at an earlier epoch and thereby reconstruct the galaxy distribution more in the linear regime. With this reconstructed field, we can correct to some extent the smearing effect in Eq. (4.49) and sharpen the acoustic peaks in the galaxy power spectrum. This is called as the BAO reconstruction method and now commonly implemented in an analysis of galaxy survey [90], which shows that in the reconstructed field the nonlinear smoothing scale is reduced from $\Sigma_{\rm nl} = 8.1\ h^{-1}$Mpc to $\Sigma_{\rm nl} = 4.4\ h^{-1}$Mpc, about a factor of 2 reduction. Thus in the Fisher matrix calculation we use $c_{\rm rec} = 0.5$ as a default choice [90].

We include the parameter for the large-scale tide for the survey volume, i.e., τ_{33} in addition to the cosmological parameters, the distances in each redshift slice, and other nuisance parameters:

$$\theta_\alpha = \{\tau_{33}, D_A(z), H(z), b_1(z), \beta(z), P_{\rm sn}(z), \Omega_{\rm m0}, A_s, n_s, \alpha_s, \Omega_{\rm m0}h^2, \Omega_{\rm b0}h^2\}, \quad (4.53)$$

where $\beta = f/b_1$ and A_s, n_s and α_s are parameters of the primordial power spectrum; A_s is the amplitude of the primordial curvature perturbation, and n_s and α_s are the spectral tilt and the running spectral index. The set of cosmological parameters determines the shape of the linear power spectrum. Since the effect of the higher-order bias, b_2 and b_{s^2}, on the power spectrum is of the order of $\mathcal{O}\left((\delta^{(1)})^2\right)$, compared with the $\mathcal{O}((\delta^{(1)}))$ effect in b_1, we ignore the higher order bias for simplicity. For the k-integration, we set $k_{\rm min} = 10^{-4}h/$Mpc and $k_{\rm max} = 0.5\ h/$Mpc, but the exponential factor in Eq. (4.49) suppresses the information from the nonlinear scales. The Fisher parameter forecasts depend on the fiducial cosmological model for which we assumed the model being consistent with the WMAP 7-year data [12]. In this section, we consider a single redshift slice, and then consider 12 parameters in total in the Fisher analysis.

In the following forecast, we consider the combination of the galaxy spectroscopic survey with the CMB constraints expected from the Planck experiment:

$$\boldsymbol{F} = \boldsymbol{F}^{\rm CMB} + \boldsymbol{F}^{\rm galaxy}, \quad (4.54)$$

where $\boldsymbol{F}^{\rm CMB}$ is the Fisher matrix for the CMB measurements. To compute the CMB Fisher matrix, we employ the method developed in Ref. [91].

4.5.2 Results

As a working example, we consider a hypothetical survey that is characterized by the central redshift $z = 0.5$, the comoving volume $V = 1\ ({\rm Gpc}/h)^3$, the mean number density of galaxies $\bar{n}_g = 10^{-3}\ (h/{\rm Mpc})^3$ and linear bias parameter $b_1 = 2$, respectively. For simplicity we consider a single redshift slice. In reality, when a

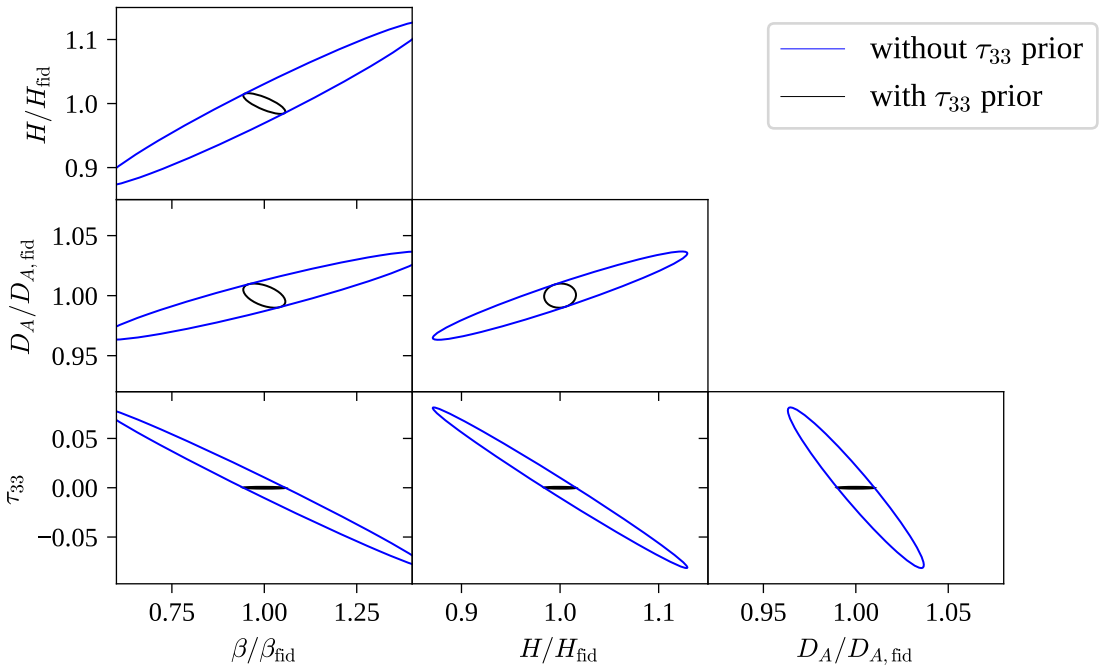

Figure 4.1: 68% CL error ellipse for the parameters, τ_{33}, D_A, H and β, including marginalization over other parameters in the Fisher analysis (see Section 4.5.1 for details). The inner black contour in each panel shows the result when $\sigma_{\tau_{33}} = 1.04 \times 10^{-3}$ is employed as the τ_{33} prior, which is taken from the rms value expected for the ΛCDM model and the assumed galaxy survey that is characterized by $V = 1\ ({\rm Gpc}/h)^3$, $\bar{n}_{\rm g} = 10^{-3}\ (h/{\rm Mpc})^3$ and $b_1 = 2$.

galaxy redshift survey probes galaxies over a wide range of redshifts, one can use the clustering analysis in multiple redshift slices and then combine their cosmological information.

In Fig. 4.1 we show the marginalized 68% CL error contours in each of two-dimensional sub-space that include either two of the large-scale tidal parameter, τ_{33}, the distance parameters, D_A or H, or the RSD parameter β, where the contours include marginalization over other parameters. Note that τ_{33} has no correlations with other parameters. More quantitatively, the cross-correlation coefficients c_{ij} with $i = \tau_{33}$, after the CMB Fisher matrix is added, is almost unity for either one of these three parameters is taken for j, while the cross-coefficients are smaller for other parameters, less than $\mathcal{O}(0.2)$. The contours in each panel of Fig. 4.1 show how an uncertainty in τ_{33} causes a degeneracy with estimation of other parameter. Since the large-scale tide causes apparent anisotropies in the observed clustering of galaxies as the radial AP anisotropy and the RSD effect do, allowing τ_{33} to freely vary in the parameter estimation causes significant degeneracies with β and H. The

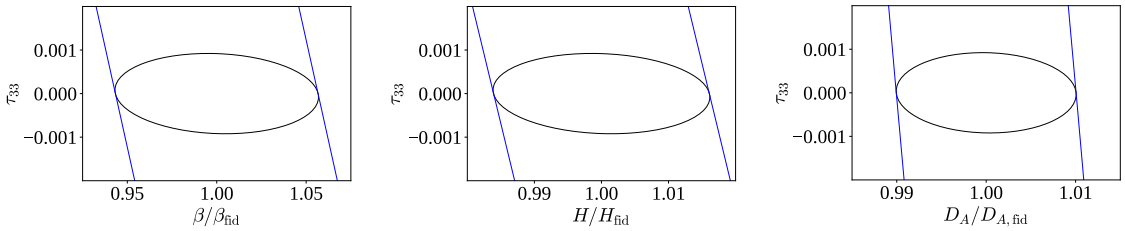

Error ellipse for τ_{33} and β | Error ellipse for τ_{33} and H | Error ellipse for τ_{33} and D_A

Figure 4.2: A zoom-in version of Fig. 4.1, around the fiducial model for the Fisher analysis.

degeneracy between τ_{33} and D_A arises from the trace-less nature of τ_{ij}; changing τ_{33} leads to a change in $\tau_{11}+\tau_{22}(=-\tau_{33})$ and therefore causes an apparent distortion in the $k_\perp$-direction, which mimics the cosmological distortion due to a change in D_A.

However, if adding the prior on τ_{33} assuming the ΛCDM model, i.e., $\tau_{33}=0$ for the expectation value and $\sigma_{\tau_{33}}=1.04\times10^{-3}$ for the rms value for $V=1$ $(\mathrm{Gpc}/h)^3$, which can be computed from Eq. (4.14), it lifts the degeneracies, recovering a high-precision measurement for each cosmological parameter. Fig. 4.2 shows a zoom-in version of the contours around the central value (the input model in the Fisher analysis) and shows that the prior of τ_{33} efficiently breaks the parameter degeneracies. In particular, even if an actual value of τ_{33} in a given survey realization is off from zero by more than a few $\sigma_{\tau_{33}}$, it does not seem to cause a significant bias in other parameters. Therefore, as long as the ΛCDM model is assumed, its effect is negligible. It should be noted that the range of marginalized error of τ_{33} in Figures 4.1 and 4.2 is sufficiently smaller than unity, for a hypothetical measurement of the redshift-space power spectrum for a volume of 1 $(\mathrm{Gpc}/h)^3$. Thus our assumption that the super-sample modes are in the linear regime is safely satisfied.

Instead of treating the super-sample effect as a new error source, it is interesting to ask whether a measurement of redshift-shift power spectrum of galaxies can be used to constrain the large-scale tide, τ_{33}, rather than employing the prior computed from the ΛCDM model, if one can include the information up to the larger k beyond the weakly nonlinear regime. As can be seen from Fig. 4.1 and Fig. 4.2, marginalized 1σ error range of the τ_{33} without prior is still small enough to take only the leading order in the Taylor expansion for the long-mode, while this error range is bigger than the rms of the τ_{33} expected from ΛCDM. This means that our formulation is valid for not assuming ΛCDM for the super-sample modes. To address this possibility, we need to know the response of the redshift-space power spectrum to the tide, $\partial P_s(\mathbf{k})/\partial\tau_{33}$, in the nonlinear regime where the perturbation theory breaks down. To estimate the response function in the nonlinear regime requires to develop a

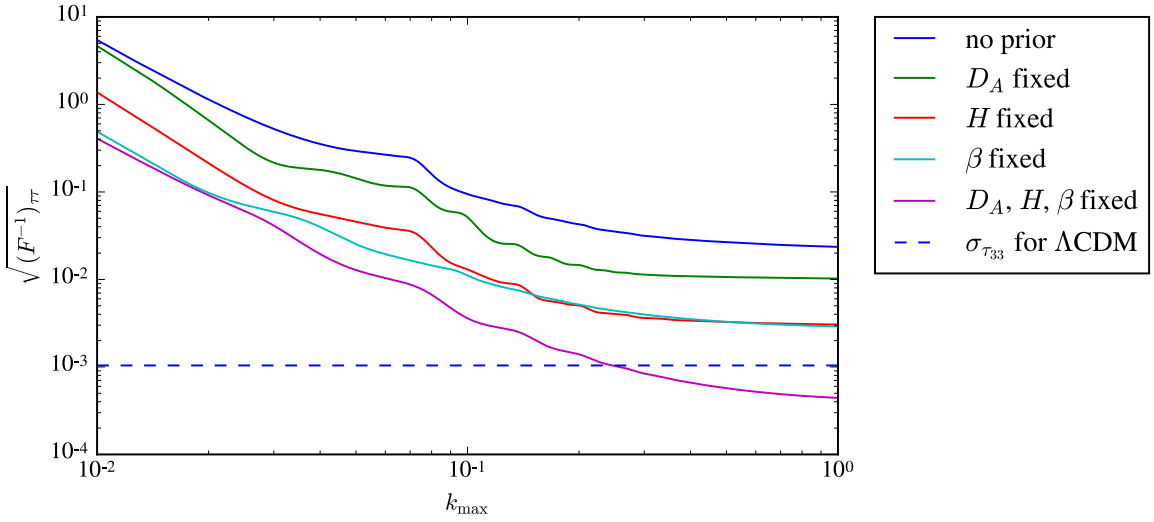

Figure 4.3: The marginalized error on the estimation of τ_{33}, $\sqrt{(F^{-1})_{\tau\tau}}$, as a function of the maximum wavenumber $k_{\rm max}$ up to which the redshift-space power spectrum information is included in the Fisher analysis (see text for the details). The different solid curves show the results when any prior on other parameters (D_A, H and β) are not employed or when some or all the parameters are fixed to their values for the ΛCDM model. The horizontal dashed curve is the rms value, $\sigma_{\tau_{33}}$, expected for the ΛCDM model and the survey volume. Note that we did not impose any prior on other parameters (Eq. (4.53)), although the CMB information is added.

separate universe simulation where the large-scale tidal effect is included in the background expansion, similarly to the method used for estimating the response for the mean density modulation, $\partial P(k)/\partial\delta_{\rm b}$, in Refs. [31, 32, 49, 92]. This issue is discussed in Chapter 5, so here we simply assume that the response function derived using the perturbation theory holds in the nonlinear regime. Furthermore, to include the effect of the large-scale tide up to the nonlinear regime, we set $\Sigma = 0$ for the BAO smearing factor in the Fisher analysis. In practice, the smearing factor also depends on nonlinear structure formation, and therefore would depend on τ_{33}. While we ignore the smearing effect and use the prediction from the perturbation theory, we consider that the following result gives a rough estimation of the genuine effect.

Fig. 4.3 shows how an accuracy of the τ_{33} estimation is improved when including the redshift-space power spectrum information up to a given maximum wavenumber $k_{\rm max}$. Without any prior, τ_{33} is estimated to about 1% accuracy for a survey volume of $V = 1\ ({\rm Gpc}/h)^3$. When fixing other parameters to their values for the ΛCDM model, the accuracy of the estimation of τ_{33} is dramatically improved. In particular,

when all the distortion parameters, D_A, H and β, are fixed, the τ_{33} parameter could be determined to an accuracy better than the rms for the ΛCDM model, if the redshift-space power spectrum information is included up to $k_{\rm max} \gtrsim 0.25\ h/{\rm Mpc}$. This result implies that the anisotropic clustering information in such a nonlinear regime could be used to infer the large-scale tide for a given survey realization, if we can separate the anisotropic signals from the super-sample tidal modes from other cosmological distortions.

4.6 The bipolar spherical harmonic expansion (BipoSH) and the super-sample signal

As discussed in Section 4.5, we can obtain the information on the super-sample tidal modes whose wavelength is beyond the survey scale, if the parameter degeneracies between the large-scale tides and RSD and AP effects are resolved. To break the parameter degeneracy, we would like to use extra degrees of freedom of the observed galaxy power spectrum, i.e., *violation of statistical isotropy*.

The super-sample tidal perturbation generates a preferred direction in a given local survey region and breaks statistical isotropy [37, 38, 50, 93]. The anisotropic distortion induced by the RSD and AP effects, where the statistical isotropy still holds, is characterized by an angle between the wave vector $\mathbf{k}$ and the line-of-sight (LOS) unit vector $\hat{n}$ and thus can entirely be decomposed using the Legendre polynomials $\mathcal{L}_\ell(\hat{k}\cdot\hat{n})$. In order to extract information on the breaking of statistical isotropy due to the super-sample tidal modes, Ref. [94] proposed an expansion scheme of the three-dimensional power spectrum with spherical harmonics functions. The authors decomposed the $\mathbf{k}$-dependence according to $P_s(\mathbf{k},\hat{n}) = \sum_{\ell m} P_{\ell m}(k)Y_{\ell m}(\hat{k})$ after the LOS direction $\hat{n}$ is defined as a z-axis. Note that the $m = 0$ mode corresponds to the coefficient in the normal Legendre expansion scheme since $Y_{\ell 0} \propto \mathcal{L}_\ell$. They found that the signals due to the RSD effect are confined to $m = 0$, while the tidal perturbation creates non-vanishing $m \neq 0$ modes. The authors further performed a Fisher matrix computation and showed that their decomposition formalism can break the degeneracy between the RSD effect and the super-sample tidal one except for its LOS component.

In this section, we examine the distinguishability between the super-sample tidal effect and the other two ones (the RSD and AP effects) by employing a more general decomposition based on bipolar spherical harmonics (BipoSH) $\{Y_\ell(\hat{k}) \otimes Y_{\ell'}(\hat{n})\}_{LM}$ [95]. This was recently applied to probing primordial statistical anisotropy induced by some sort of vector inflation models [96–98]. [1]

Through this decomposition, statistically anisotropic signals are confined to the $L \neq 0$ BipoSH coefficients. We here follow the methodology developed in Ref. [96], and, differently from Ref. [94], we do not fix $\hat{n}$ to any specific direction. This treatment is reasonable for actual data analysis because it is impossible to determine a global LOS direction $\hat{n}$ in observed galaxy samples. In Ref. [97], the BipoSH formalism was already applied to observed galaxy samples in order to constrain

[1] The BipoSH decomposition was initially introduced for dealing with the wide-angle effect in the power spectrum [99–103]. For an application to the galaxy bispectrum analysis, See Ref. [104].

statistically anisotropic signals. There, the effects of observational systematics, e.g., artificial asymmetries due to specific survey geometry, were also decomposed and hence properly subtracted. The same data analysis pipeline will also be applicable to the measurements of the super-sample tidal modes.

4.6.1 Formalism of the bipolar spherical harmonic expansion

The power spectrum which depends upon two directions, $\hat{k}$ and $\hat{n}$, can be expressed using the following coordinates:

$$\mathbf{k} = k(\sin\theta_k\cos\phi_k,\ \sin\theta_k\sin\phi_k,\ \cos\theta_k), \tag{4.55}$$

$$\hat{n} = (\sin\theta_n\cos\phi_n,\ \sin\theta_n\sin\phi_n,\ \cos\theta_n). \tag{4.56}$$

In general, to get the multiple moments that have no angular dependence requires a four-multiple integration, which is the case for the BipoSH expansion as we will see in the next section. Note that the reason why we usually need only one-dimensional integral for the power spectrum multipoles in redshift space is that the usual RSD anisotropy still preserves the three-dimensionally rotational symmetry around the observer. In that case, the four-multiple integration reduces to one-dimensional integral thanks to the rotational symmetry. We here emphasis that, differently from Ref. [94], throughout this thesis, the LOS direction is not set to the global one although the local plane-parallel approximation is adopted.

To capture the violation of the three-dimensional rotational symmetry, the three-dimensional power spectrum $P_s(\mathbf{k}, \hat{n}; \delta_\mathrm{b}, \tau_{ij})$ in redshift space should be expanded using the bipolar spherical harmonic (BipoSH) basis $X^{LM}_{\ell\ell'}$ [96],

$$P_s(\mathbf{k}, \hat{n}; \delta_\mathrm{b}, \tau_{ij}) = \sum_{LM\ell\ell'} \pi^{LM}_{\ell\ell'}(k; \delta_\mathrm{b}, \tau_{ij}) X^{LM}_{\ell\ell'}(\hat{k}, \hat{n}), \tag{4.57}$$

where the BipoSH basis is defined as [95]

$$X^{LM}_{\ell\ell'}(\hat{k}, \hat{n}) = \{Y_\ell(\hat{k}) \otimes Y_{\ell'}(\hat{n})\}_{LM} = \sum_{mm'} \mathcal{C}^{LM}_{\ell m \ell' m'} Y_{\ell m}(\hat{k}) Y_{\ell' m'}(\hat{n}) \tag{4.58}$$

$$= \sum_{mm'} (-1)^{\ell-\ell'+M} \sqrt{2L+1} \begin{pmatrix} \ell & \ell' & L \\ m & m' & -M \end{pmatrix} Y_{\ell m}(\hat{k}) Y_{\ell' m'}(\hat{n}), \tag{4.59}$$

with $\mathcal{C}^{LM}_{\ell m \ell' m'}$ being the Clebsch-Gordan coefficients and $\left(\begin{smallmatrix} \ell_1 & \ell_2 & \ell_3 \\ m_1 & m_2 & m_3 \end{smallmatrix}\right)$ being the Wigner $3j$ symbol. The inverting translation is given by

$$\pi^{LM}_{\ell\ell'}(k) = \int d^2\hat{k} \int d^2\hat{n}\ P_s(\mathbf{k}, \hat{n}) [X^{LM}_{\ell\ell'}(\hat{k}, \hat{n})]^*, \tag{4.60}$$

owing to the orthogonal property of the $X^{LM}_{\ell\ell'}$ basis:

$$\int d^2\hat{k} \int d^2\hat{n}\; X^{L_1M_1}_{\ell_1\ell'_1}(\hat{k},\hat{n})[X^{L_2M_2}_{\ell_2\ell'_2}(\hat{k},\hat{n})]^* = \delta^K_{L_1L_2}\delta^K_{M_1M_2}\delta^K_{\ell_1\ell_2}\delta^K_{\ell'_1\ell'_2}. \tag{4.61}$$

To relate the coefficients of the bipolar spherical harmonic expansion with those of usual Legendre expansion, let us introduce the *reduced* coefficients defined in Refs. [96, 97]

$$P^{LM}_{\ell\ell'}(k) \equiv \pi^{LM}_{\ell\ell'}(k)(-1)^L \frac{\sqrt{(2L+1)(2\ell+1)(2\ell'+1)}}{4\pi} H_{\ell\ell' L}, \tag{4.62}$$

where $H_{\ell_1\ell_2\ell_3} \equiv \begin{pmatrix} \ell_1 & \ell_2 & \ell_3 \\ 0 & 0 & 0 \end{pmatrix}$ and $H_{\ell\ell' L} = 0$ when $\ell + \ell' + L$ is odd. In our case, $\pi^{LM}_{\ell\ell'}$ vanishes for $\ell+\ell'+L =$ odd and hence $P^{LM}_{\ell\ell'}$ is sufficient to capture all information of three-dimensional power spectrum. The explicit relationships between the *reduced* coefficients $P^{LM}_{\ell\ell'}(k)$ and the usual Legendre coefficients $P_\ell(k)$ and between $P^{LM}_{\ell\ell'}(k)$ and the coefficients obtained via the expansion scheme of Ref. [94] are presented in Appendix C.2.

The advantages of employing the BipoSH expansion are two following aspects: (1) The BipoSH can extract the full three-dimensional anisotropic power spectrum and (2) we need not set the LOS to the z-axis. The reason why the point (1) is important is that the RSD and AP distortions generate only two-dimensional asymmetry; i.e., anisotropic signature appears only about the LOS direction, characterized by the radial components of the wave vector, $\hat{k}_\parallel = \hat{n}$, whereas the super-sample tidal effect sources the full three-dimensional asymmetry; i.e., anisotropic imprint appears not only about the LOS direction but also in the transverse plane, characterized by both $\hat{k}_\parallel$ and $\hat{k}_\perp = \widehat{\mathbf{k} - \mathbf{k}_\parallel}$.

To put the point (2) another way, the use of the BipoSH expansion requires the multiple LOS directions as implied by the integration of the LOS direction (see Eq. (4.60)). Thus, the BipoSH expansion can be applied to all-sky or wide-area surveys. In fact, different LOS directions are essential to break the degeneracies between the super-sample tidal effect and other anisotropic effects. The point is that the RSD and AP distortion respect the rotational symmetry around the observer, whereas the super-sample tidal modes violate the rotational invariance.

To elucidate this point further, let us consider a simplified situation where we have two different LOS; $\hat{n}_1 = (1,1,1)/\sqrt{3}$ and $\hat{n}_2 = (-1,-1,1)/\sqrt{3}$ (see Fig. 4.4). Under the local plane-parallel approximation, we observe the galaxy pairs on the tangential plane for each LOS (the red planes in Fig. 4.4). For both $\hat{n}_1$ and $\hat{n}_2$ direction, we should measure the same power spectrum in the absence of τ_{ij} because in that case the apparent anisotropy in the power spectrum depends only $\mu = (\hat{k}\cdot\hat{n})$, which is rotationally invariant around the observer. On the other hand,

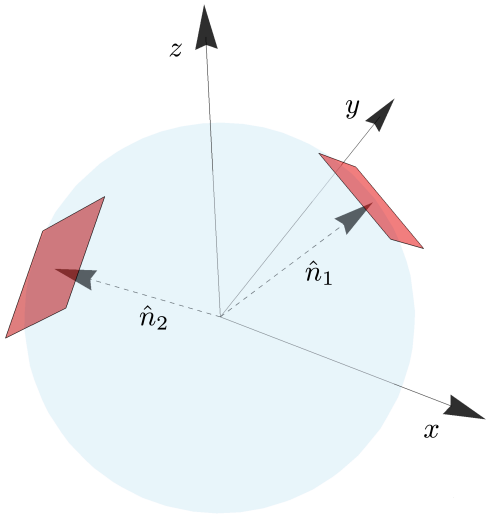

Figure 4.4: A schematic picture for an all-sky galaxy survey. The observer is at the origin. $n_1 = (1,1,1)/\sqrt{3}$ and $n_2 = (-1,-1,1)/\sqrt{3}$ depict different line-of-sight (LOS) direction. In the local plane parallel approximation, the pairs of galaxies are measured in each red plane, which is the tangential plane to each LOS direction.

the terms with super-sample tidal modes violate this rotational symmetry. For example, let us consider the term of $\tau_{ij}\hat{n}_i\hat{n}_j$. This anisotropy appears with the form of $2(\tau_{12}+\tau_{13}+\tau_{23})/3$ for $\hat{n}_1$ and $2(\tau_{12}-\tau_{13}-\tau_{23})/3$ for $\hat{n}_2$, which means that we would observe the power spectrum with the different radial distortion for each different LOS. The separation of $P^{00}_{\ell\ell}$ and $P^{2M}_{\ell\ell'}$ originates from this fact as we will see in the next subsection.

In summary, if one performs the angler average in each tangential plane by which the two-dimensional power spectrum is obtained and set $\hat{n} = \hat{z}$, only the information on the radial distortion is left, and the fact that $\tau_{ij}\hat{n}^i_1\hat{n}^j_1 \neq \tau_{ij}\hat{n}^i_2\hat{n}^j_2$ obliges us to introduce different parameters which describe the super-sample tides for various LOS. On the other hand, since the BipoSH expansion captures the full three-dimensional power spectrum including the information of the distortion on the tangential planes and taking into account the non-parallel LOS, it is expected to alleviate the degeneracies between the super-sample tidal effect and other anisotropic effects. Notice that here τ_{33} is no longer the LOS component of τ_{ij}; i.e., $\tau_{33} \neq \tau_{ij}\hat{n}^i\hat{n}^j$, but merely the zz component in the observer's coordinates; $\tau_{33} = \tau_{ij}\hat{z}^i\hat{z}^j$.

4.6.2 BipoSH coefficients of the response functions

By making use of the BipoSH formalism, we can decompose Eq. (4.40) into the following *reduced* coefficients defined in Eq. (4.62):

$$P^{00}_{\ell\ell'}(k) = \delta^K_{\ell\ell'}\left[P_\ell(k) + D_\ell(k)P_{\rm lin}(k)\delta_{\rm b}\right], \tag{4.63}$$

$$P^{20}_{\ell\ell'}(k) = T_{\ell\ell'}(k)P_{\rm lin}(k)\tau_{33}, \tag{4.64}$$

$$P^{2\pm1}_{\ell\ell'}(k) = T_{\ell\ell'}(k)P_{\rm lin}(k)\sqrt{\frac{2}{3}}(\mp\tau_{13} + i\tau_{23}), \tag{4.65}$$

$$P^{2\pm2}_{\ell\ell'}(k) = T_{\ell\ell'}(k)P_{\rm lin}(k)\frac{1}{2}\sqrt{\frac{2}{3}}(\tau_{11} - \tau_{22} \mp 2i\tau_{12}), \tag{4.66}$$

where $P_\ell(k)$ is the Legendre coefficients for the Kaiser formula Eqs. (3.33)-(3.35) and we have introduced $D_\ell(k)$ and $T_{\ell\ell'}(k)$ as the BipoSH coefficients for the response to the super-sample density mode and the tidal mode, respectively. We stress here that the isotropic signal is confined in the $L = 0$ modes ($P^{00}_{\ell\ell}(k)$) which do not suffer from the tidal mode and the $L = 2$ modes ($P^{2M}_{\ell\ell'}(k)$) successfully extracts the full five degrees of freedom of the super-sample tides. The explicit expressions of $D_\ell(k)$ and $T_{\ell\ell'}(k)$ are given by

$$\begin{aligned} D_0(k) =& \left[-2b_1^3 + \frac{47}{21}b_1^2 + 2b_1b_2 - \frac{1}{3}b_1^2\frac{d\ln P_{\rm lin}(k)}{d\ln k}\right] \\ &+ \left[\frac{26}{21}b_1 - b_1^2 + \frac{2}{3}b_2 - \frac{1}{9}b_1(2+b_1)\frac{d\ln P_{\rm lin}(k)}{d\ln k}\right] f \\ &+ \left[\frac{31}{105} - \frac{8}{45}b_1 - \frac{1}{15}(1+2b_1)\frac{d\ln P_{\rm lin}(k)}{d\ln k}\right] f^2 \\ &+ \left[-\frac{1}{105} - \frac{1}{21}\frac{d\ln P_{\rm lin}(k)}{d\ln k}\right] f^3, \end{aligned} \tag{4.67}$$

$$\begin{aligned} D_2(k) =& \left[\frac{52}{21}b_1 - \frac{4}{3}b_1^2 + \frac{4}{3}b_2 - \frac{2}{9}b_1(2+b_1)\frac{d\ln P_{\rm lin}(k)}{d\ln k}\right] f \\ &+ \left[\frac{124}{147} - \frac{8}{63}b_1 - \frac{4}{21}(1+2b_1)\frac{d\ln P_{\rm lin}(k)}{d\ln k}\right] f^2 \\ &+ \left[\frac{4}{63} - \frac{10}{63}\frac{d\ln P_{\rm lin}(k)}{d\ln k}\right] f^3, \end{aligned} \tag{4.68}$$

$$D_4(k) = \left[\frac{248}{735} + \frac{32}{105}b_1 - \frac{8}{105}(1+2b_1)\frac{d\ln P_{\rm lin}(k)}{d\ln k}\right] f^2 + \left[\frac{72}{385} - \frac{8}{77}\frac{d\ln P_{\rm lin}(k)}{d\ln k}\right] f^3, \tag{4.69}$$

$$D_6(k) = \frac{16}{693}\left[4 - \frac{d\ln P_{\rm lin}(k)}{d\ln k}\right] f^3, \tag{4.70}$$

$$T_{20}(k) = \left[\frac{8}{7}b_1^2 + 2b_1 b_{s^2} - b_1^2\frac{d\ln P_{\rm lin}(k)}{d\ln k}\right] + \left[\frac{8}{7}b_1 + \frac{2}{3}b_{s^2} - \frac{1}{3}(2b_1 + b_1^2)\frac{d\ln P_{\rm lin}(k)}{d\ln k}\right] f + \left[\frac{16}{35} + \frac{4}{5}b_1 - \frac{1}{5}(1+2b_1)\frac{d\ln P_{\rm lin}(k)}{d\ln k}\right] f^2 + \left[\frac{16}{35} - \frac{1}{7}\frac{d\ln P_{\rm lin}(k)}{d\ln k}\right] f^3, \tag{4.71}$$

$$T_{02}(k) = \left[\frac{16}{35}b_1 - b_1^2 + \frac{4}{15}b_{s^2} - \frac{1}{15}b_1(4+5b_1)\frac{d\ln P_{\rm lin}(k)}{d\ln k}\right] f + \left[\frac{64}{245} - \frac{8}{15}b_1 - \frac{1}{35}(4+14b_1)\frac{d\ln P_{\rm lin}(k)}{d\ln k}\right] f^2 + \left[\frac{13}{35} - \frac{1}{7}\frac{d\ln P_{\rm lin}(k)}{d\ln k}\right] f^3, \tag{4.72}$$

$$T_{22}(k) = \left[\frac{32}{49}b_1 + \frac{8}{21}b_{s^2} - \frac{1}{21}b_1(8+7b_1)\frac{d\ln P_{\rm lin}(k)}{d\ln k}\right] f + \left[\frac{128}{343} + \frac{20}{147}b_1 - \frac{2}{49}(4+11b_1)\frac{d\ln P_{\rm lin}(k)}{d\ln k}\right] f^2 + \left[\frac{76}{147} - \frac{25}{147}\frac{d\ln P_{\rm lin}(k)}{d\ln k}\right] f^3, \tag{4.73}$$

$$T_{42}(k) = \left[\frac{288}{245}b_1 + \frac{24}{35}b_{s^2} - \frac{24}{35}b_1\frac{d\ln P_{\rm lin}(k)}{d\ln k}\right] f + \left[\frac{1152}{1715} + \frac{144}{245}b_1 - \frac{72}{245}(1+b_1)\frac{d\ln P_{\rm lin}(k)}{d\ln k}\right] f^2 + \left[\frac{144}{245} - \frac{8}{49}\frac{d\ln P_{\rm lin}(k)}{d\ln k}\right] f^3, \tag{4.74}$$

$$T_{24}(k) = \left[\frac{256}{1715} - \frac{192}{245}b_1 - \frac{8}{245}(2+9b_1)\frac{d\ln P_{\rm lin}(k)}{d\ln k}\right] f^2 + \left[\frac{88}{245} - \frac{8}{49}\frac{d\ln P_{\rm lin}(k)}{d\ln k}\right] f^3, \tag{4.75}$$

$$T_{44}(k) = \left[\frac{512}{3773} + \frac{16}{49}b_1 - \frac{8}{539}(4+11b_1)\frac{d\ln P_{\rm lin}(k)}{d\ln k}\right] f^2 + \left[\frac{2048}{5929} - \frac{600}{5929}\frac{d\ln P_{\rm lin}(k)}{d\ln k}\right] f^3, \tag{4.76}$$

$$T_{64}(k) = \left[\frac{128}{539} - \frac{8}{77}\frac{d\ln P_{\rm lin}(k)}{d\ln k}\right] f^2 + \left[\frac{160}{847} - \frac{40}{847}\frac{d\ln P_{\rm lin}(k)}{d\ln k}\right] f^3, \tag{4.77}$$

$$T_{46}(k) = \left[\frac{72}{847} - \frac{40}{847}\frac{d\ln P_{\rm lin}(k)}{d\ln k}\right] f^3, \tag{4.78}$$

$$T_{66}(k) = \left[\frac{32}{363} - \frac{8}{363}\frac{d\ln P_{\rm lin}(k)}{d\ln k}\right] f^3. \tag{4.79}$$

Note that all the other BipoSH coefficients are zero. Details of derivations of the above expressions, are summarized in Appendix D.

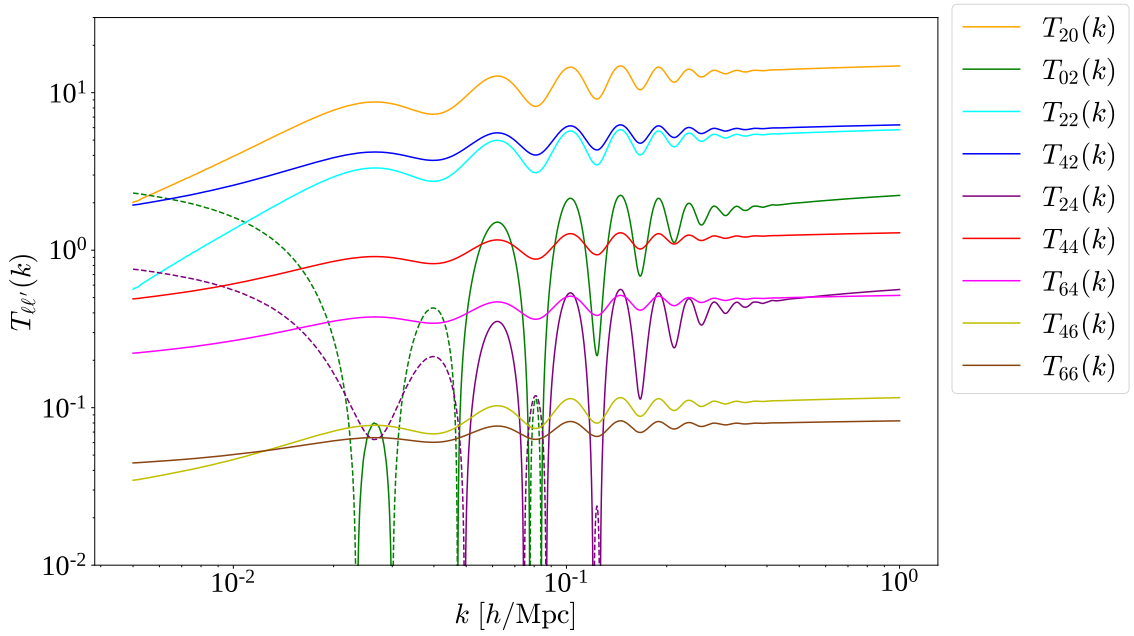

Figure 4.5: The response functions for the super-sample tides, $T_{\ell\ell'}(k)$, in terms of the BipoSH multipoles. Negative values are plotted with the dashed lines. Note that $T_{\ell\ell'}(k)$ is normalized by the matter power spectrum, i.e., $T_{\ell\ell'}(k) = \frac{\partial P^{20}_{\ell\ell'}}{\partial \tau_{33}}/P_{\rm lin}$. We assume cosmological parameters of the Planck satellite results [13] to compute $P_{\rm lin}(k)$ and for the linear growth rate and galaxy biases we use the following values: $f(z=0.8)=0.84$, $b_1=1.5$, $b_2=0.3$, and $b_{s^2}=-0.29$.

In Fig. 4.5 we show the BipoSH multipole representation of the response functions for the super-sample tides, $T_{\ell\ell'}(k)$, which are normalized by the matter power spectrum, i.e., $\frac{\partial P^{20}_{\ell\ell'}}{\partial \tau_{33}}/P_{\rm lin}$. We find that $T_{20}(k)$ has the highest magnitude, and $T_{02}(k)$, $T_{22}(k)$ and $T_{42}(k)$ have smaller magnitudes than $T_{20}(k)$. In general, there is a hierarchy of magnitudes; $|P^{2M}_{20}| > |P^{2M}_{02}| \sim |P^{2M}_{22}| \sim |P^{2M}_{42}| > |P^{2M}_{24}| \sim |P^{2M}_{44}| \sim |P^{2M}_{64}| > |P^{2M}_{66}|$, reflecting the power of the velocity. Therefore P^{2M}_{20} has a dominant contribution in the signal-to-noise ratio, similar to the usual Legendre multipole case in which P_0 is more dominant than P_2. The wiggly feature in the response function results from the BAO phase shift described by the dilation terms as explained in Section 4.3.1.

4.6.3 Fisher information matrix for the BipoSH multipoles

In the following subsection, with the BipoSH expansion, we study the degeneracies between the super-sample tidal modes and other cosmological anisotropies and the possibility to detect the super-sample tidal modes based on the Fisher information matrix formalism.

We employ the Fisher matrix formalism in order to assess the correlations between the anisotropic signals that appear in the observed power spectrum of galaxies. In terms of the reduced BipoSH coefficient $P^{LM}_{\ell_1\ell_2}(k)$, the Fisher matrix is written as

$$\begin{aligned} F_{\alpha\beta} &= -\left\langle \frac{\partial^2 \log L}{\partial\theta_\alpha \partial\theta_\beta} \right\rangle \\ &= \sum_{kk'} \sum_{\ell_1\ell_1'\ell_2\ell_2'} \sum_{LL'MM'} \frac{\partial [P^{LM}_{\ell_1\ell_2}(k)]^*}{\partial\theta_\alpha} \mathrm{Cov}^{-1}\left[[P^{LM}_{\ell_1\ell_2}(k)]^*, P^{L'M'}_{\ell_1'\ell_2'}(k') \right] \frac{\partial P^{L'M'}_{\ell_1'\ell_2'}(k')}{\partial\theta_\beta}, \end{aligned} \tag{4.80}$$

To give an expression of the covariance matrix for the reduced BipoSH coefficients $P^{LM}_{\ell_1\ell_2}(k)$, we start from the covariance for the 3D redshift-space power spectrum of galaxies $P^s(\mathbf{k};\hat{n})$ in the Gaussian limit,

$$\begin{aligned} \mathrm{Cov}\left[P^s(\mathbf{k};\hat{n}), P^s(\mathbf{k}';\hat{n'}) \right] =& 4\pi \frac{\delta^K_{k,k'}}{N_k} \left[\sum_J P^{(O)}_J(k) \mathcal{L}_J(\hat{k}\cdot\hat{n}) \right]^2 \\ & \times \left[\delta^{(2)}(\hat{k}+\hat{k}') + \delta^{(2)}(\hat{k}-\hat{k}') \right] 4\pi\delta^{(2)}(\hat{n}-\hat{n}'), \end{aligned} \tag{4.81}$$

where $N_k = 4\pi k^2 \Delta k V/(2\pi)^3$ is the number of modes with survey volume V and the interval between each Fourier mode Δk and $\mathcal{L}_J(x)$ is the Legendre polynomial. The Legendre coefficients with subscript (O) denote $P^{(O)}_0(k) = P_0(k) + 1/\bar{n}_g$, $P^{(O)}_2(k) = P_2(k)$, $P^{(O)}_4(k) = P_4(k)$ and $P^{(O)}_1(k) = P^{(O)}_3(k) = P^{(O)}_{J\geq 5}(k) = 0$ with $\bar{n}_g$ being the local number density of galaxies. By making use of the formulae in Appendix A, the covariance above leads to the following expression of the covariance for the reduced BipoSH coefficients [96],

$$\mathrm{Cov}\left[[P^{LM}_{\ell_1\ell_2}(k)]^*, P^{L'M'}_{\ell_1'\ell_2'}(k') \right] = \delta^K_{L,L'} \delta^K_{M,M'} \frac{\delta^K_{k,k'}}{N_k} \Theta^L_{\ell_1,\ell_2,\ell_1',\ell_2'}(k), \tag{4.82}$$

where

$$\begin{aligned} \Theta^L_{\ell_1,\ell_2,\ell_1',\ell_2'}(k) =& (2\ell_1+1)(2\ell_2+1)(2\ell_1'+1)(2\ell_2'+1)(2L+1)(-1)^{\ell_1} \left[1 + (-1)^{\ell_1'} \right] \\ & \times H_{\ell_1\ell_2 L} H_{\ell_1'\ell_2' L} \sum_{JJ'} P^{(O)}_J(k) P^{(O)}_{J'}(k) \sum_{L_1 L_2} (2L_1+1)(2L_2+1) \\ & \times H_{\ell_1 J L_1} H_{\ell_2 J L_2} H_{\ell_1' J' L_1} H_{\ell_1' J' L_2} \begin{Bmatrix} L & L_1 & L_2 \\ J & \ell_2 & \ell_1 \end{Bmatrix} \begin{Bmatrix} L & L_1 & L_2 \\ J' & \ell_2' & \ell_1' \end{Bmatrix}, \end{aligned} \tag{4.83}$$

with $\left\{ \begin{smallmatrix} L_1 & L_2 & L_3 \\ L_4 & L_5 & L_6 \end{smallmatrix} \right\}$ being the Wigner $6j$ symbol. The covariance matrix is therefore block-diagonalized for L, M and k. Further, the reality of the covariance means the matrix is also block-diagonalized for real part and imaginary part.

4.6.4 Results

In this subsection, we use the following cosmological parameters that are consistent with the Planck 2018 results [13]: $h = 0.6766$, $\Omega_c h^2 = 0.1193$, $\Omega_b h^2 = 0.0224$, $A_s = 2.105 \times 10^{-9}$ and $n_s = 0.9665$. We compute the Fisher matrix Eq. (4.80) for the following parameter set,

$$\theta_\alpha = \{b_1, b_2, b_{s^2}, f, D_A(z), H(z), \delta_{\rm b}, \tau_{33}, \tau_{11}, \tau_{12}, \tau_{13}, \tau_{23}\}\,. \tag{4.84}$$

As a working example, we assume a SPHEREx-like survey where we set the fiducial values of the central redshift $z = 0.8$, the comoving survey volume $V = 4.0\,({\rm Gpc}/h)^3$, the mean number density of galaxies $\bar{n}_g = 4.0 \times 10^{-3}\ (h/{\rm Mpc})^3$, the linear bias $b_1 = 1.5$, the quadratic bias $b_2 = 0.3$, the tidal bias $b_{s^2} = -\frac{4}{7}(b_1 - 1) = -0.29$ (See Eq. (3.19)), and the linear growth rate $f(z = 0.8) = 0.84$ [20]. Here we consider a single redshift slice for simplicity and the corresponding redshift width is $\Delta z \sim 0.1$. We assume that in this thin redshift slice the galaxy biases, the linear growth rate, and the distance parameters can be treated as effectively constants. Our results can be extended to include multiple redshift slice, although one should take into account the light-cone projection effect. Notice also that because the super-sample modes $\delta_{\rm b}(z_i)$ and $\tau_{ij}(z_i)$ depend on the specific survey region one should treat the $\delta_{\rm b}(z_i)$ and $\tau_{ij}(z_i)$ as independent variables for each redshift slice, unless one considers the super-sample modes that straddle multiple survey regions.

Two comments are in order. First, since the higher-order biases, b_2 and b_{s^2}, are only in the response functions at tree level calculation, then information is not sufficient to determine these higher-order biases. Therefore we employ 3σ Gaussian priors for b_2 and b_{s^2} with $\sigma_{b_2} = \sigma_{b_{s^2}} = 1$ in order to make the Fisher matrix invertible. Second, because the isotropic component of the super-sample modes $\delta_{\rm b}$ is to degenerate with the linear bias b_1 in spectroscopic surveys [32, 94], we also add a 3σ Gaussian prior to $\delta_{\rm b}$ with $\sigma_{\rm b}$ computed from Eq. (4.9) and focus on investigating the degeneracies and detectability of τ_{ij}. Note however that it is possible to constrain $\delta_{\rm b}$ in lensing surveys where the global mean density is relevant [32].

Fig. 4.6 shows the marginalized 68% error contours for the anisotropic signals $\{f, D_A, H, \tau_{33}\}$ in each of two-dimensional sub-space when adopting the minimum wavenumber $k_{\rm min} = 5.0 \times 10^{-3}\ h/{\rm Mpc}$, which is larger than the fundamental modes $k_F \sim 2\pi/V^{1/3}$, and the maximum wavenumber $k_{\rm max} = 0.2\ h/{\rm Mpc}$. We only present the results of τ_{33} because the results are identical for $\tau_{11}, \tau_{12}, \tau_{13}$, and τ_{23} in the BipoSH expansion. For comparison of the BipoSH expansion with the Legendre expansion, both expansion scheme cases are plotted. We use Eqs. (C.11)-(C.14) as the Legendre multipoles.

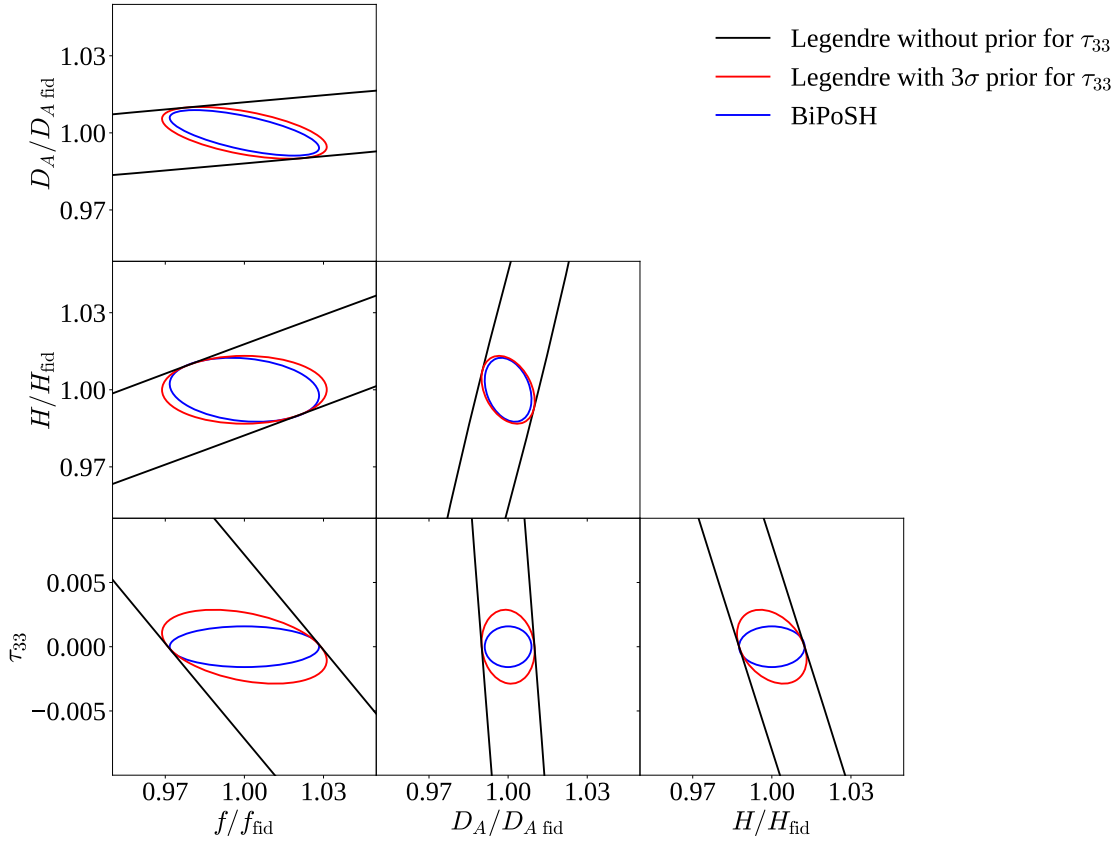

Figure 4.6: 1σ (68%) error contour for joint τ_{33} and cosmological distortion parameter, f, D_A and H, estimation with the maximum wavenumber $k_{\mathrm{max}} = 0.2\ h/\mathrm{Mpc}$. The inner blue curves in each panel show the results when employing the BipoSH expansion, which carries the full information of the three-dimensional power spectrum. The outer black curves in each panel correspond to the results when using the Legendre expansion, which contains only two-dimensional information of the power spectrum. For these two curves we do not use the prior knowledge on the super-sample tidal mode, τ_{33}. The red curves in each panel are the results when using the Legendre decomposition but adding the 3σ prior for τ_{33} with $\sigma_{\tau_{33}} = 6.4 \times 10^{-3}$.

Fig. 4.6 implies that the BipoSH decomposition formalism enables us to evade the super-sample tidal effect on the measurements of other distortion parameters, as the degradation is restored by adding the prior on τ_{33} in the analysis with the Legendre multipoles. As clearly demonstrated in Fig. 4.6, the super-sample tidal modes have little impact on the estimation of other parameters in the BipoSH expansion. More quantitatively, the absolute values of the cross-correlation coefficients between the τ_{33} and other parameters $\beta = \{b_1, f, D_A, H\}$, $c_{\tau\beta}$, are less than $\mathcal{O}(0.1)$. Notice that employing the BipoSH decomposition restores the degradation without assuming ΛCDM model.

Mathematically this is a consequence of the following facts. First, in the BipoSH expansion f, D_A and H are confined into the isotropic $L = 0$ BipoSH multipoles, $P^{00}_{\ell\ell}$, wheres the tidal signals τ_{ij} are confined into the $L = 2$ BipoSH multipoles, $P^{2M}_{\ell\ell'}$. Second, the covariance for the BipoSH coefficients (Eq. (4.82)) is block diagonal for L. Then f, D_A and H are constrained mainly from $P^{00}_{\ell\ell}(k)$, to which τ_{ij} do not contribute. On the other hand, in the Legendre expansion f, D_A, H and τ_{33} all appear in the same multipoles, $P_\ell(k)$. Accordingly, changing the AP parameters, D_A and H, leads to both the growth-like and dilation-like effect on the Legendre multipoles [83], and changing the RSD parameter f mimics the growth effect due to the super-sample mode. Hence, these parameters degenerate with each other in the Legendre expansion.

The vanishing correlation between τ_{ij} and other distortion parameters suggests that the large-scale tides τ_{ij} can be measured from the galaxy redshift-space power spectrum if using the BipoSH expansion, and therefore it is worthwhile to explore the possibility of whether a spectroscopic survey can detect τ_{ij} when including higher $k_{\rm max}$. Fig. 4.7 shows the 1σ constraint on τ_{33} as a function of $k_{\rm max}$. Again, the constraints on other super-sample tidal modes are equivalent, so we only present the τ_{33} estimation. We find that the BipoSH expansion enables us to determine τ_{33} with an accuracy better than the rms of τ_{33} expected for ΛCDM model, simultaneously measuring the RSD and AP distortion, if $P^{20}_{\ell\ell'}(k)$ is included up to $k_{\rm max} \gtrsim 0.3\ h/{\rm Mpc}$.

Although the inclusion of high $k_{\rm max}$, in general, requires to accurately model the nonlinear effect, the nonlinear evolution cannot generate the azimuthal asymmetry about the LOS, and therefore $P^{2M}_{\ell\ell'}(k)$. Hence, the fact that the appearance of $P^{2M}_{\ell\ell'}(k)$ is a distinctive feature of τ_{ij} allows us to use high $k_{\rm max}$ value. In practice, the highest $k_{\rm max}$ value we can use is limited by our knowledge of the response of the redshift-space power spectrum to the large-scale tides, $\partial P(\mathbf{k}, \hat{n})/\partial\tau_{ij}$, in the nonlinear regime where the perturbation theory breaks down. As mentioned in the previous section, to know the form of $\partial P(\mathbf{k}, \hat{n})/\partial\tau_{ij}$ in the nonlinear regime, we need to run N-body simulations with the large-scale tidal field, which is developed in the

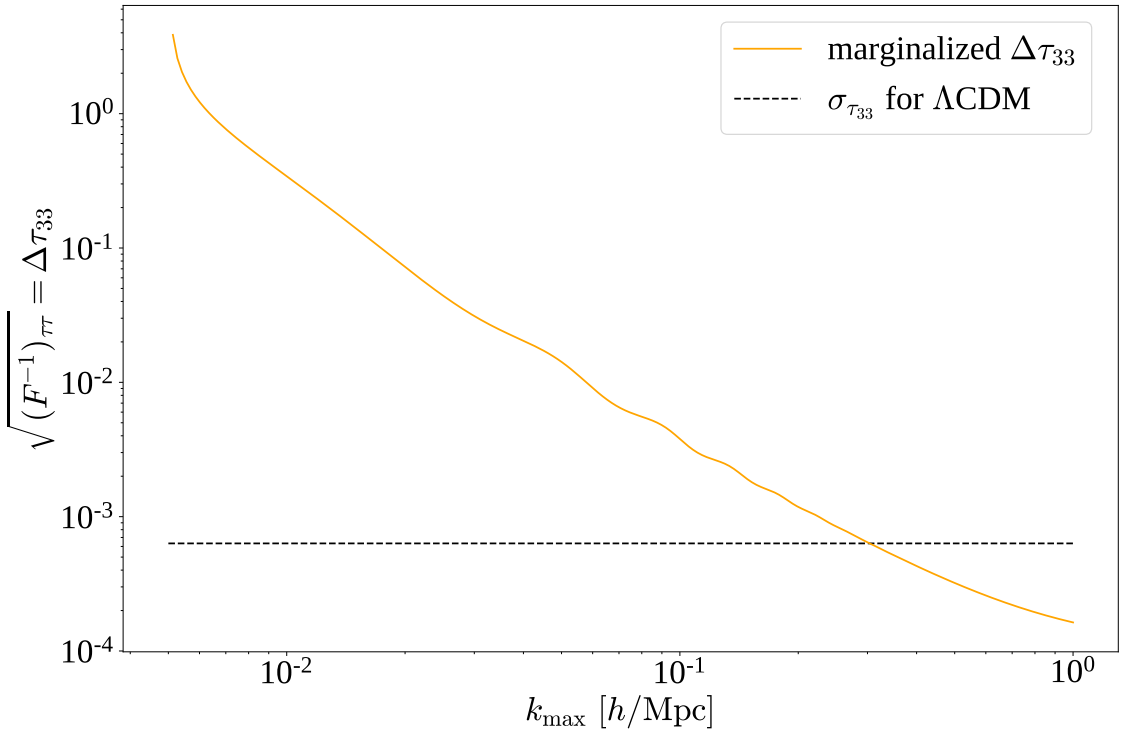

Figure 4.7: 1σ (68%) error for τ_{33} as a function of the maximum wavenumber $k_{\rm max}$. The orange curve corresponds to the 1σ constraint on τ_{33} when marginalized over other parameters, $\sqrt{(F^{-1})_{\tau\tau}}$. The horizontal dashed line represents the rms value, $\sigma_{\tau_{33}} = 6.4 \times 10^{-3}$, expected for ΛCDM cosmology and the survey volume.

next chapter. Here again we simply assume that the response function derived from the tree-level calculation of perturbation theory holds in the nonlinear regime.

Chapter 5

Cosmological simulation in an anisotropic background universe

Contents

In Chapter 4, we derive the response function to the super-sample tidal modes, using the perturbation theory, which is no longer valid on small scales. To obtain the functional form of the response function on nonlinear regime we need to run cosmological N-body simulations with long-wavelength perturbations. In practice, however, N-body simulations usually employ periodic boundary conditions to use the FFT algorithm so that longer-wavelength perturbations than the simulation

box size are not included. A naïve way to take into account long-wavelength perturbations in simulations is to run simulations in larger and larger simulation box. However to run large-box simulations requires a lot of memory and this direction will never end.

In the past few years people have started to use an alternative novel way to include the super-box mode in N-body simulation, namely, "separate universe simulation". A basic observation behind this method is that the super-box mode is effectively constant over the relevant scales rather than fluctuation. This allow us to absorb the super-box mode into the background quantities. How to implement the super-box *density* perturbation in N-body simulation is extensively studied in Refs. [27, 31, 47–49]. Since the super-box *density* mode is *isotropic*, taking the super-box density mode in the cosmological background holds isotropy; i.e, absorbing the super-box density mode into N-body simulations results in running simulation with a different FRLW background from the original FRLW cosmology. Thus what we have to do is just to run the same simulation code with different cosmological parameters. The separate universe simulation technique makes it possible to calibrate various effects such as the super-sample covariance [31] and the local halo bias [92, 105, 106], without running a large number of huge box simulations.

However, since the super-box *tidal* perturbation is *anisotropic*, taking the super-box tidal mode in the cosmological background breaks the isotropy in the background. Therefore, for the super-box tidal modes, we cannot use the same method as the density modes. Nevertheless, we show the super-box tidal modes can be absorbed into the background expansion based on the similar idea. These anisotropic simulations require modifications of N-body codes, which are presented in Section 5.2 and 5.3, after reviewing "separate universe simulation" technique in Section 5.1. As an application, we show the measurement of the growth response of the super-sample tidal modes on the sub-survey modes in Section 5.4.

5.1 Separate universe simulation

Here we briefly review the so-called "separate universe simulation" in which the large-scale density field beyond the simulation box is absorbed into the cosmological background, following the discussion in Ref. [31]. In this section we use the physical time t.

5.1.1 Separate universe technique

Suppose that a local region is embedded in the mean density fluctuation $\delta_{\rm b}(t)$ with the "global" background density $\bar{\rho}_{m,{\rm G}}$. The fact that this long wavelength density perturbation can be seen as an effective background in the local patch tempts us to define the "local" background density as

$$\bar{\rho}_{m,{\rm L}} = \bar{\rho}_{m,{\rm G}}(1+\delta_{\rm b}), \tag{5.1}$$

where the subscript G and L represent global and local quantities respectively. Then we can treat the local patch as the "separate" universe. In terms of the cosmological parameters,

$$\frac{\Omega_{m0,{\rm L}}h_{\rm L}^2}{a_{\rm L}^3} = \frac{\Omega_{m0,{\rm G}}h_{\rm G}^2}{a_{\rm G}^3}(1+\delta_{\rm b}). \tag{5.2}$$

As $\lim_{t\to 0}\delta_{\rm b}(t) = 0$, we get the initial condition for the local scale factor,

$$\lim_{t\to 0} a_{\rm L}(a_{\rm G}(t), \delta_{\rm b}(t)) = a_{\rm G}. \tag{5.3}$$

Thus at high redshift Eq. (5.2) reduces to

$$\Omega_{m0,{\rm L}}h_{\rm L}^2 = \Omega_{m0,{\rm G}}h_{\rm G}^2. \tag{5.4}$$

Substituting this into Eq. (5.2) yields

$$a_{\rm L} = \frac{a_{\rm G}}{(1+\delta_{\rm b})^{1/3}} \simeq a_{\rm G}\left(1-\frac{1}{3}\delta_{\rm b}\right), \tag{5.5}$$

at an equal physical time. The difference between the global and local scale factors naturally leads to a different expansion rate as

$$H_{\rm L}^2 - H_{\rm G}^2 \simeq -\frac{2}{3}H_{\rm G}\frac{dD}{dt}\frac{\delta_{\rm b0}}{D_0}, \tag{5.6}$$

where $\delta_{\rm b0}$ is the present-day value of $\delta_{\rm b}$ and we have used $\delta_{\rm b} = (D/D_0)\delta_{\rm b0}$ with D being the linear growth function. Using Eq. (2.38) , we find

$$H_{\rm G}\frac{dD}{dt} = \frac{\Omega_{m0,{\rm G}}H_{0,{\rm G}}}{2a_{\rm G}^2}\left[\frac{5}{D(t)} - \frac{3}{a_{\rm G}} - \frac{2\Omega_{K0,{\rm G}}}{\Omega_{m0,{\rm G}}}\right]D(t), \tag{5.7}$$

where we have included the curvature parameter Ω_{K0}. On the other hand, assuming that the Friedmann equation holds in each universe we have

$$H_{\rm L}^2 = H_{0,\rm L}^2 \left[\frac{\Omega_{m0,\rm L}}{a_{\rm L}^3} + \Omega_{\Lambda 0,\rm L} + \frac{\Omega_{K0,\rm L}}{a_{\rm L}^2} \right], \tag{5.8}$$

$$H_{\rm G}^2 = H_{0\rm G}^2 \left[\frac{\Omega_{m0,\rm G}}{a_{\rm G}^3} + \Omega_{\Lambda 0,\rm G} + \frac{\Omega_{K0,\rm G}}{a_{\rm G}^2} \right], \tag{5.9}$$

where we have defined the Hubble constant in the local separate universe as

$$H_{0,\rm L} \equiv H_{\rm L}|_{a_{\rm L}=1} \neq H_{\rm L}|_{a_{\rm G}=1}\,. \tag{5.10}$$

Eqs. (5.8) and (5.9) yields

$$H_{\rm L}^2 - H_{\rm G}^2 \simeq \frac{H_{0,\rm L}^2 - H_{0,\rm G}^2}{a_{\rm G}^2} + H_{0,\rm G}^2 \left[\frac{\Omega_{m0,\rm G}}{a_{\rm G}^3} + \frac{2}{3}\frac{\Omega_{K0,\rm G}}{a_{\rm G}^2} \right] \delta_{\rm b}. \tag{5.11}$$

where we have used Eqs. (5.4) and (5.5) and the fact that $\Omega_{\Lambda 0,\rm G} h_{\rm G}^2 = \Omega_{\Lambda 0,\rm L} h_{\rm L}^2$, which means the physical density of the cosmological constant is constant. Comparing Eq. (5.11) with Eq. (5.6) we obtain the local Hubble constant in terms of the global quantities as

$$\frac{\delta h}{h_{\rm G}} \equiv \frac{H_{0,\rm L} - H_{0,\rm G}}{H_{0,\rm G}} \simeq -\frac{5\Omega_{m0,\rm G}}{6}\frac{\delta_{\rm b}(t)}{D(t)}. \tag{5.12}$$

Other local cosmological parameters are found to be

$$\frac{\delta\Omega_{m0}}{\Omega_{m0,\rm G}} = \frac{\delta\Omega_{\Lambda 0}}{\Omega_{\Lambda 0,\rm G}} \simeq -2\frac{\delta h}{h_{\rm G}}. \tag{5.13}$$

Note that even when the global universe is flat the separate universe has a spatial curvature,

$$\Omega_{K0,\rm L} = 1 - \Omega_{m0,\rm L} - \Omega_{\Lambda 0,\rm L} \tag{5.14}$$

$$= 1 - (\Omega_{m0,\rm G} + \Omega_{\Lambda 0,\rm G}) \left(1 + \frac{5\Omega_{m0,\rm G}}{3}\frac{\delta_{\rm b}(t)}{D(t)} \right) \neq 0. \tag{5.15}$$

Thus in general the flat FLRW universe with the long-wavelength density perturbation corresponds to a curved FLRW universe effectively without the long-wavelength density perturbation.

5.1.2 Growth and dilation in separate universe picture

With a couple of separate universe simulations, we can measure the response of the power spectrum to the large-scale density field $\delta_{\rm b}$. That is, the response $\partial \ln P(k)/\partial\delta_{\rm b}$ can be evaluated as

$$\left.\frac{\partial \ln P(k)}{\partial \delta_{\rm b}}\right|_k \simeq \frac{\ln P(k;\delta_{\rm b} = +\epsilon) - \ln P(k;\delta_{\rm b} = -\epsilon)}{2\epsilon}, \tag{5.16}$$

where we measure $P(k;\delta_{\rm b}=\pm\epsilon)$ in separate universe simulations with $\epsilon \ll 1$. One of advantages of this technique lies in the fact that we can use the same initial seeds to run respective separate universe simulations. Since the initial condition is given by the Gaussian random field, the sample variances inevitably exist in measurements of the power spectrum. The separate universe technique reduces this stochasticity by sharing the initial seeds in separate universe simulations in which we take difference.

However, there are subtleties as for the comparison of the power spectra of different separate universes, since different separate universes have different units and comoving scales as discussed in the previous subsection. Cosmological N-body codes usually use the unit h Mpc^{-1} rather than Mpc^{-1} in k. To avoid confusion arisen from the difference in the units, we work with the dimensionless power spectrum $\Delta^2(k) = k^3P(k)/2\pi^2$. When we compare the power spectra of different cosmologies at some scales, this comparison is done at different scale factors given by Eq. (5.5). The fact that the physical scales should be unchanged in different cosmologies, $a_{\rm G}x_{\rm G} = a_{\rm L}x_{\rm L}$, implies that

$$k_{\rm L} = \frac{a_{\rm L}}{a_{\rm G}}k_{\rm G} \simeq \left(1-\frac{1}{3}\delta_{\rm b}\right)k_{\rm G}. \tag{5.17}$$

After all, by using the chain rule the response Eq. (5.16) is rewritten as

$$\begin{aligned}\left.\frac{\partial \ln \Delta^2_{\rm L}(k_{\rm L})}{\partial\delta_{\rm b}}\right|_{k_{\rm G}} &= \left.\frac{\partial \ln \Delta^2_{\rm L}(k_{\rm L})}{\partial\delta_{\rm b}}\right|_{k_{\rm L}} + \frac{\partial \ln \Delta^2_{\rm L}(k_{\rm L})}{\partial \ln k_{\rm L}}\frac{\partial \ln k_{\rm L}}{\partial\delta_{\rm b}} \\ &= \left.\frac{\partial \ln \Delta^2_{\rm L}(k_{\rm L})}{\partial\delta_{\rm b}}\right|_{k_{\rm L}} - \frac{1}{3}\frac{\partial \ln \Delta^2_{\rm L}(k_{\rm L})}{\partial \ln k_{\rm L}} \\ &= \left.\frac{\partial \ln \Delta^2_{\rm L}(k_{\rm L})}{\partial\delta_{\rm b}}\right|_{k_{\rm L}} - \frac{1}{3}\frac{\partial \ln \Delta^2_{\rm G}(k_{\rm G})}{\partial \ln k_{\rm G}},\end{aligned} \tag{5.18}$$

where the first and second terms correspond to the growth and dilation term respectively. Eq. (5.18) shows that the dilation term can be obtained by replacing the linear power spectrum in the perturbation theory prediction with the nonlinear one. Thus to evaluate the dilation term does not need to run separate universe simulations. On the other hand, Eq. (5.18) also shows that the growth term can be measured by taking the difference of the power spectra at fixed separate universe comoving scales $k_{\rm L}$. Several studies have already measured the response of the matter or halo power spectrum to the long-wavelength isotropic perturbation $\delta_{\rm b}$. They found that the small-scale growth is enhanced compared to the perturbation theory predictions which are given by Eqs. (4.26) and (4.29) [31, 92]. We use a similar technique to calibrate the response to the large-scale tidal field.

5.2 Methodology

5.2.1 Peculiarity-background split

In this subsection, we show that in the Newtonian cosmology the effect of infinitely long-wavelength tidal mode on dark matter particles can be absorbed by a coordinate transformation.

Consider a generalized relation between the physical and comoving coordinates,

$$r_i = a_{ij} x_j \qquad (i, j = 1, 2, 3), \tag{5.19}$$

where r_i is the physical coordinates of the dark matter particle and a_{ij} is a symmetric matrix that absorbs the large-scale stress due to the long modes so that the large-scale displacement is isotropic in the x_i coordinate. We normalize a_{ij} to the scale factor of global expansion $a\,\delta^K_{ij}$ in the absence of any long mode, when x_i reduces to the usual comoving coordinates. From Eq. (5.19) we can immediately separate the physical velocity u_i into the expansion of a local background and a peculiar component

$$u_i \equiv \dot{r}_i = H_{ij} r_j + v_i, \tag{5.20}$$

where the overdot denotes physical time derivative, $H_{ij} \equiv \dot{a}_{ik}[a^{-1}]_{kj}$ describes a local anisotropic Hubble expansion, and $v_i \equiv a_{ij}\dot{x}_j$ is the peculiar velocity.

The dark matter particle follows the Newtonian equation of motion

$$\dot{u}_i = -\frac{\partial}{\partial r_i}(\Phi + \phi). \tag{5.21}$$

Plugging Eq. (5.20) into Eq. (5.21), the acceleration also splits into a local background expansion and a peculiar piece, which are respectively driven by an effective background potential ϕ and a peculiar potential Φ

$$\ddot{a}_{ik}[a^{-1}]_{kj} r_j = -\frac{\partial \phi}{\partial r_i}, \tag{5.22}$$

$$H_{ij} v_j + \dot{v}_i = -\frac{\partial \Phi}{\partial r_i}, \tag{5.23}$$

where we have used $\dot{H}_{ij} + H_{ik}H_{kj} = \ddot{a}_{ik}[a^{-1}]_{kj}$. One can identify Eq. (5.22) with a modified Friedmann equation. The background potential ϕ absorbs the large-scale stress due to the long modes, so that the peculiar potential should be sourced only by the local structures

$$\nabla^2_{\mathbf{r}} \Phi = 4\pi G \bar{\rho}_m (1 + \Delta_0)\delta, \tag{5.24}$$

where $\nabla^2_{\mathbf{r}}$ is the Lapracian in the physical coordinates, $\bar{\rho}_m$ is the (global) mean density of matter, $\Delta_0 (= \delta_{\rm b})$ is the local mean overdensity relative to $\bar{\rho}_m$

$$1 + \Delta_0 \equiv \frac{a^3}{\det a_{ij}}, \tag{5.25}$$

and δ denotes the overdensity with respect to the local background density $\bar{\rho}_{\rm m}(1+\Delta_0)$.

Without loss of generality, we can simplify the equations (and the numerical implementation) by performing a rotation to align the principal axes of the long tide with the Cartesian axes (of the simulation box), so that $a_{ij} = a_i\delta^K_{ij}$ and $H_{ij} = H_i\delta_{ij} = \dot{a}_i\delta^K_{ij}/a_i$ with their off-diagonal degrees of freedom eliminated. Let us define Δ_i as the fractional perturbation to a_i

$$1 + \Delta_i \equiv \frac{a_i}{a}, \quad i = 1, 2, 3. \tag{5.26}$$

Therefore

$$H_i = H + \dot{\Delta}_i. \tag{5.27}$$

In order to determine the evolution of Δ_i in the presence of the large-scale tides $\tau_{ij} = \mathrm{diag}(\tau_1, \tau_2, \tau_3)$, we consider the effective background potential as

$$\phi = \frac{2}{3}\pi G(\bar{\rho} + 3\bar{\mathcal{P}})r_i^2 + \frac{2}{3}\pi G\bar{\rho}_m\tau_i r_i^2, \tag{5.28}$$

where the second term corresponds to the potential sourced by the long-wavelength tidal mode. One can easily verify substituting the first term into Eq. (5.22) gives rise to the usual Friedmann equation Eq. (2.4). Plugging Eq. (5.28) into Eq. (5.22) and using the usual Friedmann equation Eq. (2.4), we derive

$$\ddot{\Delta}_i + 2H\dot{\Delta}_i = -\frac{4}{3}\pi G\bar{\rho}_m\tau_i(1 + \Delta_i). \tag{5.29}$$

Thus given that $\tau_i = (D(t)/D_0)\tau_{i0}$ we can compute the anisotropic scale factor by solving this equation. At linear order, we get

$$\Delta_i = -\tau_i. \tag{5.30}$$

Defining the conjugate momenta of x_i as $P_i \equiv a_i^2 m\dot{x}_i$, the equation of motion for the peculiar part takes a simple form of

$$\dot{P}_i = -\frac{\partial\Phi}{\partial x^i}, \tag{5.31}$$

for the unit mass.

5.2.2 Lagrangian perturbation theory in an anisotropic background

The initial conditions for the cosmological N-body simulation are generated by making use of the second-order Lagrangian perturbation theory [107]. In the presence

of long modes, we have to solve the anisotropic perturbations to the Lagrangian displacement with the second-order Lagrangian perturbation theory.

Let us start with the Zel'dovich approximation (or linear Lagrangian perturbation theory) [108]. The displacement field $\Psi(\mathbf{q})$ is a mapping from a particle's Lagrangian position q_i to its Eulerian position x_i:

$$x_i = q_i + \Psi_i(\mathbf{q}), \tag{5.32}$$

whose determinant is related to overdensity by

$$\delta = \left|\frac{\partial \mathbf{x}}{\partial \mathbf{q}}\right|^{-1} - 1 \simeq -\Psi^{(1)}_{i,i}, \tag{5.33}$$

where $\Psi_{i,j} \equiv \partial\Psi_i/\partial q_j$, and we have only kept the leading order term in the second equality. Substituting Eq. (5.32) into Eq. (5.23) leads to

$$\ddot{\Psi}^{(1)}_i + 2H_i\dot{\Psi}^{(1)}_i = -\frac{1}{a_i}\frac{\partial\Phi}{\partial r_i}. \tag{5.34}$$

Take gradient of x_i on both sides and then sum over i:

$$\ddot{\Psi}^{(1)}_{i,i} + 2H_i\dot{\Psi}^{(1)}_{i,i} \simeq -\nabla^2_{\mathbf{r}}\Phi \simeq \frac{3}{2}H^2\Omega_m(1+\Delta_0)\Psi^{(1)}_{i,i}, \tag{5.35}$$

in which we have used Eqs. (5.24), (5.33), and the fact that at leading order $\partial\Psi^{(1)}_i/\partial x_i \simeq \Psi^{(1)}_{i,i}$. In the linear order the vorticity in $\Psi^{(1)}_{i,j}$ decays, so the displacement is a potential flow $\Psi^{(1)}_i = -\partial\psi^{(1)}/\partial q_i \equiv -\psi^{(1)}_{,i}$ with the displacement potential $\psi^{(1)}$ sourced by the overdensity in Lagrangian space:

$$\nabla^2_{\mathbf{q}}\psi^{(1)} \simeq \delta^{(1)}. \tag{5.36}$$

Rewriting Eq. (5.35) with ψ in Fourier space yields

$$\ddot{\psi}^{(1)} + 2H_i\hat{k}^2_i\dot{\psi}^{(1)} - \frac{3}{2}\Omega_{\rm m}(a)(1+\Delta_0)\psi^{(1)} = 0, \tag{5.37}$$

where $\hat{k}_i$ denotes the unit vector of the wavevector in the Lagrangian space. The above equation describes the linear growth of the displacement field, on which the effect of the long modes manifests in the quadrupolarly direction-dependent Hubble drag and the coefficients that depend on the growth history of the long modes Δ_i.

Apparently without the long modes the evolution described by Eq. (5.37) reduces to that of the usual linear growth function $D(a)$ Eq. (2.38). In the presence of the long modes, the growth function $D^{(1)}_{\rm L}(a,\hat{k})$ receives corrections of order $\mathcal{O}(\Delta_i)$. The subscript L here denotes locally averaged quantities. Let $\epsilon^{(1)}(a,\hat{k}) \equiv D^{(1)}_{\rm L} - D^{(1)}$. It follows

$$\ddot{\epsilon}^{(1)} + 2H\dot{\epsilon}^{(1)} - \frac{3}{2}\Omega_m\epsilon^{(1)} \simeq -2\dot{D}^{(1)}\hat{k}^2_i\dot{\Delta}_i + \frac{3}{2}\Omega_m D^{(1)}\Delta_0. \tag{5.38}$$

To solve this equation we can first decompose it as

$$\epsilon^{(1)}(a,\hat{k}) = \hat{k}_i^2 \epsilon_i^{(1)}(a), \tag{5.39}$$

with each component $\epsilon_i^{(1)}(a)$ solves

$$\ddot{\epsilon}_i^{(1)} + 2H\dot{\epsilon}_i^{(1)} - \frac{3}{2}\Omega_m \epsilon_i^{(1)} = -2\dot{D}^{(1)}\dot{\Delta}_i + \frac{3}{2}\Omega_m D^{(1)}\Delta_0. \tag{5.40}$$

For the simplest scenarios we assume that the universe has been matter dominated ($H = 2/3t$ and $\Omega_m = 1$) for long enough and that the long modes are well sub-horizon ($\Delta_0, \Delta_i \propto D$), so that at the Zel'dovich approximation we can set up the initial conditions of the linear growth equations Eqs. (2.38) and (5.40) as

$$\begin{aligned} D^{(1)} &= \frac{d\,D^{(1)}}{d\ln a} = a_{\rm ini}, \\ \epsilon_i^{(1)} &= \frac{1}{2}\frac{d\,\epsilon_i^{(1)}}{d\ln a} = -\frac{4}{7}\Delta_i D^{(1)} + \frac{3}{7}\Delta_0 D^{(1)}, \end{aligned} \tag{5.41}$$

at $a_{\rm ini}$ deep in the matter-dominated era.

At the second order, we have to come back to the master equation for the Lagrangian perturbation theory in the anisotropic background, which is given by

$$\left|\frac{\partial \mathbf{x}}{\partial \mathbf{q}}\right|^{-1} [\delta_{ij} + \Psi_{i,j}]^{-1} \left[\ddot{\Psi}_{i,j} + 2H_i \dot{\Psi}_{i,j}\right] = \frac{3}{2}H^2\Omega_{\rm m}(a)(1+\Delta_0)\delta. \tag{5.42}$$

Keeping up to the second-order terms, we find

$$\left|\frac{\partial \mathbf{x}}{\partial \mathbf{q}}\right|^{-1} \simeq 1 + \Psi_{i,i}^{(1)} + \Psi_{i,i}^{(2)} + \frac{1}{2}\left[\left(\Psi_{i,i}^{(1)}\right)^2 - \Psi_{i,j}^{(1)}\Psi_{j,i}^{(1)}\right], \tag{5.43}$$

$$[\delta_{ij} + \Psi_{i,j}]^{-1} \simeq \delta_{ij} - \Psi_{i,j}^{(1)}, \tag{5.44}$$

leading to the second-order equation

$$\begin{aligned} &\ddot{\Psi}_{i,i}^{(2)} + 2H_i\dot{\Psi}_{i,i}^{(2)} - \frac{3}{2}H^2\Omega_{\rm m}(a)(1+\Delta_0)\Psi_{i,i}^{(2)} \\ &\quad = -\Psi_{i,i}^{(1)}\left[\ddot{\Psi}_{j,j}^{(1)} + 2H_i\dot{\Psi}_{j,j}^{(1)}\right] + \Psi_{i,j}^{(1)}\left[\ddot{\Psi}_{i,j}^{(1)} + 2H_i\dot{\Psi}_{i,j}^{(1)}\right] \\ &\qquad + \frac{3}{2}H^2\Omega_{\rm m}(a)(1+\Delta_0)\left[\frac{1}{2}\left(\Psi_{i,i}^{(1)}\right)^2 - \frac{1}{2}\Psi_{i,j}^{(1)}\Psi_{j,i}^{(1)}\right]. \end{aligned} \tag{5.45}$$

Similar to the linear order, we introduce the second-order displacement potential thruough $\Psi_i^{(2)} = \partial\psi_{\rm L}^{(2)}/\partial q_i \equiv \psi_{{\rm L},i}^{(2)}$. In the absence of the long modes, the equation for $\psi^{(2)}$ reduces to

$$\ddot{\psi}_{,ii}^{(2)} + 2H\dot{\psi}_{,ii}^{(2)} - \frac{3}{2}H^2\Omega_{\rm m}(a)\psi_{,ii}^{(2)} = -\frac{3}{2}H^2\Omega_{\rm m}\left[\frac{1}{2}\left(\psi_{,ii}^{(1)}\right)^2 - \frac{1}{2}\psi_{,ij}^{(1)}\psi_{,ji}^{(1)}\right], \tag{5.46}$$

where we have used the linear equation Eq. (5.37) without long modes. In this usual case, we denote the time-dependent part of $\psi^{(2)}$ as $D^{(2)}$, which obeys

$$\ddot{D}^{(2)} + 2H\dot{D}^{(2)} - \frac{3}{2}H^2\Omega_m D^{(2)} = -\frac{3}{2}H^2\Omega_m \left(D^{(1)}\right)^2 . \tag{5.47}$$

In the matter dominated era, we have $D^{(2)} = -3\left[D^{(1)}\right]^2/7$. The correction induced by the long modes, which is expressed by $\epsilon^{(2)}(t,\mathbf{q}) \equiv \psi^{(2)}_{\rm L}(t,\mathbf{q}) - \psi^{(2)}(t,\mathbf{q})$, follows

$$\begin{aligned}
&\ddot{\epsilon}^{(2)}_{,ii} + 2H\dot{\epsilon}^{(2)}_{,ii} - \frac{3}{2}H^2\Omega_m\epsilon^{(2)}_{,ii} = \\
&\quad - 2\dot{\psi}^{(2)}_{,ii}\dot{\Delta}_i + 2\dot{\Delta}_i\dot{\psi}^{(1)}_{,ij}\psi^{(1)}_{,ji} - \frac{3}{2}H^2\Omega_m\epsilon^{(1)}_{,jj}\psi^{(1)}_{,ii} + \psi^{(1)}_{,ij}\left[\ddot{\epsilon}^{(1)}_{,ij} + 2H\dot{\epsilon}^{(1)}_{,ij}\right] \\
&\quad + \frac{3}{2}H^2\Omega_m\Delta_0\left[\psi^{(2)}_{,ii} + \frac{1}{2}\left(\psi^{(1)}_{,ii}\right)^2 - \frac{1}{2}\psi^{(1)}_{,ij}\psi^{(1)}_{,ji}\right],
\end{aligned} \tag{5.48}$$

where $\epsilon^{(1)}(t,\mathbf{q}) = \int \frac{d^3\mathbf{k}}{(2\pi)^3}\epsilon^{(1)}(t,\hat{k})e^{i\mathbf{k}\cdot\mathbf{q}}$ and we neglect $\mathcal{O}(\Delta_i^2)$ terms. Notice that $\epsilon^{(1)}$ is $\mathcal{O}(\Delta_i)$. For the matter dominated era the solution for Eq.(5.48) is given by

$$\begin{aligned}
\epsilon^{(2)}_{,ii}(\mathbf{q}) =& \frac{1}{4}\left[-\frac{16}{9}\psi^{(2)}_{,ii}(\mathbf{q}) + \frac{8}{9}\psi^{(1)}_{,ij}(\mathbf{q})\psi^{(1)}_{,ji}(\mathbf{q})\right]\Delta_i \\
&+ \frac{1}{6}\left[\psi^{(2)}_{,ii} + \frac{1}{2}\left(\psi^{(1)}_{,ii}\right)^2 - \frac{1}{2}\psi^{(1)}_{,ij}\psi^{(1)}_{,ji}\right]\Delta_0 \\
&+ \frac{1}{4}\left[-\frac{2}{3}\psi^{(1)}_{,ii}(\mathbf{q})\epsilon^{(1)}_{,jj}(\mathbf{q}) + \frac{20}{9}\psi^{(1)}_{,ij}(\mathbf{q})\epsilon^{(1)}_{,ij}(\mathbf{q})\right].
\end{aligned} \tag{5.49}$$

Although the modified second-order growth factor, $D^{(2)}_{\rm L}$, due to the long modes can be identified as $D^{(2)}_{\rm L}(t,\mathbf{k}) = D^{(2)}(1 + \Delta_0/6 - 4\hat{k}_i^2\Delta_i/9)$, the local gravitational tides cannot be neglected at the second order.

5.3 Numerical implementation

In this section, we describe how to modify the comsmological N-body simulation code `L-Gadget2` [109], to perform the cosmological simulation in an anisotropic expanding universe.

5.3.1 Forces

The TreePM method splits the gravity into the long-range and short-range pieces

$$\Phi = \Phi^{\rm PM} + \Phi^{\rm T}, \tag{5.50}$$

which are handled by the PM and tree algorithms, respectively [110, 111]:

$$\Phi^{\rm PM}(\mathbf{k}) = -4\pi G\bar{\rho}_m a^2 \frac{\delta(\mathbf{k})}{k^2} e^{-k^2 x_{\rm s}^2}, \tag{5.51}$$

$$\Phi^{\rm T}(\mathbf{x}) = -\frac{Gm}{a}\sum_n \frac{1}{|\mathbf{x}-\mathbf{x}_n|}\,{\rm erfc}\Big(\frac{|\mathbf{x}-\mathbf{x}_n|}{2x_{\rm s}}\Big), \tag{5.52}$$

where $x_{\rm s}$ is the comoving scale of force splitting, x_n denotes the position of the n-th particle, m represents the mass of the particle, and

$$\bar{\rho}_m\big(1+\delta(\mathbf{x})\big) = \frac{m}{a^3}\sum_n \delta_{\rm D}^3(\mathbf{x}-\mathbf{x}_n). \tag{5.53}$$

Since the Fourier transform of $e^{-k^2x_{\rm s}^2}/k^2$ is ${\rm erf}(x/x_s)/4\pi x$, one can verify the force splitting with the convolution theorem. The acceleration due to the tree force is

$$-\frac{\partial\Phi^{\rm T}}{\partial x_i} = -\frac{Gm}{a}\sum_n \frac{[\mathbf{x}-\mathbf{x}_n]_i}{|\mathbf{x}-\mathbf{x}_n|^3}\left[{\rm erfc}\Big(\frac{|\mathbf{x}-\mathbf{x}_n|}{2x_{\rm s}}\Big) + \frac{|\mathbf{x}-\mathbf{x}_n|}{x_{\rm s}\sqrt{\pi}}\exp\Big(-\frac{|\mathbf{x}-\mathbf{x}_n|^2}{4x_{\rm s}^2}\Big)\right]. \tag{5.54}$$

Now let us consider how this conventional TreePM algorithm is modified in an anisotropically expamding universe. The modified Poisson equation Eq. (5.24),

$$(1+\Delta_i)^{-2}\frac{\partial^2}{\partial x_i^2}\Phi^{\rm PM} = 4\pi G\bar{\rho}_m a^2(1+\Delta_0)\delta, \tag{5.55}$$

leads us to modify the TreePM potentials as

$$\Phi^{\rm PM}(\mathbf{k}) = -4\pi G\bar{\rho}_{\rm m} a^2(1+\Delta_0)\frac{(1+\Delta_i)^2\delta(\mathbf{k})}{k^2} e^{-\frac{k^2}{(1+\Delta_i)^2}x_{\rm s}^2}, \tag{5.56}$$

$$\Phi^{\rm T}(\mathbf{x}) = -\frac{Gm}{a}\sum_n \frac{a}{|\mathbf{r}-\mathbf{r}_n|}\,{\rm erfc}\Big(\frac{|\mathbf{r}-\mathbf{r}_n|}{2ax_{\rm s}}\Big), \tag{5.57}$$

Note that to avoid anisotropic artificial features, we split the force isotropically in physical scales, i.e., anisotropically in local comoving scales. Given that the PM

grid is now anisotropic in physical scale, having $x_{\rm s}$ bigger than the grid size helps to suppress any effect due to such anisotropic smoothing over the grid scale. The tree acceleration is now

$$-\frac{\partial\Phi^{\rm T}}{\partial x_i}=-\frac{Gm}{a}\sum_n\frac{aa_i[\mathbf{r}-\mathbf{r}_n]_i}{|\mathbf{r}-\mathbf{r}_n|^3}\left[\mathrm{erfc}\Big(\frac{|\mathbf{r}-\mathbf{r}_n|}{2ax_{\rm s}}\Big)+\frac{|\mathbf{r}-\mathbf{r}_n|}{ax_{\rm s}\sqrt{\pi}}\exp\Big(-\frac{|\mathbf{r}-\mathbf{r}_n|^2}{4a^2x_{\rm s}^2}\Big)\right], \tag{5.58}$$

We adopt the same spline kernel in `L-Gadget2` to soften the force with replacement $\mathbf{x}\to\mathbf{r}/a$.

5.3.2 Time integration

In simulations [109, 112], the kick and drift leapfrog operators

$$\text{Kick}: \quad \frac{\boldsymbol{P}}{m}\to\frac{\boldsymbol{P}}{m}-\nabla_{\mathbf{x}}\varphi\int_t^{t+\Delta t}\frac{dt}{a}, \tag{5.59}$$

$$\text{Drift}: \quad \mathbf{x}\to\mathbf{x}+\frac{\boldsymbol{P}}{m}\int_t^{t+\Delta t}\frac{dt}{a^2}, \tag{5.60}$$

are derived from canonical transformation. $\boldsymbol{P}\equiv a^2m\dot{\mathbf{x}}$ is the canonical momentum of the Hamiltonian

$$H=\sum_n\frac{\boldsymbol{P}_n^2}{2ma^2}+\sum_{n\neq n'}\frac{m^2\varphi(\mathbf{x}_n-\mathbf{x}_{n'})}{2a}, \tag{5.61}$$

in which φ is the potential of a unit-mass particle:

$$\nabla_{\mathbf{x}}^2\varphi=4\pi G\Big(\delta_{\rm D}^3(\mathbf{x}-\mathbf{x}')-\frac{1}{L^3}\Big). \tag{5.62}$$

Notice that Φ and φ are related through $\Phi=m^2\varphi/a$.

For the anisotropic system, the Hamiltonian leading to the modified EoM Eq. (5.31) is

$$H=\sum_n\sum_{i=1}^3\frac{P_{n,i}^2}{2ma_i^2}+\sum_{n\neq n'}\frac{m^2\varphi(\mathbf{x}_n-\mathbf{x}_{n'})}{2a}. \tag{5.63}$$

Thus we have

$$\text{Kick}: \quad \frac{\boldsymbol{P}}{m}\to\frac{\boldsymbol{P}}{m}-\nabla_{\mathbf{x}}\varphi\int_t^{t+\Delta t}\frac{dt}{a}, \tag{5.64}$$

$$\text{Drift}: \quad x_i\to x_i+\frac{P_i}{m}\int_t^{t+\Delta t}\frac{dt}{a_i^2}. \tag{5.65}$$

Note that since we have already considered effects of the anisotropic expansion on force (or potential) calculations in the previous subsection, we can use the same kick operators. On the other hand, the drift operator should be modified due to the modified canonical momentum.

5.4 Growth response from simulations

In this section, we show the measurement of the growth term in the response of the real-space matter power spectrum with respect to the large-scale tides from anisotorpic cosmological simulations.

5.4.1 Estimator of the growth response

Recall that in the presence of the large-scale tidal field τ_{ij} the power spectrum is modified as

$$P(\mathbf{k};\tau_{ij}) = P(k)\left[1+\frac{\partial \ln P(\mathbf{k})}{\partial \tau_{ij}}\tau_{ij}\right], \tag{5.66}$$

where $\partial \ln P(\mathbf{k})/\partial\tau_{ij}$ is called the response function. In general, the response function of the real-space power spectrum to the large-scale tides takes a form of

$$\frac{\partial \ln P(\mathbf{k})}{\partial \tau_{ij}} = \left[G(k) - \frac{\partial \ln P(k)}{\partial \ln k}\right]\hat{k}_i\hat{k}_j, \tag{5.67}$$

where $G(k)$ represents the growth term and the second term in the parenthesis represents the dilation term. As discussed in Sec. 5.1.2, the latter term arises from the coordinate transformation, namely, the difference of the expansion history in the global and local universes, which now leads to

$$k_{\mathrm{L},i} = \frac{a_{\mathrm{L},i}}{a_{\mathrm{G},i}}k_{\mathrm{G},i} \simeq (1+\Delta_i)\,k_{\mathrm{G},i} \simeq (1-\tau_i)\,k_{\mathrm{G},i}. \tag{5.68}$$

Note that due to the traceless nature of the tidal field, $\sum_{i=1}^{3}\tau_i = 0$, there is no difference in the units for different cosmologies after angle-averaging. Thus now we can work with $P(\mathbf{k})$ not $\Delta^2(\mathbf{k})$ and to evaluate the growth response, $G(k)$, we just compare the power spectrum of anisotropic simulations at fixed comoving scales.

We run anisotropic simulations with the eigenvalues of the tidal tensor at $z=0$ given by

$$(\tau_x,\tau_y,\tau_z) = \left(-\frac{1}{2},\ -\frac{1}{2},\ 1\right)\epsilon, \tag{5.69}$$

with $\epsilon = 0.01 \ll 1$. In this case, the angular dependence of the response becomes

$$\begin{aligned}\hat{k}_i\hat{k}_j\tau_{ij} =& \epsilon D(a)\frac{3\hat{k}_z^2-1}{2}\\ =& \epsilon D(a)\mathcal{L}_2(\hat{k}\cdot\hat{z}).\end{aligned} \tag{5.70}$$

Therefore to extract the growth response we find

$$G(k) = \frac{\left\langle [P(\mathbf{k};\tau_z = +\epsilon) - P(\mathbf{k};\tau_z = -\epsilon)]\, \mathcal{L}_2(\hat{k}\cdot\hat{z}) \right\rangle_{\rm angle}}{2D(a)\epsilon \left\langle P(\mathbf{k};\tau_i = 0)\mathcal{L}_2^2(\hat{k}\cdot\hat{z}) \right\rangle_{\rm angle}}, \tag{5.71}$$

where $\langle\cdots\rangle_{\rm angle}$ represents angle-averaging and the power spectrum in the denominator is measured from the usual isotropic simulation.

5.4.2 Simulation setup and results

Here we summarize our simulation setup. As discussed in the previous subsection, to calibrate the growth response, we run three simulations, two of which were performed in an anisotropic universe with $\epsilon = \pm 0.1$ and one of which was performed in the usual isotropic universe. These three simulations start from $z_{\rm init} = 49$ where the initial conditions are generated from the *same* initial seed, i.e., the same initial amplitudes and phases, and computed by the modified second-order Lagrangian perturbation theory. We choose the initial fluctuations that are consistent with the Planck 2018 result [13]. Then, we run modified `L-Gadget2` with 512^3 particles, 512^3 PM grid in the simulation box length $L = 250\ h^{-1}$Mpc. In measuring the power spectrum, we used the cloud-in-cell (CIC) assignment to 1024^3 grid.

Fig. 5.1 shows the growth response to the large-scale tides measured from the anisotropic N-body simulations at $z = 0$ and $z = 1$. We also plot the perturbation-theory prediction, namely, $G(k) = 8/7$ by the black-dashed line. On large scales where the nonlinearities is still small, the measured $G(k)$ follows the the perturbation-theory (PT) prediction value as expected. On the other hand, on small scales, the response deviates from the PT prediction because of the nonlinear structure formation.

In contrast to the response to the large-scale density perturbation, which is enhanced than the PT prediction on small scales [31, 49] because in overdense region more matter accumulates and then more halos are formed than in underdense region, we find the response to the large-scale tides decreases monotonically. Furthermore, the lower the redshift is, the less the growth response is on small scales. This suppression can be attributed to two factors. First, the suppression in intermediate scales is due to the fact that halo number density does not change at linear order of the tidal field (recall that the tidal bias starts at second order), whereas the long-wavelength density mode does. Second, the decrease in smaller scales suggests that the inner structures of halos is not significantly affected by outer tidal fields, because the inner regions of halos are virialized and thus they no longer remember

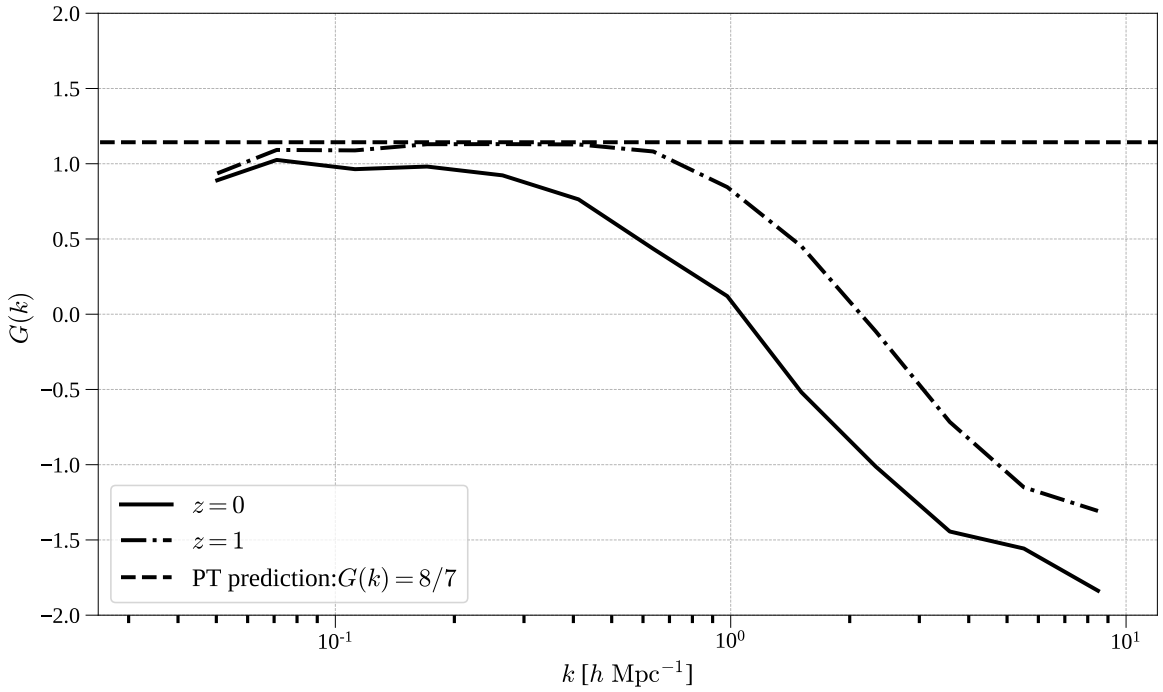

Figure 5.1: Growth response $G(k)$ of the matter power spectrum to the large-scale tides measured from tidal separate universe simulations. The dashed line depicts the tree-level perturbation theory prediction Eq. (4.27). The solid and dashdot lines depict nonlinear response at $z = 1$ and $z = 0$, respectively.

the memory of the external tidal fields. This implies that on the smallest scales the total response $\partial \ln P(k)/\partial \tau_{ij}$ goes to zero, which results in

$$G(k) \to \frac{\partial \ln P(k)}{\partial \ln k} \simeq -2. \tag{5.72}$$

The transition from the positive values to the negative of $G(k)$ seems to agree with this expectation, although to confirm this conjecture needs to run higher-resolution simulations.

Chapter 6

Conclusions

In this thesis, using the standard perturbation theory, we derived the response functions of both the real-space and redshift-space power spectrum to super-sample tidal modes. Since a given survey realization is generally embedded in the presence of super-sample modes, $\delta_{\rm b}$ and τ_{ij}, they alter the statistically averaged quantities in observations, compared with the ensemble average expectation for an infinite volume. There are two effects. First, the presence of the super-sample modes changes the growth of small-scale fluctuations via the nonlinear mode coupling. Secondly, it causes a dilation effect, the modulation of a short comoving distance scale due to the change of the local expansion factor in the finite volume region. In particular we showed that the large-scale tide, τ_{ij}, causes apparent anisotropic clustering in the redshift-space power spectrum, where the effect has directional dependence determined by an alignment of the large-scale tide, the directions of small-scale modes, and the line-of-sight direction. This effect mimics the anisotropic clustering due to the redshift-space distortion effect of the small-scale peculiar velocities of galaxies as well as the apparent cosmological distortion caused by the use of an incorrect cosmological model in the clustering analysis.

To assess a possible impact of τ_{ij} on parameter estimation from a measurement of the redshift-space power spectrum in a given survey realization, we used the Fisher information matrix formalism. To do this, we considered the two-dimensional redshift-space power spectrum, $P_s^{\rm 2D}(k_\perp, k_\parallel; \tau_{33})$ as an observable, which is obtained from the azimuthal angle average of the redshift-space power spectrum estimator in the two-dimensional plane perpendicular to the line-of-sight direction under the global plane-parallel approximation. In this case, the effects of the large-scale tide are modeled by a single quantity, τ_{33}, the line-of-sight component of the tide. We showed that, if allowing τ_{33} to freely vary, it causes a significant degradation in the parameters, D_A, H and β, due to almost perfect degeneracies between τ_{33} and the

parameters in the power spectrum. If one adopts a prior on τ_{33} assuming the rms expected for a ΛCDM model, it efficiently lifts the parameter degeneracies and restores an accuracy of the cosmological parameters that are expected for a galaxy survey without the super-sample mode. Thus the impact of the large-scale tide on the redshift-space power spectrum is not as large as the impact of the large-scale density contrast, $\delta_{\rm b}$, on the real-space power spectrum such as the weak lensing power spectrum [30, 31, 41], as long as the large-scale tide obeys the ΛCDM expectation.

We have also addressed whether a measurement of redshift-space power spectrum can be used to *constrain* the super-sample tidal modes τ_{ij} in the survey realization, rather than treating τ_{ij} as a nuisance parameter. To do so, it is essential to notice the fact that τ_{ij} breaks the statistical isotropy of the observed galaxy power spectrum. The BipoSH formalism we employed characterizes statistical anisotropic signals via a multipole index L in the BipoSH basis $\{Y_\ell(\hat{k}) \otimes Y_{\ell'}(\hat{n})\}_{LM}$, and non-zero L modes mean the presence of statistical anisotropy; in other words, we can single out only the statistical anisotropic signal by measuring the $L \neq 0$ mode. The super-sample tidal components result in the $L = 2$ mode in which all degrees of freedom of τ_{ij} are extracted. We showed emplying the BipoSH formalism τ_{ij} can be well constrained at an accuracy better than the rms for the ΛCDM model, with unbiased estimations on f, H and D_A. This is an interesting possibility, because the method gives an access to such a large-scale tide from a measurement of the small-scale fluctuations. One of possible applications is to confirm the matter-radiation equality bump in the power spectrum that is predicted in the linear cosmological perturbation theory. Assuming that there is no decrease in the power spectrum at low k unlike the ΛCDM model, the super-sample tides predicted from Eq. (4.14) should become larger than the ΛCDM prediction. To put it another way, a non-detection of such large tides can rule out the model that has no matter-radiation equality bump in the power spectrum. Related to this direction, another application lies in exploring the large-scale anomaly such as the quintessential isocurvature [113], tensor-fossils [114, 115] and super-curvature fluctuation [116], which may have a connection with the CMB large-scale anomaly. In order to detect non-ΛCDM models unambiguously, we should take into account other effects such as the survey geometry, the position dependence of biases, the selection effect, and the general relativistic effects when applying this method to an actual survey data.

In the last part in this thesis, we developed a methodology of cosmological N-body simulation with the super-box tidal field by realizing the anisotropic background expansion into which the super-box tidal field is absorbed. By using this tidal separate universe simulation, we can study various effects of τ_{ij} on nonlinear structures, although here we presented only the measurement of the growth response

to the super-sample tides. First, tidal separate universe can be used to accurately measure the non-local (tidal) bias of halos, b_{s^2}, as the usual separate universe simulations are used for measuring local halo biases b_1 and b_2 [92, 105, 106]. Since biases can be seen as a "response" of the galaxy (or halo) number density to the large-scale perturbations [79], one can measure b_{s^2} with sets of the tidal separate universe simulations; $b_{s^2} = \partial \ln n_h / \partial (\tau_{ij})^2$. Second, the the correlation between τ_{ij} and shapes of halos, which is known as the intrinsic alignments [117, 118], is also worth investigating. These applications require the modifications of a halo finder, and are our future works.

Appendix A

Useful identities

In this appendix, we summarize the useful properties of the spherical harmonics and the wigner symbols.

The addition theorem of the spherical harmonics tells us that

$$\mathcal{L}_\ell(\hat{k}\cdot\hat{x}) = \frac{4\pi}{2\ell+1}\sum_m Y_{\ell m}(\hat{k})Y^*_{\ell m}(\hat{x}), \tag{A.1}$$

where $\mathcal{L}_\ell(\mu)$ is the ℓ-th Legendre polynominal. The orthogonality for the spherical harmonics are

$$\int d^2\hat{k}\; Y_{\ell m}(\hat{k})Y^*_{\ell' m'}(\hat{k}) = \delta^K_{\ell\ell'}\delta^K_{mm'}, \tag{A.2}$$

$$\sum_{\ell m} Y_{\ell m}(\hat{k})Y^*_{\ell m}(\hat{k}') = \delta^{(2)}_D(\hat{k}-\hat{k}'). \tag{A.3}$$

The complex conjugate of the spherical harmonics becomes

$$Y^*_{\ell m}(\hat{k}) = (-1)^m Y_{\ell -m}(\hat{k}). \tag{A.4}$$

A unit vector is written by the spherical harmonics [119]

$$\hat{k}_i = \sum_m \alpha^m_i Y_{1m}(\hat{k}), \tag{A.5}$$

$$\boldsymbol{\alpha}^m = \sqrt{\frac{2\pi}{3}}\begin{pmatrix} -m(\delta^K_{m,1}+\delta^K_{m,-1}) \\ i(\delta^K_{m,1}+\delta^K_{m,-1}) \\ \sqrt{2}\delta^K_{m,0}\end{pmatrix}, \tag{A.6}$$

and the coefficient vector $\boldsymbol{\alpha}^m$ satisfies the following relations,

$$(\boldsymbol{\alpha}^m)^* = (-1)^m\boldsymbol{\alpha}^{-m}, \tag{A.7}$$

$$\boldsymbol{\alpha}^m\cdot\boldsymbol{\alpha}^{m'} = \frac{4\pi}{3}(-1)^m\delta^K_{m,-m'}, \tag{A.8}$$

$$\sum_m \alpha^m_i(\alpha^m_j)^* = \frac{4\pi}{3}\delta^K_{ij}. \tag{A.9}$$

A product of two spherical harmonics which have the same variable is reduced to a spherical harmonics

$$\begin{aligned} Y_{\ell_1 m_1}(\hat{k}) Y_{\ell_2 m_2}(\hat{k}) &= \sum_{LM} \sqrt{\frac{(2\ell_1+1)(2\ell_2+1)(2L+1)}{4\pi}} \\ &\quad \times \begin{pmatrix} \ell_1 & \ell_2 & L \\ 0 & 0 & 0 \end{pmatrix} \begin{pmatrix} \ell_1 & \ell_2 & L \\ m_1 & m_2 & M \end{pmatrix} Y^*_{LM}(\hat{k}) \\ &\equiv \sum_{LM} h_{\ell_1 \ell_2 L} \begin{pmatrix} \ell_1 & \ell_2 & L \\ m_1 & m_2 & M \end{pmatrix} Y^*_{LM}(\hat{k}). \end{aligned} \tag{A.10}$$

The orthogonalities for the Wigner 3-j symbol are

$$\sum_{\ell m} (2\ell+1) \begin{pmatrix} \ell_1 & \ell_2 & \ell \\ m_1 & m_2 & m \end{pmatrix} \begin{pmatrix} \ell_1 & \ell_2 & \ell \\ m'_1 & m'_2 & m \end{pmatrix} = \delta^K_{m_1 m'_1} \delta^K_{m_2 m'_2}, \tag{A.11}$$

$$\sum_{m_1 m_2} \begin{pmatrix} \ell_1 & \ell_2 & \ell \\ m_1 & m_2 & m \end{pmatrix} \begin{pmatrix} \ell_1 & \ell_2 & \ell' \\ m_1 & m_2 & m' \end{pmatrix} = \frac{\delta^K_{\ell \ell'} \delta^K_{m m'}}{2\ell+1}. \tag{A.12}$$

The angular momentum coupling implies

$$\sum_m (-1)^{\ell - m} \begin{pmatrix} \ell & \ell & L \\ m & -m & M \end{pmatrix} = \sqrt{2L+1} \delta_{L,0} \delta_{M,0}. \tag{A.13}$$

The wigner 6-j symbol is defined as

$$\begin{aligned} \begin{Bmatrix} \ell_1 & \ell_2 & \ell_3 \\ \ell_4 & \ell_5 & \ell_6 \end{Bmatrix} \begin{pmatrix} \ell_1 & \ell_2 & \ell_3 \\ m_1 & m_2 & m_3 \end{pmatrix} &\equiv \sum_{m_4 m_5 m_6} (-1)^{\sum_{i=4}^{6} (\ell_i - m_i)} \\ &\quad \times \begin{pmatrix} \ell_5 & \ell_1 & \ell_6 \\ m_5 & -m_1 & -m_6 \end{pmatrix} \begin{pmatrix} \ell_6 & \ell_2 & \ell_4 \\ m_6 & -m_2 & -m_4 \end{pmatrix} \begin{pmatrix} \ell_4 & \ell_3 & \ell_5 \\ m_4 & -m_3 & -m_5 \end{pmatrix}. \end{aligned} \tag{A.14}$$

Appendix B

Super-sample covariance

In this appendix, we provide the derivation of the response function by computing the collapsed trispectrum. The covariance matrix of the power spectrum estimator (Eq. 4.4) is defined as

$$C(\mathbf{k},\mathbf{k}') = \left\langle \hat{P}(\mathbf{k})\hat{P}(\mathbf{k}') \right\rangle - P(\mathbf{k})P(\mathbf{k}'). \tag{B.1}$$

Inserting Eq. (4.15) into the above equation leads us to find a formal expression of the super-sample covariance due to $\delta_{\rm b}$ and τ_{ij}:

$$C^{\rm SSC}(\mathbf{k},\mathbf{k}') = \sigma_{\rm b}^2 \frac{\partial P(k)}{\partial \delta_{\rm b}} \frac{\partial P(k')}{\partial \delta_{\rm b}} + \langle \tau_{ij}\tau_{\ell m}\rangle \frac{\partial P(k)}{\partial \tau_{ij}} \frac{\partial P(k')}{\partial \tau_{\ell m}}, \tag{B.2}$$

where we have assumed $\langle \delta_{\rm b}\tau_{ij}\rangle \simeq 0$ for a reasonably symmetric survey window. Following the formulation in Refs. [30, 32], we advocate that the squeezed trispectrum can be characterized by the responses of the power spectrum to the super-sample modes as

$$\begin{aligned}
&\lim_{q\to 0}\left[T(\mathbf{k},-\mathbf{k}+\mathbf{q},\mathbf{k}',-\mathbf{k}-\mathbf{q}) - T(\mathbf{k},-\mathbf{k},\mathbf{k}',-\mathbf{k}')\right] \\
&\simeq P_{\rm lin}(q)\left[\frac{\partial P(k)}{\partial \delta_{\rm b}} + \frac{\partial P(k)}{\partial \tau_{ij}}\left(\hat{q}_i\hat{q}_j - \frac{1}{3}\delta^K_{ij}\right)\right]\left[\frac{\partial P(k')}{\partial \delta_{\rm b}} + \frac{\partial P(k')}{\partial \tau_{\ell m}}\left(\hat{q}_\ell\hat{q}_m - \frac{1}{3}\delta^K_{\ell m}\right)\right],
\end{aligned} \tag{B.3}$$

where the Fourier modes $\mathbf{q}$ are super-sample modes satisfying $k, k' \gg q$. Then we can realize that the super-sample covariance is found to be

$$C^{\rm SSC}(\mathbf{k},\mathbf{k}') = \frac{1}{V^2}\int \frac{d^2\mathbf{q}}{(2\pi)^3}|W(\mathbf{q})|^2\left[T(\mathbf{k},-\mathbf{k}+\mathbf{q},\mathbf{k}',-\mathbf{k}'-\mathbf{q}) - T(\mathbf{k},-\mathbf{k},\mathbf{k}',-\mathbf{k}')\right], \tag{B.4}$$

where $T(\mathbf{k}_1,\mathbf{k}_2,\mathbf{k}_3,\mathbf{k}_4)$ is the tree-level trispectrum, defined as

$$\langle \delta(\mathbf{k}_1)\delta(\mathbf{k}_2)\delta(\mathbf{k}_3)\delta(\mathbf{k}_4)\rangle_c = (2\pi)^3\delta^3_{\rm D}(\mathbf{k}_{1234})T(\mathbf{k}_1,\mathbf{k}_2,\mathbf{k}_3,\mathbf{k}_4). \tag{B.5}$$

Using the perturbation theory [21], the tree-level trispectrum is given by

$$\begin{aligned} T(\mathbf{k}_1,\mathbf{k}_2,\mathbf{k}_3,\mathbf{k}_4) =& 4\left[F_2(\mathbf{k}_{13},-\mathbf{k}_1)F_2(\mathbf{k}_{13},\mathbf{k}_2)P_{\rm lin}(k_{13})P_{\rm lin}(k_1)P_{\rm lin}(k_2)+11\text{ perms.}\right] \\ &+6\left[F_3(\mathbf{k}_1,\mathbf{k}_2,\mathbf{k}_3)P_{\rm lin}(k_1)P_{\rm lin}(k_2)P_{\rm lin}(k_3)+3\text{ perms.}\right], \end{aligned} \tag{B.6}$$

with the Fourier kernels defined in Eqs. (2.76) and (2.82).

Inserting Eq. (B.6) into Eq. (B.4) leads to

$$\begin{aligned} C^{\rm SSC}(\mathbf{k},\mathbf{k}') \simeq& \frac{1}{V^2}\int\frac{d^3\mathbf{q}}{(2\pi)^3}|W(\mathbf{q})|^2 4P_{\rm lin}(q)\left[P_{\rm lin}(k)F_2(\mathbf{q},-\mathbf{k})+P_{\rm lin}(|\mathbf{k}-\mathbf{q}|)F_2(\mathbf{q},\mathbf{k}-\mathbf{q})\right] \\ &\times\left[P_{\rm lin}(k')F_2(\mathbf{q},\mathbf{k}')+P_{\rm lin}(|\mathbf{k}'+\mathbf{q}|)F_2(-\mathbf{q},\mathbf{k}'+\mathbf{q})\right], \end{aligned} \tag{B.7}$$

where we have used the fact that the window function supports $q \ll k, k'$ so the only squeezed trispectrum contribution is relevant. To further proceed the calculation, we need to care the fact that the mode coupling kernel F_2 has a pole. More especially, under the fact $k, k' \gg q$, we need to use the following expansion such as

$$\begin{aligned} P_{\rm lin}(|\mathbf{k}-\mathbf{q}|)F_2(\mathbf{q},\mathbf{k}-\mathbf{q}) \simeq& \left[P_{\rm lin}(k)-\frac{\partial P(k)}{\partial k}(\mathbf{k}\cdot\mathbf{q})\right] \\ &\times\left[\frac{5}{7}+\frac{1}{2}\left(\frac{1}{q^2}+\frac{1}{k^2}\right)(\mathbf{k}\cdot\mathbf{q}-q^2)+\frac{(\mathbf{k}\cdot\mathbf{q}-q^2)^2}{q^2k^2}\right]. \end{aligned} \tag{B.8}$$

Then we can find that the super-sample covariance can be computed as

$$\begin{aligned} C^{\rm SSC}(\mathbf{k},\mathbf{k}') \simeq& \sigma_{\rm b}^2\left[\frac{47}{21}-\frac{1}{3}\frac{\partial\ln P_{\rm lin}(k)}{\partial\ln k}\right]\left[\frac{47}{21}-\frac{1}{3}\frac{\partial\ln P_{\rm lin}(k')}{\partial\ln k'}\right]P_{\rm lin}(k)P_{\rm lin}(k') \\ &+\langle\tau_{ij}\tau_{\ell m}\rangle\,\hat{k}_i\hat{k}_j\hat{k}'_\ell\hat{k}'_m\left[\frac{8}{7}-\frac{\partial\ln P_{\rm lin}(k)}{\partial\ln k}\right]\left[\frac{8}{7}-\frac{\partial\ln P_{\rm lin}(k')}{\partial\ln k'}\right]P_{\rm lin}(k)P_{\rm lin}(k'), \end{aligned} \tag{B.9}$$

where $\hat{k}=\mathbf{k}/k$. To arrive at this equation, we have used the following identities for

the $\mathbf{q}$-integration:

$$\int \frac{d^3\mathbf{q}}{(2\pi)^3}\,|W(\mathbf{q})|^2 P_{\rm lin}(q) = \sigma_{\rm b}^2, \tag{B.10}$$

$$\begin{aligned}\int \frac{d^3\mathbf{q}}{(2\pi)^3}\,|W(\mathbf{q})|^2 P_{\rm lin}(q)\hat{q}_i\hat{q}_j &= \int \frac{d^3\mathbf{q}}{(2\pi)^3}\,|W(\mathbf{q})|^2 P_{\rm lin}(q)\left[\left(\hat{q}_i\hat{q}_j - \frac{\delta^K_{ij}}{3}\right) + \frac{\delta^K_{ij}}{3}\right] \\ &= \langle \delta_{\rm b}\tau_{ij}\rangle + \frac{\delta^K_{ij}}{3}\sigma_{\rm b}^2 \\ &\simeq \frac{\delta^K_{ij}}{3}\sigma_{\rm b}^2, \end{aligned} \tag{B.11}$$

$$\begin{aligned}\int \frac{d^3\mathbf{q}}{(2\pi)^3}\,|W(\mathbf{q})|^2 P_{\rm lin}(q)\hat{q}_i\hat{q}_j\hat{q}_\ell\hat{q}_m &\simeq \int \frac{d^3\mathbf{q}}{(2\pi)^3}\,|W(\mathbf{q})|^2 P_{\rm lin}(q) \\ &\quad\times\left[\left(\hat{q}_i\hat{q}_j - \frac{\delta^K_{ij}}{3}\right)\left(\hat{q}_\ell\hat{q}_m - \frac{\delta^K_{lm}}{3}\right) + \frac{\delta^K_{ij}\delta^K_{lm}}{9}\right] \\ &= \langle \tau_{ij}\tau_{\ell m}\rangle + \frac{\delta^K_{ij}\delta^K_{\ell m}}{9}\sigma_{\rm b}^2. \end{aligned} \tag{B.12}$$

Note that we have also used the fact that terms involving the moments with an odd power of $\hat{q}_i$ or equivalently an odd power of $\hat{k}_i$ are vanishing under the parity invariance conditions of $\mathbf{k} \leftrightarrow -\mathbf{k}$ and $\mathbf{k}' \leftrightarrow -\mathbf{k}'$.

Comparing Eqs. (B.2) and (B.9) leads us to find that the power spectrum response can be given as

$$\begin{aligned}P(\mathbf{k};\delta_{\rm b},\tau_{ij}) \simeq P(k) &+ \delta_{\rm b}\left[\frac{47}{21} - \frac{1}{3}\frac{\partial \ln P_{\rm lin}(k)}{\partial \ln k}\right] P_{\rm lin}(k) \\ &+ \hat{k}_i\hat{k}_j\tau_{ij}\left[\frac{8}{7} - \frac{\partial \ln P_{\rm lin}(k)}{\partial \ln k}\right] P_{\rm lin}(k), \end{aligned} \tag{B.13}$$

This matches Eqs. (4.26) and (4.27), which are derived from the squeezed bispectrum.

Appendix C

Muitipole power spectra

Contents

C.1 Multipole power spectra in the redshift-space power spectrum

Here, we show the multipole expansion of 2D power spectrum in redshift space. The multipole power spectrum are defined as

$$P^{\ell}_{s,\mathrm{obs}}(k;\delta_{\mathrm{b}},\tau_{33}) \equiv (2\ell+1)\int_{-1}^{1}\frac{d\mu}{2}\,P^{\mathrm{2D}}_{s,\mathrm{obs}}(k,\mu;\delta_{\mathrm{b}},\tau_{33})\mathcal{L}_{\ell}(\mu), \tag{C.1}$$

where $\mathcal{L}_{\ell}(\mu)$ is the Legendre polynomial. Making the use of Eq. (4.37) and Eq. (4.42), the multipole power spectra in redshift space can be calculated as

$$\begin{aligned}
\frac{\partial P^{\ell=0}_{s,\mathrm{obs}}}{\partial\delta_{\mathrm{b}}} =& \left(\frac{47}{21}b_1^2+2b_2+\frac{26}{21}b_1f+\frac{2}{3}b_2f+b_1^2f+\frac{31}{105}f^2+\frac{2}{3}b_1f^2+\frac{13}{105}f^3\right)P(k)\\
&-\left(\frac{1}{3}b_1^2+\frac{2}{9}b_1f+\frac{1}{9}b_1^2f+\frac{1}{15}f^2+\frac{2}{15}b_1f^2+\frac{1}{21}f^3\right)\frac{\partial P(k)}{\partial\ln k}, \qquad \text{(C.2)}\\
\frac{\partial P^{\ell=2}_{s,\mathrm{obs}}}{\partial\delta_{\mathrm{b}}} =& \left(\frac{52}{21}b_1f+\frac{4}{3}b_1^2f+\frac{4}{3}b_2f+\frac{124}{147}f^2+\frac{40}{21}b_1f^2+\frac{4}{9}f^3\right)P(k)\\
&-\left(\frac{4}{9}b_1f+\frac{2}{9}b_1^2f+\frac{4}{21}f^2+\frac{8}{21}b_1f^2+\frac{10}{63}f^3\right)\frac{\partial P(k)}{\partial\ln k}, \qquad \text{(C.3)}\\
\frac{\partial P^{\ell=4}_{s,\mathrm{obs}}}{\partial\delta_{\mathrm{b}}} =& \left(\frac{248}{735}f^2+\frac{16}{21}b_1f^2+\frac{56}{165}f^3\right)P(k)\\
&-\left(\frac{8}{105}f^2+\frac{16}{105}b_1f^2+\frac{8}{77}f^3\right)\frac{\partial P(k)}{\partial\ln k}, \qquad \text{(C.4)}\\
\frac{\partial P^{\ell=6}_{s,\mathrm{obs}}}{\partial\delta_{\mathrm{b}}} =& \frac{64}{693}f^3P(k)-\frac{16}{693}f^3\frac{\partial P(k)}{\partial\ln k}, \qquad \text{(C.5)}\\
\frac{\partial P^{\ell=0}_{s,\mathrm{obs}}}{\partial\tau_{33}} =& \left(\frac{16}{35}b_1f+\frac{4}{15}b_1^2f+\frac{8}{15}b_1b_{s^2}f+\frac{64}{245}f^2+\frac{4}{5}b_1f^2+\frac{13}{35}f^3\right)P(k)\\
&-\left(\frac{4}{15}b_1f+\frac{1}{3}b_1^2f+\frac{4}{35}f^2+\frac{2}{5}b_1f^2+\frac{1}{7}f^3\right)\frac{\partial P(k)}{\partial\ln k}, \qquad \text{(C.6)}\\
\frac{\partial P^{\ell=2}_{s,\mathrm{obs}}}{\partial\tau_{33}} =& \left(\frac{8}{7}b_1^2+2b_1b_{s^2}+\frac{88}{49}b_1f+\frac{22}{21}b_1^2f+\frac{44}{21}b_1b_{s^2}f+\frac{48}{49}f^2+\frac{16}{7}b_1f^2+\frac{4}{3}f^3\right)P(k)\\
&-\left(b_1^2+\frac{22}{21}b_1f+\frac{2}{3}b_1^2f+\frac{3}{7}f^2+\frac{8}{7}b_1f^2+\frac{10}{21}f^3\right)\frac{\partial P(k)}{\partial\ln k}, \qquad \text{(C.7)}\\
\frac{\partial P^{\ell=4}_{s,\mathrm{obs}}}{\partial\tau_{33}} =& \left(\frac{288}{245}b_1f+\frac{48}{35}b_1b_{s^2}f+\frac{2176}{2695}f^2+\frac{32}{35}b_1f^2+\frac{56}{55}f^3\right)P(k)\\
&-\left(\frac{24}{35}b_1f+\frac{136}{385}f^2+\frac{16}{35}b_1f^2+\frac{24}{77}f^3\right)\frac{\partial P(k)}{\partial\ln k}, \qquad \text{(C.8)}
\end{aligned}$$

$$\frac{\partial P_{s,\mathrm{obs}}^{\ell=6}}{\partial \tau_{33}} = \left(\frac{128}{539}f^2 + \frac{64}{231}f^3\right) P(k) - \left(\frac{128}{539}f^2 + \frac{16}{231}f^3\right) \frac{\partial P(k)}{\partial \ln k}. \tag{C.9}$$

C.2 Relationship between the BipoSH and the other expansion schemes

In this appendix, we give the connection between our formalism and other schemes to decompose anisotropic signals.

C.2.1 Relationship between the BipoSH and the Legendre expansion

The relationship between the BoPoSH and the usual Legendre expansion with the line-of-sight $\hat{n}$ setting $\hat{z}$ is

$$\begin{aligned} P_\ell(k) =&(2\ell+1)\int\frac{d^2\hat{k}}{4\pi}\int\frac{d^2\hat{n}}{4\pi}\,P^s(\mathbf{k},\hat{n};\delta_{\rm b},\tau_{ij})\mathcal{L}_\ell(\hat{k}\cdot\hat{n})(4\pi)\delta_D^{(2)}(\hat{n}-\hat{z}) \\ =&\sum_{LM\ell'}\pi^{LM}_{\ell\ell'}(k;\delta_{\rm b},\tau_{ij})(-1)^{\ell-\ell'+M}\sqrt{\frac{(2\ell+1)(2\ell'+1)(2L+1)}{(4\pi)^2}}\begin{pmatrix}\ell & \ell' & L\\ 0 & 0 & -M\end{pmatrix} \\ =&\sum_{L\ell'}P^{L0}_{\ell\ell'}(k;\delta_{\rm b},\tau_{ij}), \end{aligned} \tag{C.10}$$

where we used $Y_{\ell m}(\hat{z})=\sqrt{(2\ell+1)/(4\pi)}\delta_{m0}$. Notice that the summation of L and ℓ' is limited by the Wigner $3j$ symbol $\left(\begin{smallmatrix}\ell & \ell' & L\\ 0 & 0 & 0\end{smallmatrix}\right)$. For instance,

$$P_{\ell=0}(k) =P^{00}_{00}(k)+P^{20}_{02}(k), \tag{C.11}$$
$$P_{\ell=2}(k) =P^{00}_{22}(k)+P^{20}_{20}(k)+P^{20}_{22}(k)+P^{20}_{24}(k), \tag{C.12}$$
$$P_{\ell=4}(k) =P^{00}_{44}(k)+P^{20}_{42}(k)+P^{20}_{44}(k)+P^{20}_{46}(k), \tag{C.13}$$
$$P_{\ell=6}(k) =P^{20}_{64}(k)+P^{20}_{66}(k)., \tag{C.14}$$
$$\tag{C.15}$$

This reproduces the result presented in Eqs. (C.2)-(C.9).

C.2.2 Relationship between the BipoSH and the single spherical harmonic expansion

In Ref. [94], the authors defined the spherical multipole expansion,

$$P_{gg}(\mathbf{k};\hat{n}\parallel\hat{z})=\sum_{\ell m}P_{gg;\ell m}(k)Y_{\ell m}(\hat{k}), \tag{C.16}$$
$$P_{gg;\ell m}(k)=\int d^2\hat{k}\;P_{gg}(\mathbf{k};\hat{n}\parallel\hat{z})Y^*_{\ell m}(\hat{k}). \tag{C.17}$$

The transformation from the BipoSH expansion to the spherical multipole expansion is

$$\begin{aligned} P_{gg,\ell m}(k) &= \int \frac{d^2\hat{k}}{4\pi} \int \frac{d^2\hat{n}}{4\pi}\ P^s(\mathbf{k},\hat{n};\delta_{\rm b},\tau_{ij}) Y^*_{\ell m}(\hat{k})(4\pi)\delta_D^{(2)}(\hat{n}-\hat{z}) \\ &= \sum_{L\ell'} \pi^{Lm}_{\ell\ell'}(k;\delta_{\rm b},\tau_{ij})(-1)^{\ell-\ell'+m}\sqrt{\frac{(2\ell'+1)(2L+1)}{(4\pi)^3}} \begin{pmatrix} \ell & \ell' & L \\ m & 0 & -m \end{pmatrix}. \end{aligned} \tag{C.18}$$

Appendix D

BipoSH coefficients for the super-samle modes

Contents

In this appendix, we provide how to derive the explicit expressions of the BipoSH coefficients for the responses to the super-sample modes, especially, we give a derivation of each BipoSH coefficient for each type of the anisotropic terms. Using the resultant BipoSH coefficients for each type of the anisotropic terms, we finally show how to compute $D_\ell(k)$ and $T_{\ell\ell'}(k)$.

D.1 BipoSH coefficients from $(\hat{k}\cdot\hat{n})^\lambda$ terms

For later convenience, we decompose $(\hat{k}\cdot\hat{n})^\lambda$ into the spherical harmonic basis as

$$(\hat{k}\cdot\hat{n})^\lambda = \sum_{n=0}^{\lambda} A_{n\lambda}\mathcal{L}_n(\hat{k}\cdot\hat{n}) = \sum_{n=0}^{\lambda}\frac{4\pi A_{n\lambda}}{2n+1}\sum_{\nu} Y_{n\nu}(\hat{k})Y^*_{n\nu}(\hat{n}), \tag{D.1}$$

where

$$\begin{aligned} A_{n\lambda} &= \frac{2n+1}{2}\int_{-1}^{1} d\mu\ \mu^\lambda\mathcal{L}_n(\mu) \\ &= \frac{2n+1}{2}[(-1)^{n+\lambda}+1]\int_0^1 d\mu\ \mu^\lambda\mathcal{L}_n(\mu) \\ &= \frac{2n+1}{2}\frac{(-1)^{n+\lambda}+1}{2^n}\frac{\Gamma(\lambda+1)\Gamma(\frac{\lambda-n+3}{2})}{\Gamma(\lambda-n+2)\Gamma(\frac{\lambda+n+3}{2})}\Theta_{\lambda\geq n}, \end{aligned} \tag{D.2}$$

with $\Theta_{\lambda\geq n} \equiv \begin{cases} 1:\lambda\geq n \\ 0:\lambda<n \end{cases}$ being the step function. Then, the BipoSH coefficients from $(\hat{k}\cdot\hat{n})^\lambda$ terms are calculated as

$$\begin{aligned} \pi^{LM}_{\ell\ell'}(k) &= \int d^2\hat{k}\int d^2\hat{n}\ (\hat{k}\cdot\hat{n})^\lambda\sum_{mm'}\mathcal{C}^{LM}_{\ell m\ell' m'}Y^*_{\ell m}(\hat{k})Y^*_{\ell' m'}(\hat{n}) \\ &= \frac{4\pi A_{\ell\lambda}}{2\ell+1}\delta^K_{\ell\ell'}\sqrt{2L+1}(-1)^\ell\sum_m(-1)^{\ell-m}\begin{pmatrix}\ell & \ell & L\\ m & -m & M\end{pmatrix} \\ &= \frac{4\pi A_{\ell\lambda}}{\sqrt{2\ell+1}}(-1)^\ell\delta^K_{L0}\delta^K_{M0}\delta^K_{\ell\ell'}. \end{aligned} \tag{D.3}$$

D.2 BipoSH coefficients from $(\hat{k}\cdot\hat{n})^\lambda \tau_{ij}\hat{k}_i\hat{k}_j$ terms

$$
\begin{aligned}
(\hat{k}\cdot\hat{n})^\lambda \tau_{ij}\hat{k}_i\hat{k}_j &= \sum_{n=0}^{\lambda}\frac{4\pi A_{n\lambda}}{2n+1}\sum_{\nu} Y^*_{n\nu}(\hat{k})Y_{n\nu}(\hat{n})\left(\tau_{ij}\sum_{m_i m_j}\alpha_i^{m_i}Y_{1m_i}(\hat{k})\alpha_j^{m_j}Y_{1m_j}(\hat{k})\right)\\
&= \sum_{n=0}^{\lambda}\frac{4\pi A_{n\lambda}}{2n+1}\sum_{\nu} Y^*_{n\nu}(\hat{k})Y_{n\nu}(\hat{n})\tau_{ij}\\
&\qquad\times\sum_{m_i m_j}\alpha_i^{m_i}\alpha_j^{m_j}\sum_{\ell_3 m_3} h_{11\ell_3}Y^*_{\ell_3 m_3}(\hat{k})\begin{pmatrix}1 & 1 & \ell_3\\ m_i & m_j & m_3\end{pmatrix}\\
&= \sum_{n=0}^{\lambda}\frac{4\pi A_{n\lambda}}{2n+1}\tau_{ij}\sum_{\nu} Y_{n\nu}(\hat{n})\sum_{m_i m_j}\alpha_i^{m_i}\alpha_j^{m_j}\sum_{\ell_3 m_3} h_{11\ell_3}\begin{pmatrix}1 & 1 & \ell_3\\ m_i & m_j & m_3\end{pmatrix}\\
&\qquad\times\sum_{\ell'' m''} h_{n\ell_3\ell''}\begin{pmatrix}n & \ell_3 & \ell''\\ \nu & m_3 & m''\end{pmatrix}Y_{\ell'' m''}(\hat{k}),
\end{aligned}
\tag{D.4}
$$

where $h_{l_1 l_2 l_3}\equiv\sqrt{\frac{(2l_1+1)(2l_2+1)(2l_3+1)}{4\pi}}\begin{pmatrix}l_1 & l_2 & l_3\\ 0 & 0 & 0\end{pmatrix}$. Then, we have

$$
\begin{aligned}
\pi^{LM}_{\ell\ell'}(k) &= \int d^2\hat{k}\int d^2\hat{n}\,(\hat{k}\cdot\hat{n})^\lambda\tau_{ij}\hat{k}_i\hat{k}_j\sum_{mm'}\mathcal{C}^{LM}_{\ell m\ell' m'}Y^*_{\ell m}(\hat{k})Y^*_{\ell' m'}(\hat{n})\\
&= \frac{4\pi A_{\ell'\lambda}}{2\ell'+1}\tau_{ij}\sum_{m_i m_j}\alpha_i^{m_i}\alpha_j^{m_j}\sum_{\ell_3 m_3}h_{11\ell_3}\begin{pmatrix}1 & 1 & \ell_3\\ m_i & m_j & m_3\end{pmatrix}\\
&\qquad\times\sum_{mm'}\mathcal{C}^{LM}_{\ell m\ell' m'}h_{\ell'\ell_3\ell}\begin{pmatrix}\ell' & \ell_3 & \ell\\ m' & m_3 & m\end{pmatrix}\\
&= \frac{4\pi A_{\ell'\lambda}}{2\ell'+1}\tau_{ij}\sum_{m_i m_j}\alpha_i^{m_i}\alpha_j^{m_j}\begin{pmatrix}1 & 1 & L\\ m_i & m_j & -M\end{pmatrix}\frac{(-1)^{\ell-\ell'+M}}{\sqrt{2L+1}}h_{11L}h_{\ell\ell' L}.
\end{aligned}
\tag{D.5}
$$

D.3 BipoSH coefficients from $(\hat{k}\cdot\hat{n})^{\lambda}\tau_{ij}\hat{n}_i\hat{n}_j$ terms

$$
\begin{aligned}
(\hat{k}\cdot\hat{n})^{\lambda}\tau_{ij}\hat{n}_i\hat{n}_j &= \sum_{n=0}^{\lambda}\frac{4\pi A_{n\lambda}}{2n+1}\sum_{\nu}Y_{n\nu}(\hat{k})Y^{*}_{n\nu}(\hat{n})\left(\tau_{ij}\sum_{m_i m_j}\alpha_i^{m_i}Y_{1m_i}(\hat{n})\alpha_j^{m_j}Y_{1m_j}(\hat{n})\right)\\
&= \sum_{n=0}^{\lambda}\frac{4\pi A_{n\lambda}}{2n+1}\sum_{\nu}Y_{n\nu}(\hat{k})Y^{*}_{n\nu}(\hat{n})\tau_{ij}\sum_{m_i m_j}\alpha_i^{m_i}\alpha_j^{m_j}\\
&\qquad\times\sum_{\ell_3 m_3}h_{11\ell_3}Y^{*}_{\ell_3 m_3}(\hat{n})\begin{pmatrix}1 & 1 & \ell_3\\ m_i & m_j & m_3\end{pmatrix}\\
&= \sum_{n=0}^{\lambda}\frac{4\pi A_{n\lambda}}{2n+1}\tau_{ij}\sum_{\nu}Y_{n\nu}(\hat{k})\sum_{m_i m_j}\alpha_i^{m_i}\alpha_j^{m_j}\sum_{\ell_3 m_3}h_{11\ell_3}\begin{pmatrix}1 & 1 & \ell_3\\ m_i & m_j & m_3\end{pmatrix}\\
&\qquad\times\sum_{\ell'' m''}h_{n\ell_3\ell''}\begin{pmatrix}n & \ell_3 & \ell''\\ \nu & m_3 & m''\end{pmatrix}Y_{\ell'' m''}(\hat{n}).
\end{aligned}
\tag{D.6}
$$

Then, we have

$$
\begin{aligned}
\pi^{LM}_{\ell\ell'}(k) &= \int d^2\hat{k}\int d^2\hat{n}\;(\hat{k}\cdot\hat{n})^{\lambda}\tau_{ij}\hat{n}_i\hat{n}_j\sum_{mm'}\mathcal{C}^{LM}_{\ell m\ell' m'}Y^{*}_{\ell m}(\hat{k})Y^{*}_{\ell' m'}(\hat{n})\\
&= \frac{4\pi A_{\ell\lambda}}{2\ell+1}\tau_{ij}\sum_{m_i m_j}\alpha_i^{m_i}\alpha_j^{m_j}\sum_{\ell_3 m_3}h_{11\ell_3}\begin{pmatrix}1 & 1 & \ell_3\\ m_i & m_j & m_3\end{pmatrix}\\
&\qquad\times\sum_{mm'}\mathcal{C}^{LM}_{\ell m\ell' m'}h_{\ell\ell_3\ell'}\begin{pmatrix}\ell & \ell_3 & \ell'\\ m & m_3 & m'\end{pmatrix}\\
&= \frac{4\pi A_{\ell\lambda}}{2\ell+1}\tau_{ij}\sum_{m_i m_j}\alpha_i^{m_i}\alpha_j^{m_j}\begin{pmatrix}1 & 1 & L\\ m_i & m_j & -M\end{pmatrix}\frac{(-1)^{\ell-\ell'+M}}{\sqrt{2L+1}}h_{11L}h_{\ell'\ell L}.
\end{aligned}
\tag{D.7}
$$

D.4 BipoSH coefficients from $(\hat{k}\cdot\hat{n})^\lambda\tau_{ij}\hat{k}_i\hat{n}_j$ terms

$$
\begin{aligned}
(\hat{k}\cdot\hat{n})^\lambda\tau_{ij}\hat{k}_i\hat{n}_j &= \sum_{n=0}^{\lambda}\frac{4\pi A_{n\lambda}}{2n+1}\sum_{\nu}Y_{n\nu}(\hat{k})Y^*_{n\nu}(\hat{n})\left(\tau_{ij}\sum_{m_im_j}\alpha_i^{m_i}Y_{1m_i}(\hat{k})\alpha_j^{m_j}Y_{1m_j}(\hat{n})\right)\\
&= \sum_{n=0}^{\lambda}\frac{4\pi A_{n\lambda}}{2n+1}\tau_{ij}\sum_{\nu}\sum_{m_im_j}(-1)^{\nu+m_i+m_j}\alpha_i^{m_i}\alpha_j^{m_j}\sum_{\ell_3m_3}\sum_{\ell_3'm_3'}Y_{\ell_3m_3}(\hat{k})Y_{\ell_3'm_3'}(\hat{n})\\
&\qquad\times h_{n1\ell_3}h_{n1\ell_3'}\begin{pmatrix}n & 1 & \ell_3\\ -\nu & -m_i & m_3\end{pmatrix}\begin{pmatrix}n & 1 & \ell_3'\\ \nu & -m_j & m_3'\end{pmatrix}.
\end{aligned}
\tag{D.8}
$$

Then, we have

$$
\begin{aligned}
\pi^{LM}_{\ell\ell'}(k) &= \int d^2\hat{k}\int d^2\hat{n}\ (\hat{k}\cdot\hat{n})^\lambda\tau_{ij}\hat{k}_i\hat{n}_j\sum_{mm'}\mathcal{C}^{LM}_{\ell m\ell' m'}Y^*_{\ell m}(\hat{k})Y^*_{\ell' m'}(\hat{n})\\
&= \sum_{n=0}^{\lambda}\frac{4\pi A_{n\lambda}}{2n+1}\tau_{ij}\sum_{\nu}\sum_{m_im_j}(-1)^{\nu+m_i+m_j}\alpha_i^{m_i}\alpha_j^{m_j}h_{n1\ell}h_{n1\ell'}\\
&\qquad\times\sum_{mm'}\mathcal{C}^{LM}_{\ell m\ell' m'}\begin{pmatrix}n & 1 & \ell\\ -\nu & -m_i & m\end{pmatrix}\begin{pmatrix}n & 1 & \ell'\\ \nu & -m_j & m'\end{pmatrix}\\
&= \sum_{n=0}^{\lambda}\frac{4\pi A_{n\lambda}}{2n+1}(-1)^{n+L+M}\sqrt{2L+1}\tau_{ij}\sum_{m_im_j}\alpha_i^{m_i}\alpha_j^{m_j}h_{n1\ell}h_{n1\ell'}\\
&\qquad\times\begin{pmatrix}1 & 1 & L\\ m_i & m_j & -M\end{pmatrix}\begin{Bmatrix}1 & 1 & L\\ \ell' & \ell & n\end{Bmatrix}.
\end{aligned}
\tag{D.9}
$$

D.5 $D_\ell(k)$ and $T_{\ell\ell'}(k)$

Since the response to $\delta_{\rm b}$ depends only on $\mu = (\hat{k}\cdot\hat{n})$, $D_\ell(k)$ are computed as

$$D_\ell(k) = (\text{coefficients to } \mu^\lambda \text{ in the response to } \delta_{\rm b}) \times A_{\ell\lambda}\sqrt{2\ell+1}H_{\ell\ell 0}. \tag{D.10}$$

The response to τ_{ij} includes three types of angular dependence, $\mu^\lambda\tau_{ij}\hat{k}_i\hat{k}_j$, $\mu^\lambda\tau_{ij}\hat{n}_i\hat{n}_j$, and $\mu^\lambda\tau_{ij}\hat{k}_i\hat{n}_j$ and therefore $T_{\ell\ell'}(k)$ are computed as

$$\begin{aligned}
T_{\ell\ell'}(k) =& (\text{coefficients to } \mu^\lambda\tau_{ij}\hat{k}_i\hat{k}_j \text{ in the response to } \tau_{ij}) \\
&\times \frac{A_{\ell'\lambda}\sqrt{2\ell+1}}{\sqrt{2\ell'+1}}\tau_{ij}H_{\ell\ell' 2}\sum_{m_i m_j}\alpha_i^{m_i}\alpha_j^{m_j}\begin{pmatrix}1 & 1 & 2\\ m_i & m_j & -M\end{pmatrix}h_{112}h_{\ell\ell' 2} \\
&+ (\text{coefficients to } \mu^\lambda\tau_{ij}\hat{n}_i\hat{n}_j \text{ in the response to } \tau_{ij}) \\
&\times \frac{A_{\ell\lambda}\sqrt{2\ell'+1}}{\sqrt{2\ell+1}}\tau_{ij}H_{\ell\ell' 2}\sum_{m_i m_j}\alpha_i^{m_i}\alpha_j^{m_j}\begin{pmatrix}1 & 1 & 2\\ m_i & m_j & -M\end{pmatrix}h_{112}h_{\ell\ell' 2} \\
&+ (\text{coefficients to } \mu^\lambda\tau_{ij}\hat{k}_i\hat{n}_j \text{ in the response to } \tau_{ij}) \\
&\times \sum_{n=0}^{\lambda}\frac{A_{n\lambda}}{2n+1}(-1)^{n+M}5\cdot\sqrt{(2\ell+1)(2\ell'+1)}\tau_{ij}\sum_{m_i m_j}\alpha_i^{m_i}\alpha_j^{m_j}h_{n1\ell}h_{n1\ell'} \\
&\qquad\times\begin{pmatrix}1 & 1 & 2\\ m_i & m_j & -M\end{pmatrix}\begin{Bmatrix}1 & 1 & 2\\ \ell' & \ell & n\end{Bmatrix}.
\end{aligned} \tag{D.11}$$

Bibliography

[1] A. A. Starobinsky, *A New Type of Isotropic Cosmological Models Without Singularity*, *Phys. Lett.* **B91** (1980) 99.

[2] K. Sato, *First Order Phase Transition of a Vacuum and Expansion of the Universe*, *Mon. Not. Roy. Astron. Soc.* **195** (1981) 467.

[3] A. H. Guth, *The Inflationary Universe: A Possible Solution to the Horizon and Flatness Problems*, *Phys. Rev.* **D23** (1981) 347.

[4] V. F. Mukhanov and G. V. Chibisov, *Quantum Fluctuations and a Nonsingular Universe*, *JETP Lett.* **33** (1981) 532.

[5] E. L. Turner, *Gravitational lensing limits on the cosmological constant in a flat universe*, *Astrophys. J.* **365** (1990) L43.

[6] G. Efstathiou, W. J. Sutherland and S. J. Maddox, *The cosmological constant and cold dark matter*, *Nature* **348** (1990) 705.

[7] M. Fukugita and E. L. Turner, *Gravitational lensing frequencies: Galaxy cross-sections and selection effects*, *Mon. Not. Roy. Astron. Soc.* **253** (1991) 99.

[8] M. Fukugita and P. J. E. Peebles, *Visibility of gravitational lenses and the cosmological constant problem*, astro-ph/9305002.

[9] Supernova Cosmology Project collaboration, *Measurements of* Ω *and* Λ *from 42 high redshift supernovae*, *Astrophys. J.* **517** (1999) 565 [astro-ph/9812133].

[10] Supernova Search Team collaboration, *Observational evidence from supernovae for an accelerating universe and a cosmological constant*, *Astron. J.* **116** (1998) 1009 [astro-ph/9805201].

[11] COBE collaboration, *Structure in the COBE differential microwave radiometer first year maps*, *Astrophys. J.* **396** (1992) L1.

[12] WMAP collaboration, *Seven-Year Wilkinson Microwave Anisotropy Probe (WMAP) Observations: Cosmological Interpretation*, *Astrophys. J. Suppl.* **192** (2011) 18 [1001.4538].

[13] Planck collaboration, *Planck 2018 results. VI. Cosmological parameters*, 1807.06209.

[14] BOSS collaboration, *The clustering of galaxies in the completed SDSS-III Baryon Oscillation Spectroscopic Survey: cosmological analysis of the DR12 galaxy sample*, *Mon. Not. Roy. Astron. Soc.* **470** (2017) 2617 [1607.03155].

[15] PFS Team collaboration, *Extragalactic science, cosmology, and Galactic archaeology with the Subaru Prime Focus Spectrograph*, *Publ. Astron. Soc. Jap.* **66** (2014) R1 [1206.0737].

[16] LSST Science, LSST Project collaboration, *LSST Science Book, Version 2.0*, 0912.0201.

[17] DESI collaboration, *The DESI Experiment Part I: Science,Targeting, and Survey Design*, 1611.00036.

[18] D. Spergel et al., *Wide-Field InfraRed Survey Telescope-Astrophysics Focused Telescope Assets WFIRST-AFTA Final Report*, 1305.5422.

[19] EUCLID collaboration, *Euclid Definition Study Report*, 1110.3193.

[20] O. Doré et al., *Cosmology with the SPHEREX All-Sky Spectral Survey*, 1412.4872.

[21] F. Bernardeau, S. Colombi, E. Gaztanaga and R. Scoccimarro, *Large scale structure of the universe and cosmological perturbation theory*, *Phys. Rept.* **367** (2002) 1 [astro-ph/0112551].

[22] V. Desjacques, D. Jeong and F. Schmidt, *Large-Scale Galaxy Bias*, *Phys. Rept.* **733** (2018) 1 [1611.09787].

[23] R. Scoccimarro, *Redshift-space distortions, pairwise velocities and nonlinearities*, *Phys. Rev.* **D70** (2004) 083007 [astro-ph/0407214].

[24] S. Dodelson, *Modern Cosmology*. Academic Press, Amsterdam, 2003.

[25] M. Takada and B. Jain, *Three-point correlations in weak lensing surveys: Model predictions and applications*, *Mon. Not. Roy. Astron. Soc.* **344** (2003) 857 [astro-ph/0304034].

[26] A. J. S. Hamilton, C. D. Rimes and R. Scoccimarro, *On measuring the covariance matrix of the nonlinear power spectrum from simulations*, *Mon. Not. Roy. Astron. Soc.* **371** (2006) 1188 [astro-ph/0511416].

[27] T. Baldauf, U. Seljak, L. Senatore and M. Zaldarriaga, *Galaxy Bias and non-Linear Structure Formation in General Relativity*, *JCAP* **1110** (2011) 031 [1106.5507].

[28] B. D. Sherwin and M. Zaldarriaga, *The Shift of the Baryon Acoustic Oscillation Scale: A Simple Physical Picture*, *Phys. Rev.* **D85** (2012) 103523 [1202.3998].

[29] R. de Putter, C. Wagner, O. Mena, L. Verde and W. Percival, *Thinking Outside the Box: Effects of Modes Larger than the Survey on Matter Power Spectrum Covariance*, *JCAP* **1204** (2012) 019 [1111.6596].

[30] M. Takada and W. Hu, *Power Spectrum Super-Sample Covariance*, *Phys. Rev.* **D87** (2013) 123504 [1302.6994].

[31] Y. Li, W. Hu and M. Takada, *Super-Sample Covariance in Simulations*, *Phys. Rev.* **D89** (2014) 083519 [1401.0385].

[32] Y. Li, W. Hu and M. Takada, *Super-Sample Signal*, *Phys. Rev.* **D90** (2014) 103530 [1408.1081].

[33] J. Carron and I. Szapudi, *The impact of supersurvey modes on cosmological constraints from cosmic shear fields*, *Mon. Not. Roy. Astron. Soc.* **447** (2015) 671 [1408.1744].

[34] R. Takahashi, S. Soma, M. Takada and I. Kayo, *An optimal survey geometry of weak lensing survey: minimizing supersample covariance*, *Mon. Not. Roy. Astron. Soc.* **444** (2014) 3473 [1405.2666].

[35] L. Dai, E. Pajer and F. Schmidt, *On Separate Universes*, *JCAP* **1510** (2015) 059 [1504.00351].

[36] H. Y. Ip and F. Schmidt, *Large-Scale Tides in General Relativity*, *JCAP* **1702** (2017) 025 [1610.01059].

[37] K. Akitsu, M. Takada and Y. Li, *Large-scale tidal effect on redshift-space power spectrum in a finite-volume survey*, *Phys. Rev.* **D95** (2017) 083522 [1611.04723].

[38] A. Barreira and F. Schmidt, *Responses in Large-Scale Structure*, *JCAP* **1706** (2017) 053 [1703.09212].

[39] K. C. Chan, A. Moradinezhad Dizgah and J. Noreña, *Bispectrum Supersample Covariance*, *Phys. Rev.* **D97** (2018) 043532 [1709.02473].

[40] DES collaboration, *Dark Energy Survey Year 1 Results: Multi-Probe Methodology and Simulated Likelihood Analyses*, *Submitted to: Phys. Rev. D* (2017) [1706.09359].

[41] A. Barreira, E. Krause and F. Schmidt, *Complete super-sample lensing covariance in the response approach*, *JCAP* **1806** (2018) 015 [1711.07467].

[42] N. Kaiser, *Clustering in real space and in redshift space*, *Mon. Not. Roy. Astron. Soc.* **227** (1987) 1.

[43] A. J. S. Hamilton, *Linear redshift distortions: A Review*, in *Ringberg Workshop on Large Scale Structure Ringberg, Germany, September 23-28, 1996*, 1997, astro-ph/9708102, DOI.

[44] C. Alcock and B. Paczyński, *An evolution free test for non-zero cosmological constant*, *Nature* **281** (1979) 358.

[45] H.-J. Seo and D. J. Eisenstein, *Probing dark energy with baryonic acoustic oscillations from future large galaxy redshift surveys*, *Astrophys. J.* **598** (2003) 720 [astro-ph/0307460].

[46] W. Hu and Z. Haiman, *Redshifting rings of power*, *Phys. Rev.* **D68** (2003) 063004 [astro-ph/0306053].

[47] E. Sirko, *Initial conditions to cosmological N-body simulations, or how to run an ensemble of simulations*, *Astrophys. J.* **634** (2005) 728 [astro-ph/0503106].

[48] N. Y. Gnedin, A. V. Kravtsov and D. H. Rudd, *Implementing the DC Mode in Cosmological Simulations with Supercomoving Variables*, *Astrophys. J. Suppl.* **194** (2011) 46 [1104.1428].

[49] C. Wagner, F. Schmidt, C.-T. Chiang and E. Komatsu, *Separate Universe Simulations*, *Mon. Not. Roy. Astron. Soc.* **448** (2015) L11 [1409.6294].

[50] K. Akitsu and M. Takada, *Impact of large-scale tides on cosmological distortions via redshift-space power spectrum*, *Phys. Rev.* **D97** (2018) 063527 [1711.00012].

[51] K. Akitsu, N. S. Sugiyama and M. Shiraishi, *Super-sample tidal modes on the celestial sphere*, *Phys. Rev.* **D100** (2019) 103515 [1907.10591].

[52] S. Weinberg, *Cosmological fluctuations of short wavelength*, *Astrophys. J.* **581** (2002) 810 [astro-ph/0207375].

[53] D. H. Lyth, K. A. Malik and M. Sasaki, *A General proof of the conservation of the curvature perturbation*, *JCAP* **0505** (2005) 004 [astro-ph/0411220].

[54] D. Blas, J. Lesgourgues and T. Tram, *The Cosmic Linear Anisotropy Solving System (CLASS) II: Approximation schemes*, *JCAP* **1107** (2011) 034 [1104.2933].

[55] N. E. Chisari and M. Zaldarriaga, *Connection between Newtonian simulations and general relativity*, *Phys. Rev.* **D83** (2011) 123505 [1101.3555].

[56] B. Jain and E. Bertschinger, *Selfsimilar evolution of cosmological density fluctuations*, *Astrophys. J.* **456** (1996) 43 [astro-ph/9503025].

[57] R. Scoccimarro and J. Frieman, *Loop corrections in nonlinear cosmological perturbation theory 2. Two point statistics and selfsimilarity*, *Astrophys. J.* **473** (1996) 620 [astro-ph/9602070].

[58] M. Peloso and M. Pietroni, *Galilean invariance and the consistency relation for the nonlinear squeezed bispectrum of large scale structure*, *JCAP* **1305** (2013) 031 [1302.0223].

[59] A. Kehagias and A. Riotto, *Symmetries and Consistency Relations in the Large Scale Structure of the Universe*, *Nucl. Phys.* **B873** (2013) 514 [1302.0130].

[60] J. J. M. Carrasco, S. Foreman, D. Green and L. Senatore, *The 2-loop matter power spectrum and the IR-safe integrand*, *JCAP* **1407** (2014) 056 [1304.4946].

[61] P. Creminelli, J. Noreña, M. Simonović and F. Vernizzi, *Single-Field Consistency Relations of Large Scale Structure*, *JCAP* **1312** (2013) 025 [1309.3557].

[62] P. Valageas, *Kinematic consistency relations of large-scale structures*, *Phys. Rev.* **D89** (2014) 083534 [1311.1236].

[63] R. Takahashi, *Third Order Density Perturbation and One-loop Power Spectrum in a Dark Energy Dominated Universe*, *Prog. Theor. Phys.* **120** (2008) 549 [0806.1437].

[64] J. N. Fry, *The Minimal power spectrum: Higher order contributions*, *Astrophys. J.* **421** (1994) 21.

[65] P. J. E. Peebles, *The large-scale structure of the universe*. Princeton Univ Press, 1980.

[66] T. Nishimichi, F. Bernardeau and A. Taruya, *Response function of the large-scale structure of the universe to the small scale inhomogeneities*, *Phys. Lett.* **B762** (2016) 247 [1411.2970].

[67] N. Dalal, O. Dore, D. Huterer and A. Shirokov, *The imprints of primordial non-gaussianities on large-scale structure: scale dependent bias and abundance of virialized objects*, *Phys. Rev.* **D77** (2008) 123514 [0710.4560].

[68] N. Kaiser, *On the Spatial correlations of Abell clusters*, *Astrophys. J.* **284** (1984) L9.

[69] J. M. Bardeen, J. R. Bond, N. Kaiser and A. S. Szalay, *The Statistics of Peaks of Gaussian Random Fields*, *Astrophys. J.* **304** (1986) 15.

[70] J. R. Bond, S. Cole, G. Efstathiou and N. Kaiser, *Excursion set mass functions for hierarchical Gaussian fluctuations*, *Astrophys. J.* **379** (1991) 440.

[71] J. N. Fry and E. Gaztanaga, *Biasing and hierarchical statistics in large scale structure*, *Astrophys. J.* **413** (1993) 447 [astro-ph/9302009].

[72] K. C. Chan, R. Scoccimarro and R. K. Sheth, *Gravity and Large-Scale Non-local Bias*, *Phys. Rev.* **D85** (2012) 083509 [1201.3614].

[73] T. Baldauf, U. Seljak, V. Desjacques and P. McDonald, *Evidence for Quadratic Tidal Tensor Bias from the Halo Bispectrum*, *Phys. Rev.* **D86** (2012) 083540 [1201.4827].

[74] S. Saito, T. Baldauf, Z. Vlah, U. Seljak, T. Okumura and P. McDonald, *Understanding higher-order nonlocal halo bias at large scales by combining the power spectrum with the bispectrum*, *Phys. Rev.* **D90** (2014) 123522 [1405.1447].

[75] M. Mirbabayi, F. Schmidt and M. Zaldarriaga, *Biased Tracers and Time Evolution*, *JCAP* **1507** (2015) 030 [1412.5169].

[76] R. Angulo, M. Fasiello, L. Senatore and Z. Vlah, *On the Statistics of Biased Tracers in the Effective Field Theory of Large Scale Structures*, *JCAP* **1509** (2015) 029 [1503.08826].

[77] P. McDonald, *Clustering of dark matter tracers: Renormalizing the bias parameters*, *Phys. Rev.* **D74** (2006) 103512 [astro-ph/0609413].

[78] P. McDonald and A. Roy, *Clustering of dark matter tracers: generalizing bias for the coming era of precision LSS*, *JCAP* **0908** (2009) 020 [0902.0991].

[79] F. Schmidt, D. Jeong and V. Desjacques, *Peak-Background Split, Renormalization, and Galaxy Clustering*, *Phys. Rev.* **D88** (2013) 023515 [1212.0868].

[80] V. Assassi, D. Baumann, D. Green and M. Zaldarriaga, *Renormalized Halo Bias*, *JCAP* **1408** (2014) 056 [1402.5916].

[81] T. Matsubara and Y. Suto, *Cosmological redshift distortion of correlation functions as a probe of the density parameter and the cosmological constant*, *Astrophys. J.* **470** (1996) L1 [astro-ph/9604142].

[82] W. E. Ballinger, J. A. Peacock and A. F. Heavens, *Measuring the cosmological constant with redshift surveys*, *Mon. Not. Roy. Astron. Soc.* **282** (1996) 877 [astro-ph/9605017].

[83] N. Padmanabhan and M. J. White, *Constraining Anisotropic Baryon Oscillations*, *Phys. Rev.* **D77** (2008) 123540 [0804.0799].

[84] BOSS collaboration, *The clustering of galaxies in the completed SDSS-III Baryon Oscillation Spectroscopic Survey: Anisotropic galaxy clustering in Fourier-space*, *Mon. Not. Roy. Astron. Soc.* **466** (2017) 2242 [1607.03150].

[85] C.-T. Chiang, C. Wagner, F. Schmidt and E. Komatsu, *Position-dependent power spectrum of the large-scale structure: a novel method to measure the squeezed-limit bispectrum*, *JCAP* **1405** (2014) 048 [1403.3411].

[86] T. Nishimichi and P. Valageas, *Redshift-space equal-time angular-averaged consistency relations of the gravitational dynamics*, *Phys. Rev.* **D92** (2015) 123510 [1503.06036].

[87] H. A. Feldman, N. Kaiser and J. A. Peacock, *Power spectrum analysis of three-dimensional redshift surveys*, *Astrophys. J.* **426** (1994) 23 [astro-ph/9304022].

[88] D. J. Eisenstein, H.-j. Seo, E. Sirko and D. Spergel, *Improving Cosmological Distance Measurements by Reconstruction of the Baryon Acoustic Peak*, *Astrophys. J.* **664** (2007) 675 [astro-ph/0604362].

[89] D. J. Eisenstein, H.-j. Seo and M. J. White, *On the Robustness of the Acoustic Scale in the Low-Redshift Clustering of Matter*, *Astrophys. J.* **664** (2007) 660 [astro-ph/0604361].

[90] N. Padmanabhan, X. Xu, D. J. Eisenstein, R. Scalzo, A. J. Cuesta, K. T. Mehta et al., *A 2 per cent distance to z=0.35 by reconstructing baryon acoustic oscillations - I. Methods and application to the Sloan Digital Sky Survey*, *Mon. Not. Roy. Astron. Soc.* **427** (2012) 2132 [1202.0090].

[91] G. Jungman, M. Kamionkowski, A. Kosowsky and D. N. Spergel, *Cosmological parameter determination with microwave background maps*, *Phys. Rev.* **D54** (1996) 1332 [astro-ph/9512139].

[92] T. Baldauf, U. Seljak, L. Senatore and M. Zaldarriaga, *Linear response to long wavelength fluctuations using curvature simulations*, *JCAP* **1609** (2016) 007 [1511.01465].

[93] Y. Li, M. Schmittfull and U. Seljak, *Galaxy power-spectrum responses and redshift-space super-sample effect*, *JCAP* **1802** (2018) 022 [1711.00018].

[94] C.-T. Chiang and A. Slosar, *Power spectrum in the presence of large-scale overdensity and tidal fields: breaking azimuthal symmetry*, 1804.02753.

[95] D. A. Varshalovich, A. N. Moskalev and V. K. Khersonsky, *Quantum Theory of Angular Momentum: Irreducible Tensors, Spherical Harmonics, Vector Coupling Coefficients, 3nj Symbols*. World Scientific, Singapore, 1988.

[96] M. Shiraishi, N. S. Sugiyama and T. Okumura, *Polypolar spherical harmonic decomposition of galaxy correlators in redshift space: Toward testing cosmic rotational symmetry*, *Phys. Rev.* **D95** (2017) 063508 [1612.02645].

[97] N. S. Sugiyama, M. Shiraishi and T. Okumura, *Limits on statistical anisotropy from BOSS DR12 galaxies using bipolar spherical harmonics*, *Mon. Not. Roy. Astron. Soc.* **473** (2018) 2737 [1704.02868].

[98] N. Bartolo, A. Kehagias, M. Liguori, A. Riotto, M. Shiraishi and V. Tansella, *Detecting higher spin fields through statistical anisotropy in the CMB and galaxy power spectra*, *Phys. Rev.* **D97** (2018) 023503 [1709.05695].

[99] A. S. Szalay, T. Matsubara and S. D. Landy, *Redshift space distortions of the correlation function in wide angle galaxy surveys*, *Astrophys. J.* **498** (1998) L1 [astro-ph/9712007].

[100] I. Szapudi, *Wide angle redshift distortions revisited*, *Astrophys. J.* **614** (2004) 51 [astro-ph/0404477].

[101] P. Papai and I. Szapudi, *Non-Perturbative Effects of Geometry in Wide-Angle Redshift Distortions*, *Mon. Not. Roy. Astron. Soc.* **389** (2008) 292 [0802.2940].

[102] D. Bertacca, R. Maartens, A. Raccanelli and C. Clarkson, *Beyond the plane-parallel and Newtonian approach: Wide-angle redshift distortions and convergence in general relativity*, *JCAP* **1210** (2012) 025 [1205.5221].

[103] A. Raccanelli, D. Bertacca, O. Doré and R. Maartens, *Large-scale 3D galaxy correlation function and non-Gaussianity*, *JCAP* **1408** (2014) 022 [1306.6646].

[104] N. S. Sugiyama, S. Saito, F. Beutler and H.-J. Seo, *A complete FFT-based decomposition formalism for the redshift-space bispectrum*, *Mon. Not. Roy. Astron. Soc.* **484** (2019) 364 [1803.02132].

[105] Y. Li, W. Hu and M. Takada, *Separate Universe Consistency Relation and Calibration of Halo Bias*, *Phys. Rev.* **D93** (2016) 063507 [1511.01454].

[106] T. Lazeyras, C. Wagner, T. Baldauf and F. Schmidt, *Precision measurement of the local bias of dark matter halos*, *JCAP* **1602** (2016) 018 [1511.01096].

[107] M. Crocce, S. Pueblas and R. Scoccimarro, *Transients from Initial Conditions in Cosmological Simulations*, *Mon. Not. Roy. Astron. Soc.* **373** (2006) 369 [astro-ph/0606505].

[108] Ya. B. Zeldovich, *Gravitational instability: An Approximate theory for large density perturbations*, *Astron. Astrophys.* **5** (1970) 84.

[109] V. Springel, *The Cosmological simulation code GADGET-2*, *Mon. Not. Roy. Astron. Soc.* **364** (2005) 1105 [astro-ph/0505010].

[110] J. S. Bagla, *A TreePM code for cosmological N-body simulations*, *J. Astrophys. Astron.* **23** (2002) 185 [astro-ph/9911025].

[111] J. S. Bagla and S. Ray, *Performance characteristics of treepm codes*, *New Astron.* **8** (2003) 665 [astro-ph/0212129].

[112] T. R. Quinn, N. Katz, J. Stadel and G. Lake, *Time stepping N body simulations*, *Submitted to: Astrophys. J.* (1997) [astro-ph/9710043].

[113] D. Jamieson and M. LoVerde, *Quintessential Isocurvature in Separate Universe Simulations*, 1812.08765.

[114] E. Dimastrogiovanni, M. Fasiello, D. Jeong and M. Kamionkowski, *Inflationary tensor fossils in large-scale structure*, *JCAP* **1412** (2014) 050 [1407.8204].

[115] F. Schmidt, E. Pajer and M. Zaldarriaga, *Large-Scale Structure and Gravitational Waves III: Tidal Effects*, *Phys. Rev.* **D89** (2014) 083507 [1312.5616].

[116] Y. Nan, K. Yamamoto, H. Aoki, S. Iso and D. Yamauchi, *Large-scale inhomogeneity of dark energy produced in the ancestor vacuum*, *Phys. Rev.* **D99** (2019) 103512 [1901.11181].

[117] P. Catelan, M. Kamionkowski and R. D. Blandford, *Intrinsic and extrinsic galaxy alignment*, *Mon. Not. Roy. Astron. Soc.* **320** (2001) L7 [astro-ph/0005470].

[118] C. M. Hirata and U. Seljak, *Intrinsic alignment-lensing interference as a contaminant of cosmic shear*, *Phys. Rev.* **D70** (2004) 063526 [astro-ph/0406275].

[119] M. Shiraishi, D. Nitta, S. Yokoyama, K. Ichiki and K. Takahashi, *CMB Bispectrum from Primordial Scalar, Vector and Tensor non-Gaussianities*, *Prog. Theor. Phys.* **125** (2011) 795 [1012.1079].